Spatial and Temporal Analysis of Glutamate Receptor Localisation at the Drosophila Neuromuscular Junction

D I S S E R T A T I O N

zur Erlangung des akademischen Grades

d o c t o r r e r u m n a t u r a l i u m
(Dr. rer. nat.)

im Fach Biophysik

eingereicht an der
Lebenswissenschaftlichen Fakultät
der Humboldt-Universität zu Berlin

von
Dipl. Biophysiker Yue-Hien Lee

Präsident der Humboldt-Universität zu Berlin
Prof. Dr. Jan-Hendrik Olbertz

Dekan der Lebenswissenschaftlichen Fakultät
Prof. Dr. Richard Lucius

Gutachter:

1. Prof. Dr. Hanspeter Herzel
2. Prof. Dr. Stephan J. Sigrist
3. Prof. Dr. Stefan Hallermann

eingereicht am: 9. September 2014
Tag der mündlichen Prüfung: 25. Juni 2015

Abstract

Synapses are one of the basic elements in the neural network of our brain. The activity-dependent change in synaptic strength between neurons, called synaptic plasticity, is supposed to be the molecular basis of learning and memory formation. One major mechanism involved in the regulation of the synaptic strength is the trafficking of glutamate receptors to and from the synapse. The quantity of glutamate receptors is directly related to the transmission strength of a synapse.

In this thesis the neuromuscular junction (NMJ) of *Drosophila* larva is used as a model system to study basic mechanisms of glutamate receptor trafficking. In particular confocal images of glutamate receptors, tagged to fluorophores, are analysed. For this, statistical parameters are developed and used to quantitatively describe the distributions of glutamate receptors.

The results show that gating dynamics are an important variable in glutamate receptor trafficking. Glutamate receptors with reduced charge transfer have strong altered localisation and accumulate prematurely at young synapses. Furthermore, their abundance are uncoupled from presynaptic assembly. The thesis also shows that glutamate receptors compete for synaptic anchoring sites in postsynaptic densities (PSDs). Therefore, the trafficking of one receptor is also dependent on the trafficking of other receptors. Moreover, at the NMJ the density of synaptic proteins is not regulated on the level of single synapses, but instead is regulated in clusters of synapses. Interestingly, the density of the presynaptic protein Bruchpilot is tightly coupled to the total receptor density. Suggesting a trans-synaptic mechanism that couples the protein densities between pre- and postsynaptic sites.

Contents

Chapter 1

Introduction

The information that we perceive from our environment is processed by neurons in our central nervous system. One of the hallmarks of a neuron is its ability to form multiple connections to other neurons. It is estimated that in average a neuron has about 1000 connections. Thus, taking into account that there are about 10^{11} neurons in our brain, the overall number of connections is astronomically high. In this huge neural network electrical signals are actively propagated from one neuron to subsequent neurons. The transmission of electrical signals between neurons takes place at highly specialised junctions called synapses.

Structure and function of a chemical synapse

The general structure of a chemical synapse consists of a presynaptic and a postsynaptic terminal that are separated by a synaptic cleft (Fig. 1.1). In the presynaptic terminal arriving electrical signals are translated into a chemical signal by releasing neurotransmitter into the synaptic cleft. The release of neurotransmitter is a highly organised process that requires the interplay of many different proteins (Sheng et al., 2012). At the active zone vesicles are closely docked to the membrane, which release neurotransmitter by quick fusion with the membrane. The fusion is initiated by an increase in intracellular calcium (Fig. 1.1a,b).

The postsynaptic density (PSD) is an electron-dense structure at the postsynaptic terminal that is directly located opposite the active zone. Neurotransmitter receptors are located within the PSD, which can be activated by the binding of neurotransmitter from the synaptic cleft. Most neurotransmitter receptors translate the chemical signal back into an electrical signal by changing the postsynaptic membrane potential (Fig. 1.1c). Depending on whether the postsynaptic membrane potential is depolarised or hyperpolarised, the chemical synapse is defined as excitatory or inhibitory. At excitatory synapses glutamate is often used as a neurotransmitter. One prominent neurotransmitter receptor, which is activated by glutamate, is the AMPA receptor (AMPAR) (Fig. 1.2). In the central nervous system AMPARs are responsible for most fast excitatory synaptic transmissions (Shepherd and Huganir, 2007).

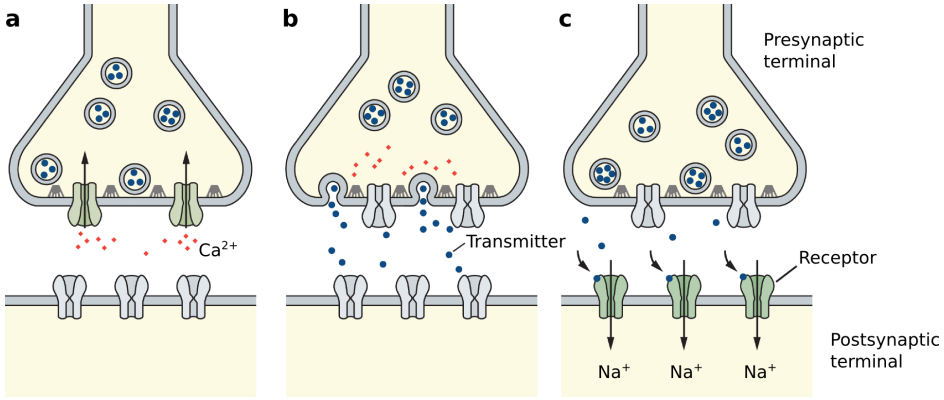

Figure 1.1. Signal transmission at a chemical synapse. This is an illustration that shows the most important aspects of an excitatory synapse during signal transmission. **(a)** Voltage-gated calcium channels are triggered by an action potential that arrives at the presynaptic terminal. As a consequence calcium flows through the calcium channels from the extracellular space into the presynaptic terminal. **(b)** Due to the intracellular increase of calcium, vesicles filled with neurotransmitter fuse with the membrane at the active zone. Neurotransmitters are released from the vesicles into the synaptic cleft, where they diffuse to the postsynaptic site and bind to ligand-gated receptors. **(c)** The binding results in the opening of the ion pore of the receptors. Ions flow into the postsynaptic terminal, which depolarises the postsynaptic membrane. Adapted from Kandel et al. (2013).

1.1 The molecular basis of learning and memory

One of the major goals in neuroscience is to understand the molecular basis of learning and memory. The brain consists of a huge number of neurons that form a highly interconnected network. What changes take place in this network during learning and memory formation? The view today is that the synaptic connections between the neurons are plastic. New connections can be formed and already existing connections can be altered. The process where existing connections get stronger or weaker is called synaptic plasticity. Very early on Hebb proposed a learning rule called "fire together, wire together" which took into account that synaptic connections can get modified (Hebb, 1949). He proposed that when a neuron A takes part in firing a neuron B repeatedly, then the synaptic connection between neuron A and B becomes stronger such that the efficiency of neuron A firing neuron B increases.

Synaptic plasticity and receptor trafficking

The best studied forms of synaptic plasticity are long-term potentiation (LTP) and long-term depression (LTD). LTP describes the increase and LTD the decrease of the synaptic transmission strength due to changes in neuronal activity. On the molecular level calcium plays an important role during synaptic plasticity. The influx of calcium through NMDA receptors (NMDARs) at the postsynaptic site and the subsequent activation of CaMKII, a protein kinase, is necessary for the induction of LTP (Fig. 1.3). The

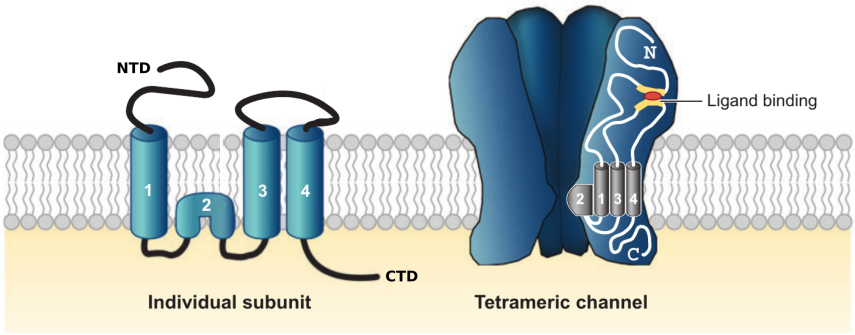

Figure 1.2. The structure and function of AMPA receptors. In the central nervous system AMPARs mediate fast excitatory synaptic transmission, i.e. they depolarise the postsynaptic membrane potential upon binding to glutamate. The binding of glutamate results in a conformational change that opens their ion pore. AMPARs are tetramers that consist of four subunits. Altogether there are four different AMPAR subunits known: GluA1-4. However only maximal two different subunits are assembled into one AMPAR complex. AMPARs have an intracellular, a transmembrane and an extracellular domain. The extracellular domain consists of the N-terminal domain (NTD) and the ligand binding domain, which is essential for neurotransmitter binding. The transmembrane domain consists of the channel pore, which, when opened, conducts ion. The intracellular domain consists mainly of the C-terminal domain (CTD). The four subunits show high variations in their CTDs, which is responsible for their different binding partners. Modified from Shepherd and Huganir (2007).

increase in synaptic efficacy due to LTP can theoretically be mediated by changes at the pre- or postsynaptic site. Presynaptically the glutamate release can be increased, postsynaptically the sensitivity to glutamate can be enhanced. Several evidences suggest that the postsynaptic site undergoes significant modifications during LTP. Postsynaptic silent synapses (Malinow et al., 2000), which have only NMDARs but no AMPARs, recruit AMPARs to the PSD from extrasynaptic membrane sites or intracellular pools to increase the synaptic strength during LTP (Fig. 1.3). This dynamic recruitment of AMPARs to the PSD is regulated by lateral membrane trafficking and exocytosis mechanisms. In the last decade it became apparent that AMPAR trafficking is highly important for the expression of LTP and LTD (Malinow and Malenka, 2002; Bredt and Nicoll, 2003; Shepherd and Huganir, 2007; Anggono and Huganir, 2012; Huganir and Nicoll, 2013).

Regulation of receptor trafficking

Since the discovery of silent synapses and the importance of AMPAR recruitment for LTP, many studies have focused on the mechanisms of AMPAR trafficking. Until recently a general view was that AMPAR trafficking is regulated by their C-terminal domains (CTDs). The CTDs of AMPAR subunits show high sequence variations, have different phosphorylation sites and interact with distinct proteins. In particular results have shown that AMPAR subunits have different functional roles. The GluA1 sub-

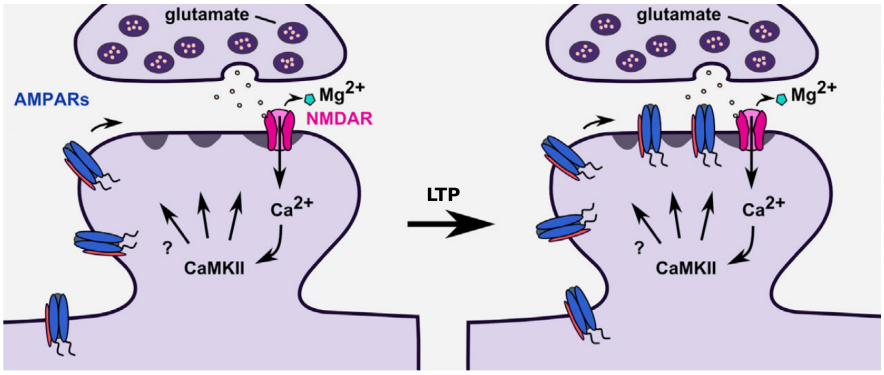

Figure 1.3. AMPA receptor trafficking is crucial for synaptic plasticity. The induction of LTP requires a postsynaptic depolarisation, which can be achieved by a short period of high frequency stimulation. This depolarisation unblocks the voltage-dependent NMDARs from magnesium. The activation of NMDARs leads to the influx of calcium into the postsynaptic site. Calcium then activates the protein kinase CaMKII, which can phosphorylate diverse PSD proteins, including the GluA1 subunit of AMPARs and the GluN2B subunit of NMDARs. Although the signalling cascade downstream of CaMKII is still under investigation, it is known that AMPAR recruitment to the PSD accounts for the increased synaptic transmission strength. The changes in synaptic efficacy can last for several hours. Modified from Huganir and Nicoll (2013).

unit is necessary for LTP, whereas the GluA2 subunit is necessary for LTD expression (Malinow and Malenka, 2002; Huganir and Nicoll, 2013). However a recent study has cast doubt on the CTD as the major factor in controlling receptor trafficking during LTP. Granger et al. (2013) have shown that during LTP the synapse can accumulate, as opposed to the common view, a broad variety of glutamate receptors independent of subunit type. Even kainate receptors, normally not found at those synapses, can be recruited to induce LTP. Therefore the molecular mechanisms of receptor trafficking during synaptic plasticity remain still unclear. The exact details of how receptor trafficking is regulated is of great interest in the neuroscience field, since it helps to understand the molecular basis of learning and memory.

1.2 The *Drosophila* neuromuscular synapse

The motivation to develop new molecular and cellular techniques to monitor and perturb trafficking of receptors comes from the discovery that AMPAR trafficking is involved in LTP (Malinow and Malenka, 2002). In this thesis the *Drosophila melanogaster* neuromuscular synapse is used as a model system to understand receptor trafficking and localisation. Model systems have always played a major role in the discovery of basic mechanisms of biological processes. They have been used when vertebrate systems have been too complex and too hard to access by experiments. For example Eric R. Kandel used the sea slug *Aplysia californica*, an invertebrate, as a model system to show that learning and memory storage are related to changes in synapses. Later it

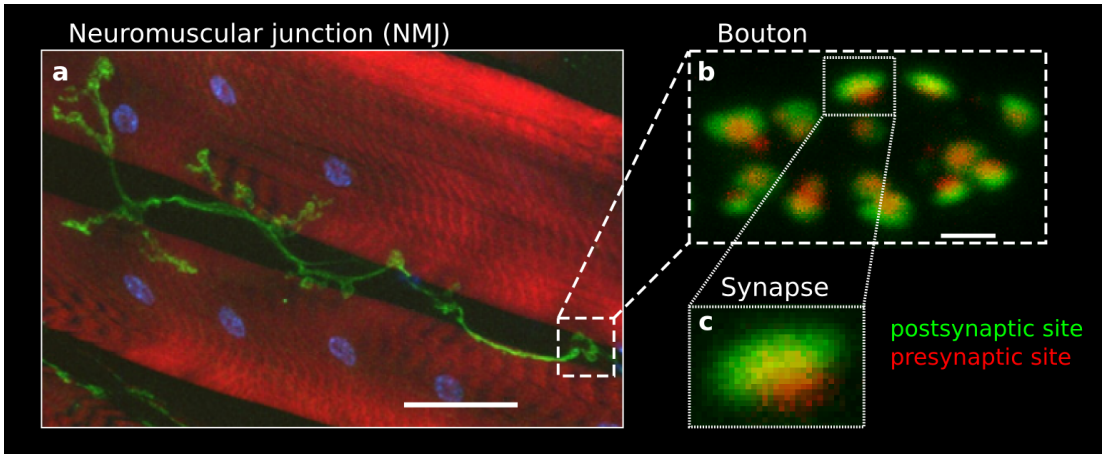

Figure 1.4. The neuromuscular junction of a 3rd instar larva. (a) The neuromuscular junction consists of a presynaptic terminal (motoneuron, green) and a postsynaptic terminal (muscle, red). Muscle nuclei are in blue. Scale bar, 50 μm. Modified from Peron et al. (2009). **(b)** A confocal image showing a single bouton with multiple synapses. Glutamate receptors at postsynaptic densities are in green. Bruchpilot proteins at presynaptic active zones are in red. Scale bar, 1 μm. Image by Astrid Petzoldt. **(c)** Magnified image section from (b) showing a single synapse.

became apparent that basic learning mechanisms are conserved between invertebrates and vertebrates (Bailey et al., 1996).

The hallmarks of model systems are their easy accessibility by various experimental techniques and their easy manipulability. Both properties are highly fulfilled by the neuromuscular junction (NMJ) of the *Drosophila* larva (Collins and DiAntonio, 2007; Frank et al., 2013). For the fruit fly there exist a vast amount of genetic tools to manipulate gene function not only for a specific tissue but also for a certain developmental stage. Besides the high genetic manipulability, the NMJ is also accessible to various established experimental techniques. Thus mutations introduced into the model system can be studied under many physiological aspects (e.g. electrophysiology or behavioural studies). Often it is even possible to study mutations *in vivo* at the living animal.

This all makes the *Drosophila* larval NMJ an ideal system to study the development of synapses under many aspects, including receptor trafficking and localisation. The following introduction of the NMJ briefly describes the experimental methods on which this thesis is based on. For a deeper understanding of the NMJ and the existing methods the book by Budnik and Ruiz-Canada (2006) is recommended.

The structure of the NMJ

The NMJ connects the motoneuron with its target muscle cell and can reach the length of several hundred micrometers. The NMJ is organised in several boutons that are lined up in a chain, which often show complex branching patterns (Fig. 1.4). In a single bouton there are up to ~ 20 synapses depending on its size. NMJs are divided

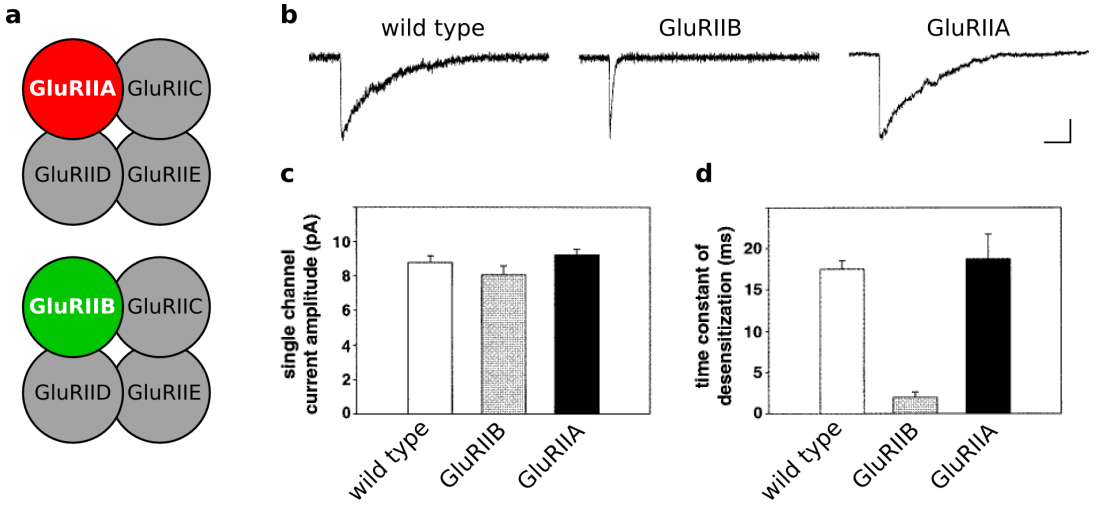

Figure 1.5. Glutamate receptor subunit composition determines desensitisation rate. (a) Two tetrameric glutamate receptor complexes at the NMJ exist that differ in only one subunit: GluRIIA or GluRIIB. **(b)** The fourth subunit, GluRIIA or GluRIIB, is crucially determining the postsynaptic response to glutamate application in outside-out patches of isolated muscle membrane. Scale bar: 10 msec, 2 pA. **(c)** The single channel amplitude does not depend on GluRIIA or GluRIIB. However, **(d)** receptor complexes with GluRIIB show an increased desensitisation rate. (b-d) are modified from DiAntonio et al. (1999).

into three types (I, II and II) depending on their morphology. Type I NMJs are the most common ones and are further subdivided into type Ib and Is. Type Ib NMJs are larger (3-6 μm diameter) than type Is NMJs (2-4 μm diameter) (Hoang and Chiba, 2001). In this thesis only type Ib NMJs are analysed.

Glutamate receptors at the NMJ

The synapses at the NMJ share similarities with the excitatory synapses in the central nervous system of vertebrates. The synapses are mainly glutamatergic and contain non-NMDA-type ionotropic glutamate receptors, which mediate fast excitatory synaptic transmissions. Five glutamate receptor subunits are known: GluRIIA, GluRIIB, GluRIIC, GluRIID and GluRIIE (Schuster et al., 1991; Petersen et al., 1997; Marrus et al., 2004; Qin et al., 2005). Interestingly, the glutamate receptor subunits show homology to AMPA and kainate receptors of vertebrates (Marrus et al., 2004; Qin et al., 2005). Several studies suggest that the glutamate receptor subunits assemble as heteromeric tetramers. Three of them (GluRIIC, GluRIID and GluRIIE) are essential for receptor formation and function. The fourth subunit in the receptor complex is either GluRIIA or GluRIIB and has a major influence on the postsynaptic response to glutamate (Fig. 1.5). Receptor complexes with GluRIIB desensitises about ten times faster than complexes with GluRIIA (DiAntonio et al., 1999).

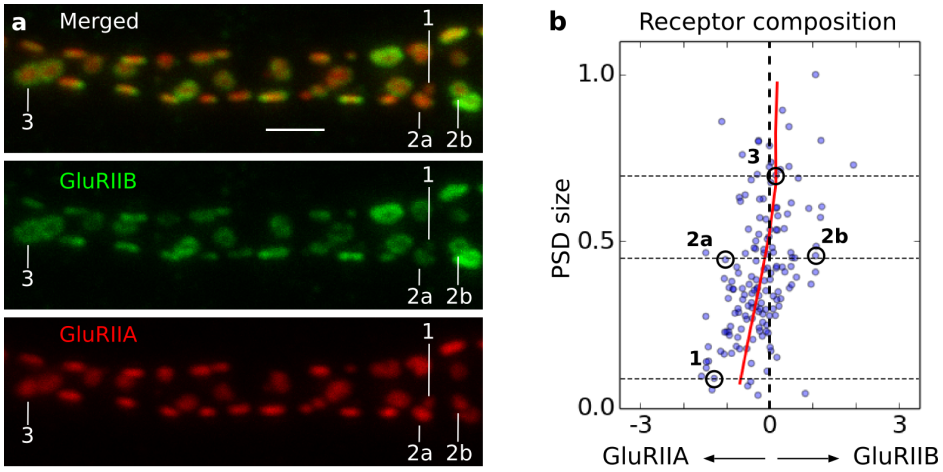

Figure 1.6. GluRIIA and GluRIIB segregate at the NMJ. (a) Confocal image of an NMJ expressing GluRIIA and GluRIIB that are genetically fused to RFP and GFP, respectively. Scale bar, 2 μm. Image by Astrid Petzoldt. **(b)** GluRIIA and GluRIIB show distinct localisations at the level of single PSDs (compare 2a with 2b). Nascent synapses are mainly rich in GluRIIA (1), while mature synapses (3) have a rather balanced receptor composition (Schmid et al., 2008). N = 155 PSDs. The red line represents the average receptor ratio in a window length of 0.2 PSD size. The receptor composition is given as: $\log_2$(GluRIIB/GluRIIA).

Monitoring glutamate receptor composition of single PSDs

The strength of the *Drosophila* larval NMJ as a model system is its genetic accessibility. It is possible to re-express genetic constructs of the receptor subunits in a genetic background, where the endogenous receptor subunits are knocked out (Schmid et al., 2008). The receptor subunits can be re-expressed at physiological levels using their own endogenous promoters. Using this system one can insert targeted mutations into certain receptor subunits and study the implications of the mutations without the interference of the wild type receptors.

For instance one can re-express GluRIIA and GluRIIB with a fluorescent tag (RFP and GFP) to study their localisation at the NMJ. Importantly, the genetic tag does not influence their gating properties (Schmid et al., 2008). Analysing the localisation of GluRIIA and GluRIIB in detail shows that their localisation differs on the level of single synapses (Fig. 1.6). This distinct localisation of GluRIIA and GluRIIB have been previously observed and termed as segregation (Marrus et al., 2004; Chen and Featherstone, 2005). The molecular mechanisms underlying the segregation of GluRIIA and GluRIIB are not yet understood. Several studies revealed proteins that have subunit specific effects on the synaptic expression levels of either GluRIIA or GluRIIB (Chen et al., 2005; Chen and Featherstone, 2005; Liebl and Featherstone, 2008; Morimoto et al., 2010; Lee et al., 2013). However, none of them can explain the different localisation.

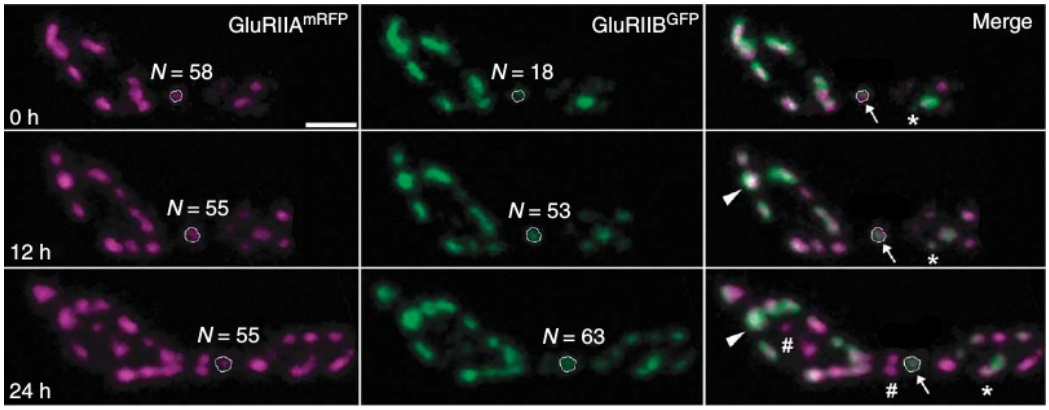

Figure 1.7. ***In vivo*** **imaging of glutamate receptors.** Confocal image of a 3rd instar larval NMJ expressing GluRIIA and GluRIIB, which are genetically fused to mRFP and GFP, respectively. Glutamate receptor composition of single PSDs can be monitored *in vivo* over 24 hours. During this period new synapses form (#) and mature (arrow and asterisk). Small PSDs are mainly rich in GluRIIA, but during maturation the receptor composition becomes balanced (arrow). Large PSDs are stable and barely increase in size (arrowhead). N indicates estimated receptor number for GluRIIA and GluRIIB. Scale bar, 2 μm. Modified from Schmid et al. (2008).

In vivo imaging of glutamate receptors over time

The NMJ is a dynamic structure, where new boutons are constantly formed. During larval development the NMJ can increase its size by up to 100 fold. The cuticle of the larva is translucent, which allows to image the NMJ in a noninvasive manner in the living animal (Zito et al., 1999). Therefore the NMJ can be imaged *in vivo* over several hours during which the larva continues to grow. The size of the NMJ makes it easy to re-identify the NMJ at different time points. During the recordings it is then possible to follow the formation of new boutons and the growth of existing boutons (Zito et al., 1999).

The Sigrist lab (Rasse et al., 2005; Füger et al., 2007; Schmid et al., 2008) developed a system, where the protein levels at single synapses can be monitored over time *in vivo*. 3rd instar larvae can be anaesthetised with desflurane in an imaging chamber to stop any movements of the larvae. In this way the confocal image recordings are not impaired by the movement of the larvae. Importantly, the anaesthetisation does not affect the normal development of the larvae. Combined with the available genetic tools, synaptic proteins of interest can be monitored during synapse formation and assembly. That makes this system a very powerful analytical tool to study synapse assembly *in vivo* at glutamatergic synapses.

Using this system, it is for example possible to analyse the dynamics of synaptic receptor incorporation using fluorescence recovery after photo-bleaching (Schmid et al., 2008). Another application, which is especially relevant for this thesis, is the possibility to analyse receptor composition of single synapses over time during which synapses ma-

ture and grow (Fig. 1.7). For example, Schmid et al. (2008) have shown that small PSDs are mainly dominated by GluRIIA. However during PSD maturation more GluRIIB than GluRIIA is incorporated, which in turn leads to a balanced receptor composition of mature PSDs.

1.3 Overview of the thesis

The main aim of this thesis is to understand how glutamate receptor trafficking is regulated on the molecular level. In a close collaboration with the Sigrist lab from the Freie Universität Berlin, the trafficking of glutamate receptors is studied at the larval NMJ using the experimental setup introduced in the last section. For this, several mutant receptors were created in the Sigrist lab with altered electrophysiological or structural properties. Using a confocal microscope the mutant receptors were imaged at the NMJ. Confocal images were taken by Astrid Petzoldt and Omid Khorramshahi from the Sigrist lab.

In this thesis the confocal images are processed and the receptor quantities of single synapses are extracted from these images. A new statistical parameter is defined and other statistical parameters are used to compare the distribution of receptors at the NMJ. Using the extracted data and the statistical parameters the effects of the mutations and their implications on receptor trafficking are studied. Moreover the spatial distribution of receptors is analysed to test if receptor trafficking is location dependent. Also, a model is derived that describes the relation between GluRIIA and GluRIIB. The thesis is divided into the following chapters:

- In chapter (2) it is investigated if the experimental setup, as used in Schmid et al. (2008), is capable of measuring the *absolute* ratio between GluRIIA and GluRIIB over time. For this purpose an imaging protocol is proposed to measure the relative brightness between an GFP and RFP molecule. Furthermore the precision of the experimental setup is analysed.

- In chapter (3) the hypothesis is tested if gating dynamics of a receptor influence its localisation during synapse formation and maturation. Confocal images of wild type and mutant receptors are processed and compared. A segregation parameter is defined to quantify the colocalisation of two receptors.

- In chapter (4) the spatial distribution of receptors at the NMJ is analysed. The aim is to examine if the relative position of a synapse at the NMJ has any influence on the localisation of receptors.

- In chapter (5) the relation between GluRIIA and GluRIIB is analysed on the level of single synapses. In particular the mechanism underlying the segregation between GluRIIA and GluRIIB is examined. A simple model describing their relation is derived from image analysis.

Chapter 2

Quantification of Receptor Ratios

2.1 Introduction

The system for *in vivo* imaging of GluRIIA and GluRIIB at single synapse resolution has been developed and used in the Sigrist lab to analyse receptor composition and dynamics over time (Rasse et al., 2005; Füger et al., 2007; Schmid et al., 2008). For this purpose GluRIIA and GluRIIB have been genetically tagged with the fluorophores RFP and GFP. GluRIIA$^{\mathrm{RFP}}$ and GluRIIB$^{\mathrm{GFP}}$ are expressed using their own endogenous promoters in a gluRIIA^{null};gluRIIB^{null} background, where no endogenous GluRIIA and GluRIIB are present. Two questions arise when quantifying receptor compositions in time (Fig. 2.1). Can the *absolute* ratio of GluRIIA and GluRIIB be measured? And is it possible to track the *absolute* ratio over time?

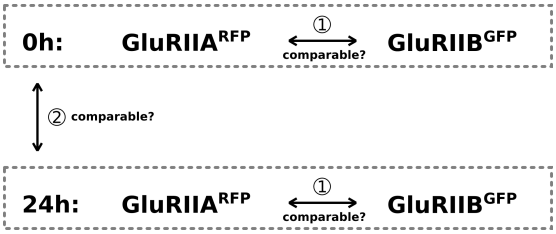

Figure 2.1. Comparability issues between different fluorophores and time points. **(1)** Is there a way to compare the measured quantities of GluRIIA and GluRIIB with each other although they are labelled with different fluorophores? **(2)** Is the experimental setup robust enough to track the absolute receptor ratio over time?

These two questions are not easy to answer, since GluRIIA and GluRIIB are labelled with different fluorophores that differ in their brightness. GFP has a much higher quantum yield than RFP, preventing a direct comparison of the fluorescence intensities. Next, for the monitoring of receptor ratios over time the same NMJ needs to be imaged twice. As a result, the variability of the experimental setup increases. For instance the imaging chamber containing the larva has to be reassembled. Here an imaging protocol is proposed for measuring the absolute receptor ratio at the NMJ.

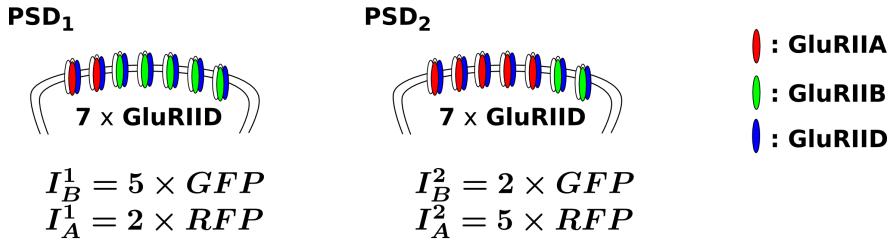

Figure 2.2. Illustration of measuring GFP/RFP. In theory two PSDs with equal number of total receptors are enough to calculate the relative brightness GFP/RFP. The fluorescence intensity of GluRIID will guide the detection of those two PSDs. Then the ratio of the difference in GluRIIB (ΔI_B) and GluRIIA (ΔI_B) fluorescence intensity between the two PSDs equals GFP/RFP.

2.2 Measuring the absolute receptor ratio

The key to measure the absolute ratio of GluRIIA and GluRIIB lies in the quantification of the relative brightness between one GFP and one RFP molecule (GFP/RFP). Once the relative brightness GFP/RFP is known, immediately the absolute ratio of GluRIIA and GluRIIB can be calculated. To measure GFP/RFP the following fact is exploited here: both GluRIIA and GluRIIB are assembled with three other subunits (GluRIIC, GluRIID and GluRIIE) into a tetrameric receptor complex. As a consequence, the number of GluRIID subunits in one PSD have to represent the total number of GluRIIA and GluRIIB subunits in that PSD. This additional information can be used to measure GFP/RFP (Fig. 2.2). However it is important to mention that this approach only works, because the ratio of GluRIIA and GluRIIB differs from PSD to PSD. In other words the segregation between GluRIIA and GluRIIB is absolutely necessary.

The approach in (Fig. 2.2) is slightly modified to take into account that more than two PSDs are measured in one NMJ. As a first step all PSDs are plotted into a three-dimensional space, where the x-, y- and z-axes represent the fluorescence intensities of GluRIIA, GluRIIB and GluRIID. In this graph all PSDs are constrained on a plain, since GluRIID corresponds to the sum of GluRIIA and GluRIIB (Fig. 2.4a). In particular the plain has the following form:

$$m_1 * I_{\mathrm{GFP}} + m_2 * I_{\mathrm{RFP}} = I_{\mathrm{Cy5}} \tag{2.1}$$

where I_{Cy5}, I_{GFP} and I_{RFP} are the fluorescence intensities of GluRIID, GluRIIB and GluRIIA, respectively. In a final step a plain is fitted to the data points in the three-dimensional space to obtain m_1 and m_2. Then GFP/RFP can be calculated as:

$$\mathrm{GFP/RFP} = m_2/m_1 \tag{2.2}$$

Image processing

In the experiments GluRIID was labelled with Cy5 using antibodies. Nine NMJs from four larvae were imaged with the same microscope settings (staining and imaging by Astrid Petzoldt). Confocal image stacks of type Ib NMJs were processed as described in (Banovic et al., 2010; Owald et al., 2012). Each channel (GFP, RFP, Cy5) was processed the same way. The image stacks were preprocessed in ImageJ (1.47v) by applying a Gaussian blur filter after background subtraction. Processed stacks were transferred to Imaris 6.15 (Bitplane) to create 3D surface masks for each PSD using the seed point detection algorithm. The segmentation was checked afterwards, if necessary, PSDs that were connected together, were separated manually. Finally, for each PSD the following data were extracted using Imaris for further analysis: receptor number (represented by the fluorescence intensity), receptor density, volume and position of a PSD. The receptor density (Fig. 2.3) was calculated the following way:

$$\rho = N/V$$

where ρ is the receptor density, N is the receptor number and V is the volume of the PSD. The question whether it is possible to measure the receptor density of a PSD using a confocal microscope will be discussed in chapter (4), section (4.3.4).

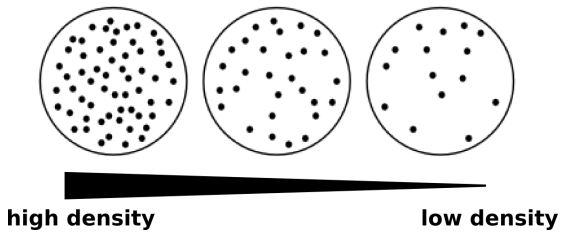

Figure 2.3. PSDs with different receptor densities. Circles represent PSDs, black dots represent receptors. Three PSDs with the same volume but with different number of receptors are shown. Consequently their receptor densities differ.

The measurement of GFP/RFP is robust

After image processing and data extraction, equation (2.1) is used to obtain GFP/RFP for each NMJ. The result (Fig. 2.4b) shows that the measurement of GFP/RFP is quite robust, since the standard deviation is relatively small (GFP/RFP = 1.32 ± 0.12; mean $\pm$ standard deviation). Unexpectedly, this result suggests that GFP is only slightly brighter than RFP. In the literature it is indicated that GFP is about three times brighter than RFP (Shaner et al., 2007). However, this can be explained by a stronger excitation beam used for RFP, thus increasing the number of emitted photons without changing its quantum yield.

The obtained GFP/RFP can now be used to calculate the absolute receptor ratio at the NMJ. For instance it is now possible to state if GluRIIA or GluRIIB is

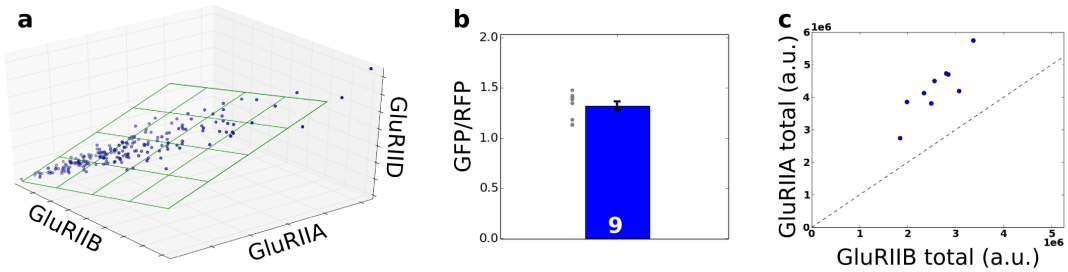

Figure 2.4. Measuring GFP/RFP. (a) The fluorescence intensities of GluRIID, GluRIIA and GluRIIB are located on a plain in a three-dimensional space, since GluRIID corresponds to the sum of GluRIIA and GluRIIB. **(b)** Nine NMJs are imaged with the same microscope settings. GFP/RFP is calculated by fitting a plain to the obtained data. GFP/RFP = 1.32 ± 0.04. Dots are single measurements. Error bars represent mean ± SEM. **(c)** For all nine NMJs the total abundance of GluRIIA (corrected with the factor 1.32) is scattered against that of GluRIIB. At all NMJs the quantity of GluRIIA is higher than GluRIIB (on average 1.6 times more frequent). The bisector is indicated by the dashed black line.

more abundant at one NMJ. The calculated absolute receptor ratio indicates that at NMJs GluRIIA is more abundant than GluRIIB, on average 1.6 times more frequent (Fig. 2.4c). Altogether this imaging protocol seems to be suitable to measure the absolute receptor ratio. However, control experiments need to be conducted to exclude any artefacts or bias in the measurement.

2.3 The variance of measuring the receptor ratio

Using the imaging protocol from last section the absolute receptor ratio at one time point can be determined. However is it possible to track the absolute receptor ratio in time? In other words, is the experimental setup robust enough to allow the comparison of receptor ratios over time? To answer this question it is necessary to quantify the variability of the experimental setup between different time points. For this purpose, larval NMJs are analysed, where two genetic copies of GluRIIA, labelled with GFP and RFP, are coexpressed in a gluRIIA^{null};gluRIIB^{null} background. This larva will be called hereafter IIA/IIA genotype. This system has the advantage that the measured ratio of GFP and RFP should be the same for all PSDs. Any variance in the measurement of the ratio can be attributed to either noise in the experimental setup or to biological noise.

RFP is significantly bleached during imaging

To start analysing the experimental variability, a single NMJ of the IIA/IIA genotype was imaged twice in quick succession. The larva was remounted into the imaging chamber for the second recording to include mounting variance (Fig. 2.5a,b). Confocal images were processed as before. First of all, the total fluorescence intensity of GFP

Table 2.1. Significant photobleaching of RFP. Imaging leads to a 31 % loss of RFP signal, whereas almost no GFP signal is lost.

	Image 1 (*a.u.*)	Image 2 (*a.u.*)	Loss (%)	Bleaching factor
GFP	818630	810367	1	1.01
RFP	610159	423223	31	1.44

and RFP between the two recordings was compared. Unexpectedly, a significant decrease in the RFP signal was observed, whereas the GFP signal did not change from image 1 to image 2 (Tab. 2.1). The RFP used to tag GluRIIA is called mRFP and its photostability is more than a magnitude smaller than the photostability of GFP (Campbell et al., 2002; Shaner et al., 2007). Since the microscope settings have not been changed between the two recordings, the decrease in RFP fluorescence is therefore likely caused by photobleaching.

The receptor ratio of single PSDs can be measured with good accuracy

Next, the fluorescence intensities of single PSDs were compared between image 1 and 2. For this, single PSDs were tracked manually in Imaris between images. The results show that the PSD size, the fluorescence intensities and the densities of $\text{GluRIIA}^{\text{GFP}}$ and $\text{GluRIIA}^{\text{RFP}}$ can all be reproduced with good accuracy, when corrected for the loss of RFP signal (Fig. 2.5). Importantly, the receptor ratio can be measured with an average error of $\pm$ 0.1 fold changes (Fig. 2.5e). Thus the receptor ratio from single PSDs can be followed between two recordings with good accuracy.

Interestingly the receptor ratios of image 1 and 2 are positively correlated (Fig. 2.5e). This result suggests that different receptor ratios at the NMJ exist and are not caused by noise from the experimental setup. It is conceivable that fluctuations in receptor number can cause this kind of variation. The total receptor number in PSDs lies in the order of about 100 receptors (Schmid et al., 2008).

The receptor ratio can be tracked over 24 hours with high precision

Last, the variability of measuring the receptor ratio over a longer time period, e.g. 24 hours, is analysed. During this period the larva increases its size considerably. It is therefore interesting to know if the growth of the larva influences the measurement of the receptor ratio. To address this issue, six NMJs from three larvae of the IIA/IIA genotype have been tracked over 24 hours (imaging by Omid Khorramshahi). The receptor ratio of $\text{GluRIIA}^{\text{GFP}}$ and $\text{GluRIIA}^{\text{RFP}}$ of the whole NMJ was quantified.

The result indicates that the receptor ratio of a whole NMJ can be tracked over time with high precision, i.e. with an average error of $\pm$ 0.06 fold changes (Fig. 2.6). Also, this shows that the receptor ratio does not change over time. Another conclusion is that bleaching effects, as quantified above, can be neglected after 24 hours. The RFP signal has not been corrected here. Interestingly, the total range of receptor ratios, which

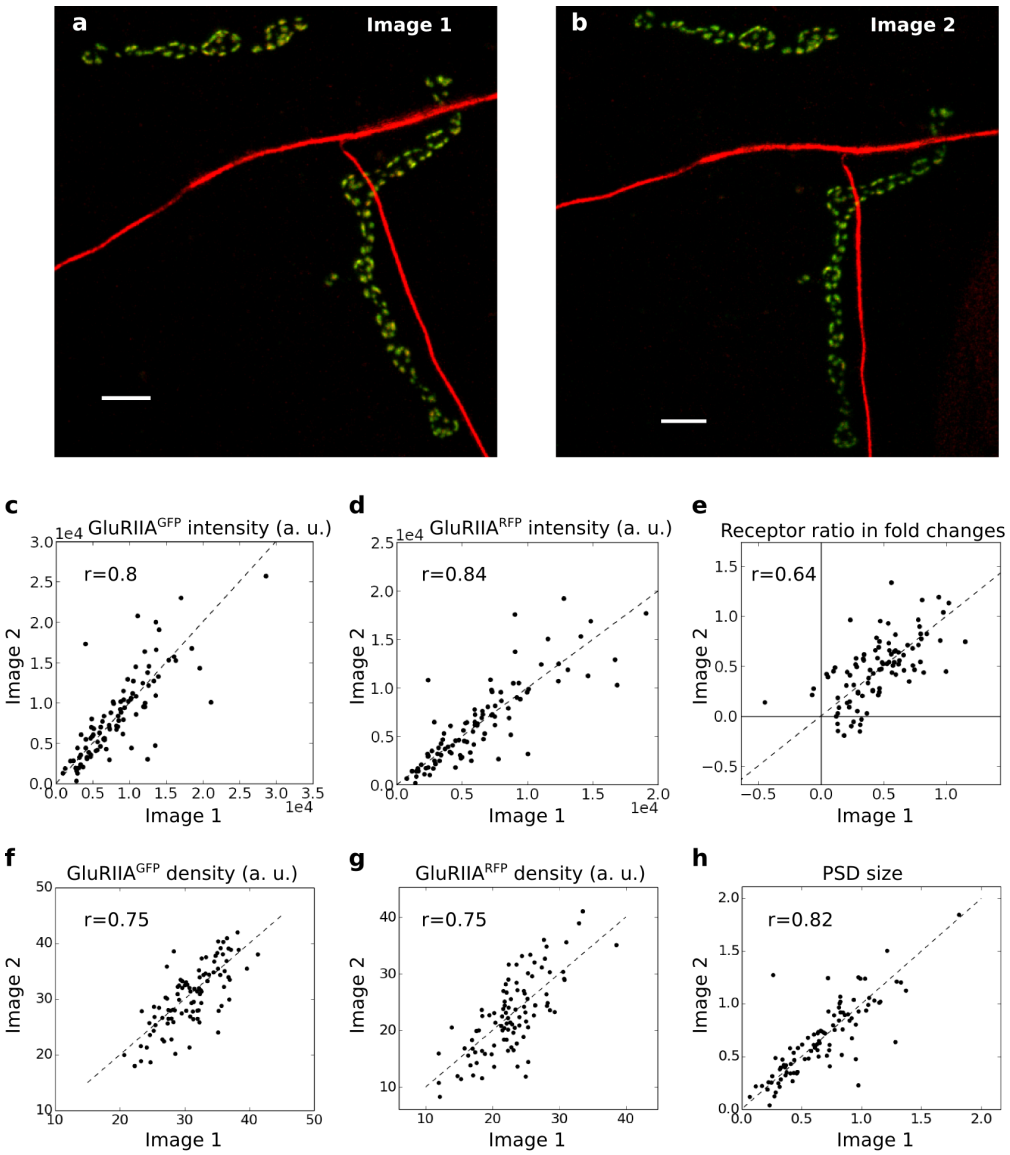

Figure 2.5. The receptor ratio of single PSDs is reproducible. (a,b) The variance of the experimental setup is studied by imaging one NMJ of the IIA/IIA genotype twice. The larva is remounted into the imaging chamber before the second recording to include mounting variance. PSDs have been tracked from image 1 to image 2 manually. Imaging by Omid Khorramshahi. Scale bar, $5\,\mu m$. **(c-h)** The loss of RFP signal is corrected to analyse the variance of the experimental setup under the condition when there is no photobleaching. The average relative errors are: RFP intensity = $\pm$ 14 %, GFP intensity = $\pm$ 14 %, RFP density = $\pm$ 9 %, GFP density = $\pm$ 5 % and PSD size = $\pm$ 11 %. The relative error of each data point is calculated as: rel = $|\bar{X} - X_i|/\bar{X}$. Moreover the receptor ratio can be reproduced with good accuracy, since the average error is only $\pm$ 0.1 fold changes. The error of single data points is calculated as: err = $|\bar{X} - X_i|$. The bisector is indicated by the dashed black line. The receptor ratio is given as: $\log_2(\mathrm{GluRIIA}^{\mathrm{GFP}}/\mathrm{GluRIIA}^{\mathrm{RFP}})$. N = 96 PSDs.

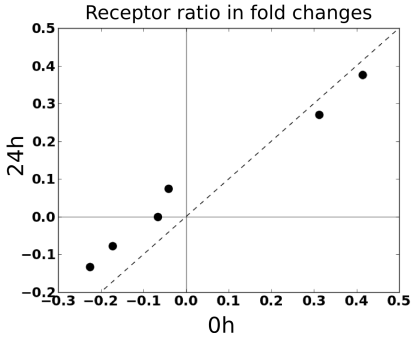

Figure 2.6. The receptor ratio of a whole NMJ can be tracked over 24 hours. The receptor ratio of six NMJs of three larvae were tracked over 24 hours. The analysis show that the receptor ratio of a single NMJ is quite stable over time. Therefore it is possible to conclude that the receptor ratio can be measured with high precision over a time period of 24 hours. The average error is only ± 0.06 fold changes. The bisector is indicated by the dashed black line. The receptor ratio is given as: $\log_2(\text{GluRIIA}^{\text{GFP}}/\text{GluRIIA}^{\text{RFP}})$.

is about 0.6 fold changes, is much larger than the measurement error of ± 0.06 fold changes. Thus NMJs differ in their absolute receptor ratios. The answer to question two in (Fig. 2.1) is yes. The absolute ratio of GluRIIA and GluRIIB can be tracked over a time period of 24 hours.

2.4 The receptor expression varies from larva to larva

The 24 hours experiment did not only reveal that receptor ratios can be measured with high precision, but also that the absolute receptor ratio differ from NMJ to NMJ (Fig. 2.6). As a consequence this would mean that the expression levels of $\text{GluRIIA}^{\text{GFP}}$ and/or $\text{GluRIIA}^{\text{RFP}}$ is different between NMJs.

Here, the difference in receptor ratio is analysed systematically in 9 larvae. The receptor ratio of at least two NMJs per larva is quantified and compared to each other. As a first step it is analysed, if the depth of the NMJ under the cuticle is responsible for the distinct receptor ratios. The measurements show that there is no correlation at all between the depth of the NMJ and the receptor ratio (Fig. 2.7). Surprisingly, when analysing the distribution of receptor ratios in more detail, the variability within one larva is much smaller than the variability from larva to larva (Fig. 2.8). The average range of observed receptor ratios within one larva is 0.2 fold changes, while the entire range of observed receptor ratios is 1.14 fold changes. In comparison, the accuracy of the experimental setup is ± 0.06 fold changes. Thus one can conclude that the observed variability of the receptor ratio has a biological source.

Since the variability between NMJs within the same larva is small compared to the overall variability, it is possible that the large inter-variability is genetically determined. One possible explanation could be that the landing sites of the genetic constructs differ from larva to larva, since they had been randomly introduced into the genome.

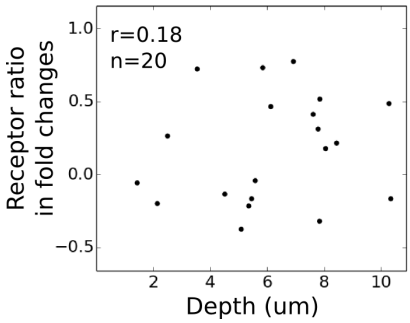

Figure 2.7. The receptor ratio is independent from the depth of the NMJ. The depth of the NMJ under the cuticle was measured as the distance between the cover glass and the centre of the NMJ along the z-axis. There is no significant correlation (P=0.45) between the receptor ratio and the depth of the NMJ.

2.5 Discussion

In this chapter an imaging protocol was introduced to quantify the absolute ratio of GluRIIA and GluRIIB at the NMJ. Since GluRIIA and GluRIIB are genetically fused to one RFP and one GFP molecule, it is necessary to measure the relative brightness between one GFP and one RFP molecule (GFP/RFP). For this purpose the essential GluRIID subunit of the tetrameric receptor complex has been additionally tagged by antibody with the fluorophore Cy5. The measurement of GFP/RFP is based on the fact that the fluorescence signal of Cy5 corresponds to the sum of GluRIIA and GluRIIB (Fig. 2.4).

The results indicate that this imaging protocol is suitable, since the measurement of GFP/RFP show little variation. However, the measurement of GFP/RFP should be confirmed by control experiments in order to exclude any bias. For example, a previous study has shown that only about 80 % of expressed GFP molecules are actually functional (Ulbrich and Isacoff, 2007). Two proteins with known stoichiometry fused to GFP and RFP can serve as a control. Any deviations from the expected ratio is a bias that can be considered in future experiments.

The 24 hour experiment has revealed that the receptor ratio of a whole NMJ can be measured with high precision (average error is $\pm$ 0.06 fold changes). Therefore, if the experimental settings are hold constant, the absolute receptor ratio can be tracked over time. However, this is only possible when the photobleaching of RFP can be neglected (Tab. 2.1), which was the case for the 24 hour experiment. In summary, the two questions from (Fig. 2.1) can be answered, in principle, with yes. The experimental setup is robust enough to compare receptor ratios between different measurements. Also, other quantities like the size of PSDs could be reproduced well. Thus, it should be possible to analyse relationships between different protein quantities. The following chapters will make use of this and derive models based on the precision of this experimental setup.

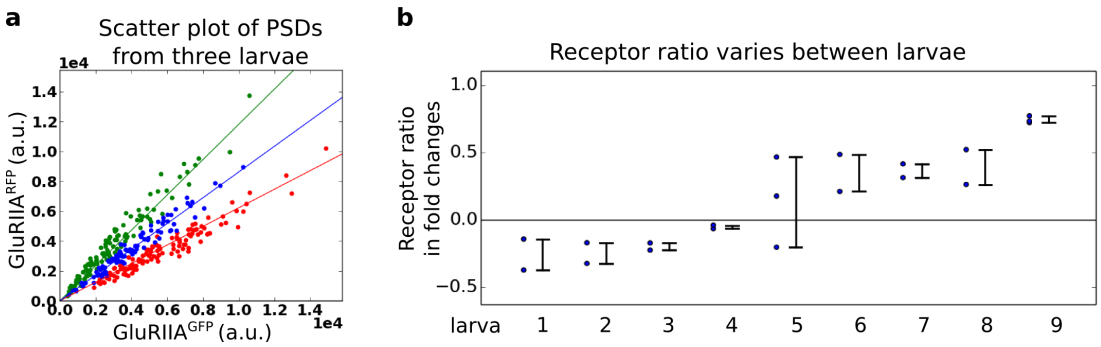

Figure 2.8. The receptor ratio is from larva to larva different. (a) Three NMJs from different larvae (represented by green, blue and red dots) are shown. The receptor ratios of PSDs within the same NMJ are similar, but differ noticeably from larva to larva. **(b)** The receptor ratio distributions of 9 larvae are shown. The entire range of the observed receptor ratios is 1.14 fold changes. Whereas the average range within one larva is only 0.2 fold changes. Each dot represents the receptor ratio of a single NMJ, while the bar indicates the range of receptor ratios within one larva. The receptor ratio is given as: $\log_2(\text{GluRIIA}^{\text{GFP}}/\text{GluRIIA}^{\text{RFP}})$.

Measuring the stoichiometry of other synaptic proteins?

If it is possible to accurately determine the relative brightness between one GFP and one RFP molecule (GFP/RFP) using the approach from section (2.2), then it should be possible to measure the stoichiometry of other proteins at the synapse. Once GFP/RFP is determined using NMJs of the IIA/IIA genotype, other larvae with synaptic proteins tagged to GFP and RFP can be measured using the same microscope settings. GFP/RFP should also apply to the new larvae, since the experimental setup is robust enough. Then using the measured GFP/RFP their absolute ratio can be determined and thus their stoichiometry. The advantage of this approach would be that it could be applied *in vivo* and to proteins that occur in high densities, as it is the case at the synapse. However one should be aware of quenching effects which can influence the measurement.

Main conclusions

In principle, the relative brightness between one GFP and one RFP molecule can be determined. Thus, the absolute ratio of two receptors, labelled with GFP and RFP, can be measured. Moreover, the ratio of two receptors can be tracked with high precision over a time period of 24 hours.

Chapter 3

Gating Dynamics Control Receptor Localisation

3.1 Introduction

Glutamate receptors change their conformation during gating (Fig. 3.1). Therefore the gating dynamics of a receptor determine how long it remains in a certain conformational state. Several studies have shown that glutamate receptors interact with auxiliary subunits, which can modify their trafficking and electrophysiological properties (Guzman and Jonas, 2010; Jackson and Nicoll, 2011). It is conceivable that gating dynamics can influence the interaction of receptors with auxiliary subunits and thus control receptor trafficking and localisation.

To test if gating dynamics indeed have an influence on receptor localisation, point mutations were introduced into GluRIIA that are known to slow or accelerate the desensitisation rate of glutamate receptors in mammalians (Tab. 3.1). The acceleration of the desensitisation rate has the effect that the opening time of the receptor, after binding to glutamate, is reduced. Consequently the charge flow through the receptor is also reduced - here termed fast-gating. On the contrary, by slowing down the desensitisation rate, the opening time of the receptor is prolonged, which in turn enhances charge flow through the receptor - here termed slow-gating. The larval NMJ is an ideal model system to study if gating dynamics determine receptor localisation, because the mutant receptors can be monitored *in vivo* over several hours, during which new synapses form and mature (Schmid et al., 2008).

Distinct gating dynamics are sufficient for receptor segregation

The created GluRIIA mutants (GFP-tagged) were coexpressed with a control wild type GluRIIA (RFP-tagged) in a genetic background, where endogenous GluRIIA and GluRIIB were knockout. Importantly, the point mutations did not block the GluRIIA mutants from ER export or prevent their trafficking to PSDs, because they colocalised with wild type GluRIIA opposite active zones. Furthermore, quantitative image anal-

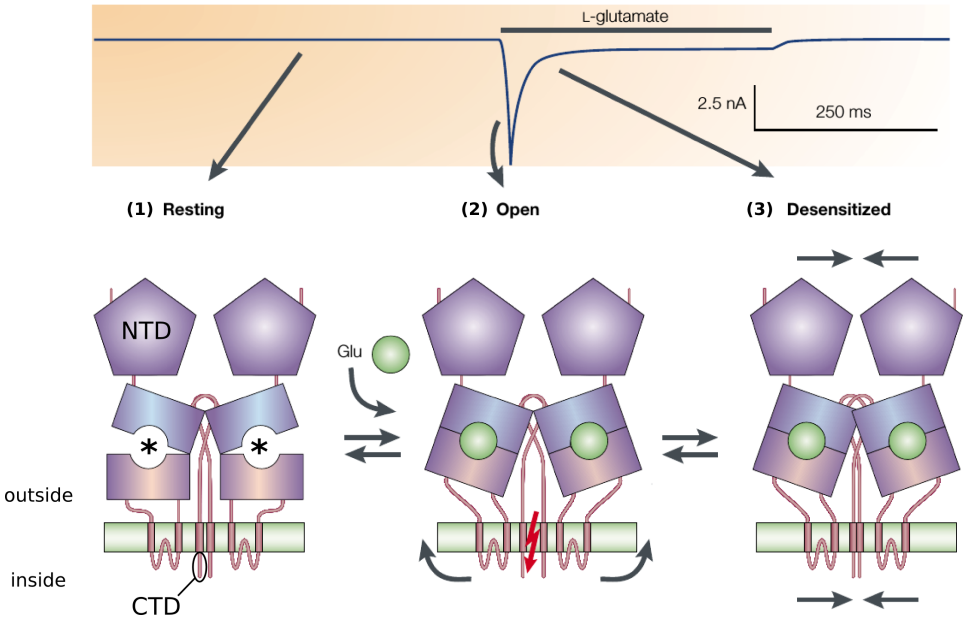

Figure 3.1. Activation and desensitisation of ionotropic glutamate receptors. The upper row shows the electrophysiology of glutamate receptors before and after glutamate application. The lower row shows the corresponding conformational changes of the glutamate receptor channel from a side view. (1) In the resting state the ion pore is closed. No ions can flow through the channel. (2) Binding of glutamate in the ligand binding domain of the channel (asterisks) opens the ion pore. Now ions can flow through the channel (lightning bolt). (3) The channel desensitises, i.e. the ion pore closes although glutamate is still bound. Modified from Madden (2002).

ysis suggests that the GluRIIA mutants formed normal receptor complexes with the other essential receptor subunits (Petzoldt et al., 2014).

To assess, if the gating dynamics of the GluRIIA mutants behave as it has been predicted (Tab. 3.1), each mutant was either coexpressed with GluRIIB or expressed in a genetic background, where the level of GluRIIA was drastically reduced. Indeed, the electrophysiological recordings of spontaneous and evoked synaptic currents at those larval muscles were consistent with the predicted gating dynamics of the GluRIIA mutants. The slow-gating GluRIIA-KE substantially increased the charge flow of spontaneous and evoked excitatory junctional currents (mEJC and eEJC). On the contrary the very-fast-gating GluRIIA-EA did not change the charge flow of mEJC and eEJC, which is in consistence with a very-fast closing receptor. The fast-gating GluRIIA-EQ had an intermediate effect on the charge flow of mEJC and eEJC (Petzoldt et al., 2014).

Strikingly, the very-fast-gating GluRIIA-EA exhibited altered synaptic localisation and trafficking behaviours when compared to wild type GluRIIA. On the single synapse level the localisation of GluRIIA-EA and GluRIIA differed strongly, even between neighbouring synapses (Fig. 3.2, IIA/IIA-EA). Additional fluorescence recovery after

Table 3.1. GluRIIA mutants. Point mutations in the region of the ligand binding domain or the pore of mammalian glutamate receptors had either an accelerating or deaccelerating effect on the desensitisation kinetics (Horning and Mayer, 2004; Yelshansky et al., 2004). Homologous point mutations were introduced into GluRIIA to achieve similar results (Petzoldt et al., 2014). Additional mutants were created, where the intracellular C-terminal domains (CTD) of GluRIIA, GluRIIA-EQ and GluRIIA-EA were exchanged with the CTD of GluRIIB (CTD_{IIB}).

Mutant name	Mutation	Expected electrophysiological behaviour
GluRIIA-KE	$K_{661} \rightarrow E$	slow-gating (long opening)
GluRIIA-EQ	$E_{783} \rightarrow Q$	fast-gating (short opening)
GluRIIA-EA	$E_{783} \rightarrow A$	very-fast-gating (very short opening)
$GluRIIA_{IIB}$	$CTD_{IIA} \rightarrow CTD_{IIB}$	same as GluRIIA
$GluRIIA\text{-}EQ_{IIB}$	$CTD_{IIA} \rightarrow CTD_{IIB}$	same as GluRIIA-EQ
$GluRIIA\text{-}EA_{IIB}$	$CTD_{IIA} \rightarrow CTD_{IIB}$	same as GluRIIA-EA

photobleaching (FRAP) experiments showed that the mobility of GluRIIA-EA, i.e. the in and out-rate of GluRIIA-EA from synapses, was considerably increased when compared to wild type GluRIIA (Petzoldt et al., 2014).

The fast-gating GluRIIA-EQ also segregated from GluRIIA, but in a less pronounced way (Fig. 3.2, IIA/IIA-EQ). On the contrary, the slow-gating GluRIIA-KE appeared to have the same localisation as GluRIIA (Fig. 3.2, IIA/IIA-KE). However, the overall fluorescence intensity of GluRIIA-KE, and thus its overall synaptic expression level, seemed to be reduced by a factor of two (Petzoldt et al., 2014). It could not be deduced visually from the confocal images of the NMJs, whether the genetic CTD-swap changed the segregation strength of the GluRIIA mutants (Fig. 3.2). In order to test if the segregation strength between two genotypes was indeed different, a quantitative parameter describing the segregation strength is introduced.

3.2 Quantifying the segregation between receptors

Here the strength of receptor segregation for one NMJ is defined as the logarithm of the fold change between the minimum and maximum observed receptor ratio at single PSDs:

$$S = \log_2(\frac{r_{max}}{r_{min}}) \tag{3.1}$$

where r_{max} is the maximum and r_{min} is the minimum observed receptor ratio (Fig. 3.3). The receptor ratio itself was calculated from the fluorescence intensity of the fluorophores (GFP and RFP). Since the measurements were error prone, five PSDs with the highest and lowest receptor ratio were used to estimate r_{max} and r_{min}, respectively. However, noise in the measurements and the biological system can cause fluctuations of the ratio between two receptors. Thus two receptors can appear segregated although they are not. Therefore the IIA/IIA genotype was always used as a baseline for measuring the segregation strength, since no segregation is expected here (Fig. 3.3a).

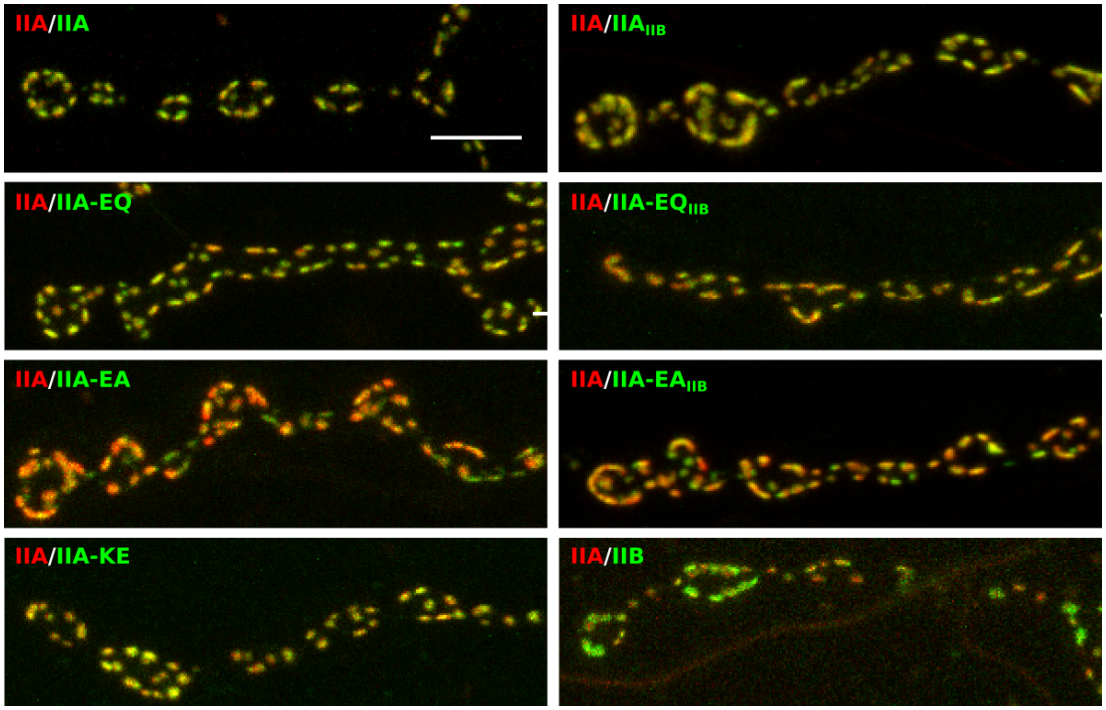

Figure 3.2. Accelerated gating dynamics change synaptic localisation of glutamate receptors. GluRIIA mutants and GluRIIB (labelled with GFP) were coexpressed with control wild type GluRIIA (labelled with RFP) in the gluRIIA^{null};gluRIIB^{null} background. Abbreviations used for receptors: IIA (GluRIIA), IIA$_{IIB}$ (GluRIIA$_{IIB}$), IIA-KE (GluRIIA-KE), IIA-EQ (GluRIIA-EQ), IIA-EQ$_{IIB}$ (GluRIIA-EQ$_{IIB}$), IIA-EA (GluRIIA-EA), IIA-EA$_{IIB}$ (GluRIIA-EA$_{IIB}$), IIB (GluRIIB). Abbreviation used to describe coexpressed receptors: */*. For instance IIA/IIA-EA means: GluRIIA and GluRIIA-EA were coexpressed. One representative NMJ (muscle 26/27) of each genotype is shown here. The IIA/IIA genotype, where no segregation is expected, was used as a reference point to estimate the segregation strength of the other genotypes "by eye". IIA/IIA$_{IIB}$: no segregation, IIA/IIA-KE: no segregation, IIA/IIA-EQ: weak or no segregation, IIA/IIA-EQ$_{IIB}$: weak segregation, IIA/IIA-EA: very strong segregation, IIA/IIA-EA$_{IIB}$: strong segregation, IIA/IIB: very strong segregation. Scale bar for all images, 5 μm. Images by Astrid Petzoldt.

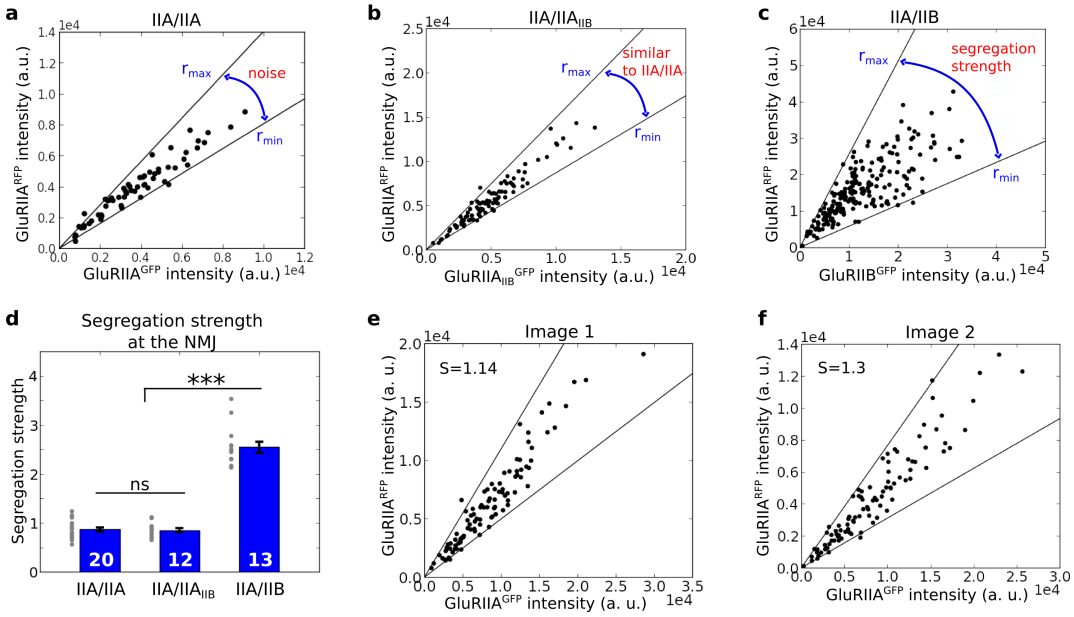

Figure 3.3. Quantifying the segregation strength. (a-c) The fluorescence intensity of the 1st and 2nd receptor at single PSDs is scattered against each other (each genotype one NMJ). r_{max} is the maximum and r_{min} is the minimum ratio that were estimated from five PSDs each. **(d)** The quantification shows that the segregation strength of IIA/IIA (S = 0.87 ± 0.04) and IIA/IIA$_{\text{IIB}}$ (S = 0.85 ± 0.04) does not differ significantly, whereas the IIA/IIB genotype exhibited a strong segregation between GluRIIA and GluRIIB (S = 2.55 ± 0.11). ns: not significant, *** P < 0.001, two-sided t-test. Dots are single measurements. Error bars represent mean ± SEM. **(e, f)** A single NMJ (muscle 26/27) of a IIA/IIA genotype was imaged twice in quick succession with the same settings. The larva was remounted into the imaging chamber before the second recording to include mounting variance. The quantification showed that the segregation strength between image 1 and image 2 had a relatively small deviation (0.16) when compared to the standard deviation (σ = 0.18) of the IIA/IIA genotype at the population level.

Confocal images of NMJs were processed as described in section (2.2). As expected, the measured segregation strength between GluRIIA and GluRIIB was significantly higher than in the control IIA/IIA genotype (Fig. 3.3a,c,d; IIA/IIA, S = 0.87 ± 0.04; IIA/IIB, S = 2.55 ± 0.11). The verification of this method showed that the segregation strength was reproducible, when the whole imaging procedure was repeated, which included the remounting of the larva into the imaging chamber (Fig. 3.3e,f).

Segregation strength scales with the accelerated gating dynamics

Using the new defined segregation parameter the segregation strength of the other genotypes can be quantified and compared to each other. As speculated from the images (Fig. 3.2), the fast- and very-fast-gating GluRIIA mutants (GluRIIA-EQ, GluRIIA-EA) showed significant segregation from control wild type GluRIIA (Fig. 3.4). Inter-

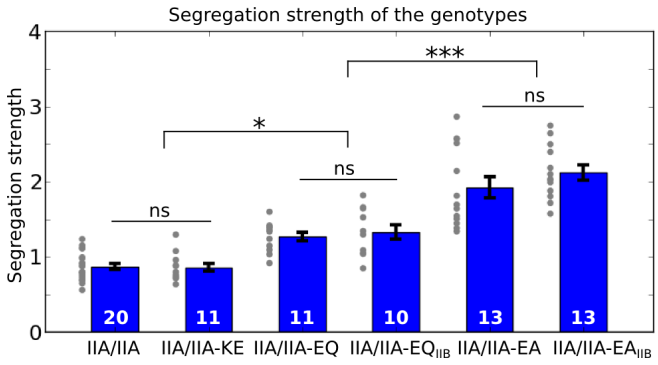

Figure 3.4. Subunit localisation is not mediated by the CTD. The segregation strength for each GluRIIA mutant was quantified (muscle 4 and muscle 26/27). The CTD-swap does not affect the segregation strength, whereas the point mutations accelerating the gating dynamics had a considerable effect on the segregation strength. IIA/IIA-EA$_{\mathrm{IIB}}$ = 2.12 ± 0.1, IIA/IIA-EA = 1.92 ± 0.14, IIA/IIA-EQ$_{\mathrm{IIB}}$ = 1.33 ± 0.1, IIA/IIA-EQ = 1.27 ± 0.06, IIA/IIA-KE = 0.86 ± 0.05, IIA/IIA = 0.87 ± 0.04. ns: not significant, * P < 0.05, *** P < 0.001, one way ANOVA with Tukey's multiple comparison post test. Dots are single measurements. Error bars represent mean ± SEM.

estingly, the CTD$_{\mathrm{IIB}}$ did not change the localisation characteristics of GluRIIA$_{\mathrm{IIB}}$ when compared to wild type GluRIIA. The segregation strength did not increase in comparison to the baseline (Fig. 3.3d). Also the exchange of the CTD of the other genotypes, GluRIIA-EA$_{\mathrm{IIB}}$ and GluRIIA-EQ$_{\mathrm{IIB}}$, did not change the segregation strength (Fig. 3.4). Taken together this indicates that the CTD does not mediate subunit localisation to PSDs. Moreover the quantitative segregation parameter showed that the slow-gating GluRIIA-KE did not segregate from GluRIIA. Therefore, its localisation on the single synapse level resembled that of GluRIIA. In particular, the segregation strengths of the genotypes differed significantly in the following order (mean ± SEM): IIA/IIA-EA$_{\mathrm{IIB}}$ (2.12 ± 0.1) ≈ IIA/IIA-EA (1.92 ± 0.14) > IIA/IIA-EQ$_{\mathrm{IIB}}$ (1.33 ± 0.1) ≈ IIA/IIA-EQ (1.27 ± 0.06) > IIA/IIA-KE (0.86 ± 0.05) ≈ IIA/IIA (0.87 ± 0.04).

In sum, these results revealed that by accelerating the gating dynamics of receptors, the *in vivo* synaptic localisation could be substantially changed. The very-fast-gating GluRIIA-EA had the strongest segregation phenotype, whereas the fast-gating GluRIIA-EQ had an intermediate segregation phenotype. Thus the segregation strength scaled with the gating dynamics of receptors. By changing the gating dynamics in the other direction (GluRIIA-KE), i.e. making it slower, however did not alter receptor localisation on the single synapse level.

3.3 GluRIIA mutants show distinct localisation during synaptic maturation

The results revealed the interesting fact that gating dynamics have a significant effect on receptor localisation. To understand this altered trafficking behaviour in more detail,

the fast- and very-fast-gating GluRIIA mutants are studied under the aspect of synaptic assembly and maturation.

3.3.1 Premature accumulation of fast- and very-fast-gating receptors

At the NMJ new synapses constantly form *de novo* and grow until they reach a mature and stable size (Rasse et al., 2005). This developmental process at the NMJ is tightly coordinated in time and space (Fouquet et al., 2009; Owald et al., 2012). Interestingly, the synaptic trafficking and localisation of GluRIIA during this developmental process, seems to be highly regulated. The entry of GluRIIA into PSDs is directly associated with the growth of PSDs (Rasse et al., 2005) and the expression level of GluRIIA is correlated with the number of PSDs (Sigrist et al., 2002). Furthermore, a study showed (Schmid et al., 2006) that receptors are essential for synaptic maturation. Thus, receptor trafficking and synaptic assembly and maturation are tightly linked to each other.

To find out, if the accelerated gating dynamics affects receptor localisation during synaptic maturation, the size of a PSD was used as an estimator for the maturity of a synapse. Small PSDs were considered as young and large PSDs were considered as old synapses. Therefore analysing the distribution of PSD size and receptor composition would yield information about the localisation preferences of the GluRIIA mutants with regard to the maturity of synapses. The analysis shows that the receptor composition of the control IIA/IIA genotype had, as expected, a uniform distribution, which was centred around the dashed midline (Fig. 3.5, IIA/IIA). The deviations from the midline, observed for single PSDs, are very likely due to noise in the experimental setup and in the biological system itself. The slow-gating GluRIIA-KE had a similar receptor distribution with regard to PSD size (Fig. 3.5, IIA/IIA-KE). PSDs were mostly uniformly centred around the dashed midline, which is indicated by the red line. In contrast, GluRIIA-EQ and GluRIIA-EA had a strong accumulation at small PSDs (Fig. 3.5, IIA/IIA-EQ and IIA/IIA-EA). However, with increasing PSD size this imbalance was resolved and the receptor composition became more uniform. Therefore these results suggest that fast- and very-fast-gating receptors are enriched in young and immature PSDs and that this enrichment is lost with the maturation of the PSDs.

Indeed, when the receptor composition was analysed *in vivo* over either 7h or 24h, it can be confirmed that young and immature PSDs are rich in fast- and very-fast-gating receptors (Fig. 3.6a,b; 24h new and 7h/24h new). Furthermore, PSDs that were previously enriched with GluRIIA-EA or GluRIIA-EQ, lost this enrichment over time. Resulting in an uniformly distributed receptor composition at 7h or 24h (Fig. 3.6a,b; compare 0h with 24 old and 7h/24h old). Moreover, a significant decrease in the segregation strength was observed for the IIA/IIA-EA genotype for "old" PSDs (Fig. 3.6c). This confirms that with synapse maturation the receptor composition becomes more balanced. Altogether, these results suggest that fast- and very-fast-gating receptors have a substantial coordination deficit in synaptic maturation. They over-accumulate at immature synapses.

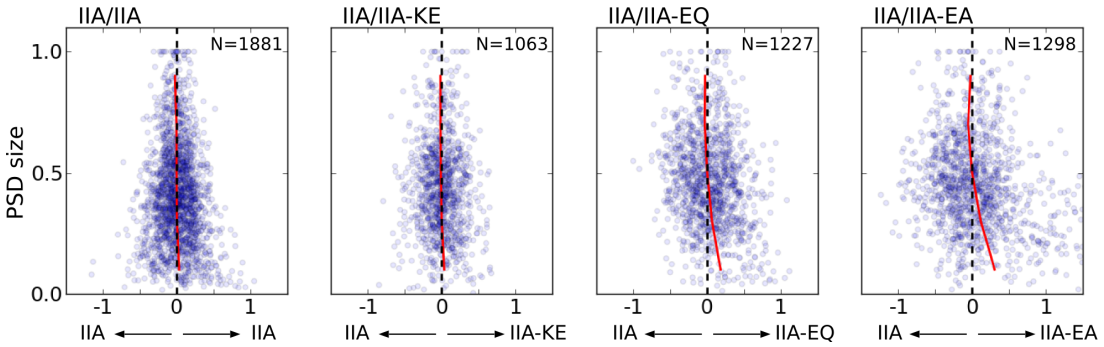

Figure 3.5. Receptor composition as a function of PSD size. The red line represents the average receptor ratio in a window length of 0.2 PSD size and the dashed midline represents equal receptor composition. The comparison of the wild type GluRIIA with the mutant receptors yields that small PSDs are preferentially occupied by receptors with fast-gating dynamics (GluRIIA-EA and GluRIIA-EQ), which is visualised by the red line bending rightwards for small PSDs. The receptor ratio is given as: $\log_2(\text{GluRIIA-X}^{\text{GFP}}/\text{GluRIIA}^{\text{RFP}})$. The receptor ratio distribution is centred at 0. IIA/IIA = 20 NMJs, IIA/IIA-KE = 11 NMJs, IIA/IIA-EQ = 11 NMJs, IIA/IIA-EA = 13 NMJs.

3.3.2 Very-fast-gating receptors are uncoupled from presynaptic assembly

Next the receptor localisation was analysed with regard to the presynaptic assembly state, since synapse assembly is a process, where pre- and postsynaptic proteins interact and accumulate in a temporally well-orchestrated way. The assembly state of the postsynaptic site can be accessed through the size of the receptor field and the quantity of receptors within. Presynaptically the assembly state can be accessed through the protein Bruchpilot, which is accumulated continuously in the synaptic maturation process (Schmid et al., 2008). Bruchpilot is a scaffolding protein at the active zone that is essential for efficient evoked glutamate release (Wagh et al., 2006; Kittel et al., 2006; Fouquet et al., 2009; Matkovic et al., 2013). Furthermore, it is a marker for synapses with a high probability of evoked release (Peled et al., 2014).

To directly investigate receptor localisation during synapse assembly, Bruchpilot was labelled with antibody in larval NMJs of the IIA/IIA-EQ and IIA/IIA-EA genotype (Fig. 3.7a,b). Each presynaptic active zone, represented by the Bruchpilot fluorescence signal, was manually connected to its corresponding PSD using Imaris (confocal images were processed as before in section 2.2). The size of the Bruchpilot puncta and the PSD were both three-dimensionally estimated from the volume of the fluorescence signals. The analysis of the obtained data revealed that Bruchpilot and PSD size were correlated (Fig. 3.7c,d). This is consistent with the fact that the pre- and postsynaptic sites are coupled during synaptic maturation and assembly. Furthermore, the postsynaptic accumulation of wild type GluRIIA was linked to the presynaptic accumulation of Bruchpilot. In both genotypes (IIA/IIA-EA and IIA/IIA-EQ), the density of GluRIIA has a high correlation to the density of Bruchpilot (Fig. 3.8b,c,e,f; r = 0.61 and r =

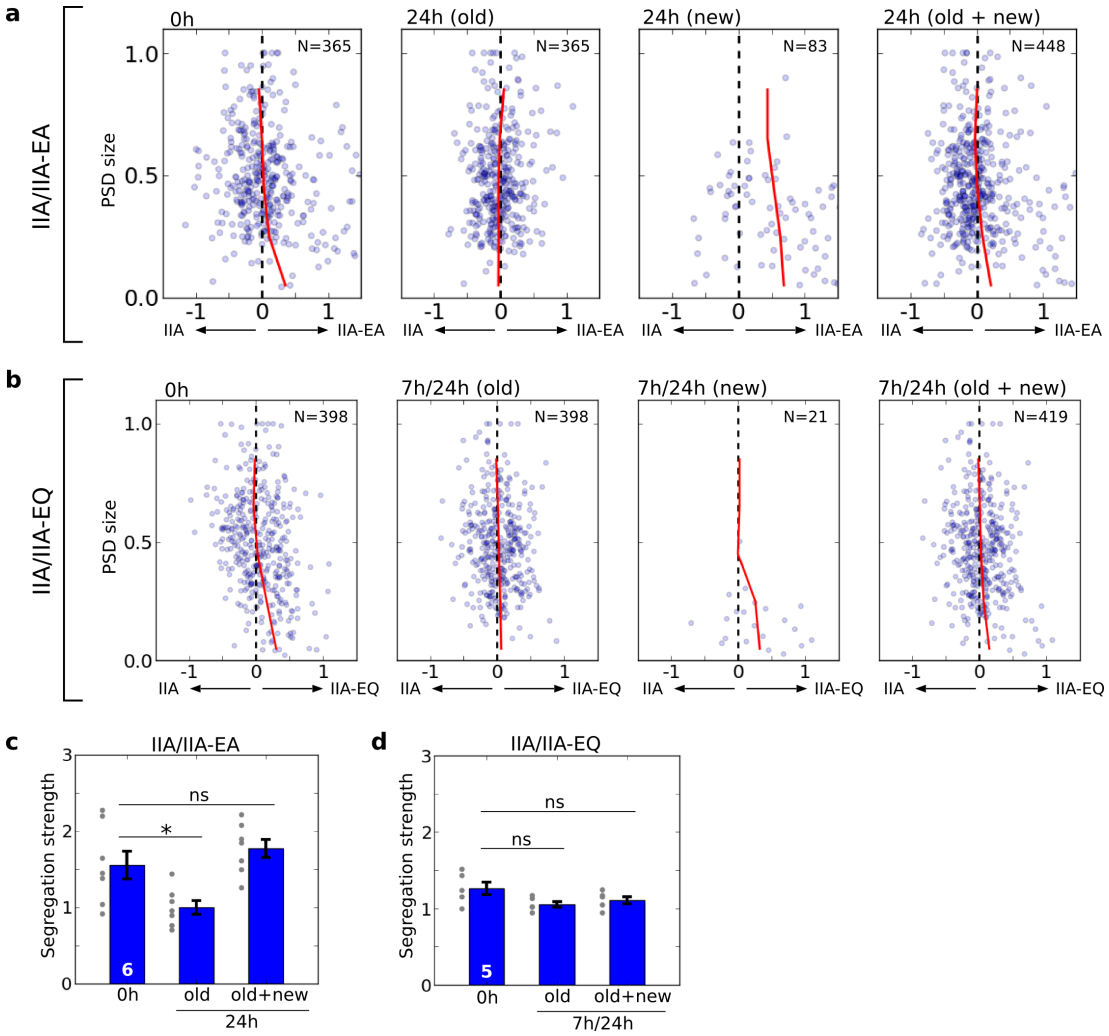

Figure 3.6. Time development of receptor composition and segregation strength. NMJs of muscle 26/27 were imaged *in vivo* over time as described previously by Schmid et al. (2008). Imaging by Astrid Petzoldt. PSDs were tracked manually in Imaris between two time points. PSDs reidentified at either 7h or 24h are termed as "old" PSDs, whereas PSDs that were imaged the first time at 7h or 24h are referred to as "new" PSDs. **(a, b)** Time development of receptor ratio with regard to PSD size. The red line indicates the average receptor ratio in a window length of 0.2 PSD size. Both GluRIIA mutants were enriched in small and young PSDs as indicated by the right shift of the red line for small PSDs at 24h or 7h/24h. The enrichment of GluRIIA-EA and GluRIIA-EQ in small PSDs was lost with the maturation of the PSDs (compare 0h with 24h and 7h/24h old). The receptor ratio is given as: $\log_2(\text{GluRIIA-X}^{\text{GFP}}/\text{GluRIIA}^{\text{RFP}})$. The receptor ratio distribution is centred at 0. IIA/IIA-EA: 6 NMJs, IIA/IIA-EQ: 5 NMJs. **(c, d)** Time development of the segregation strength. In the IIA/IIA-EA genotype, the segregation of "old" PSDs decreased significantly after 24h (0h vs 24h old), whereas the total segregation at 24h did not change (0h vs 24h old+new). No significant changes were observed for the IIA/IIA-EQ genotype. ns: not significant, * $P < 0.05$, paired t-test. Dots are single measurements. Error bars represent mean ± SEM.

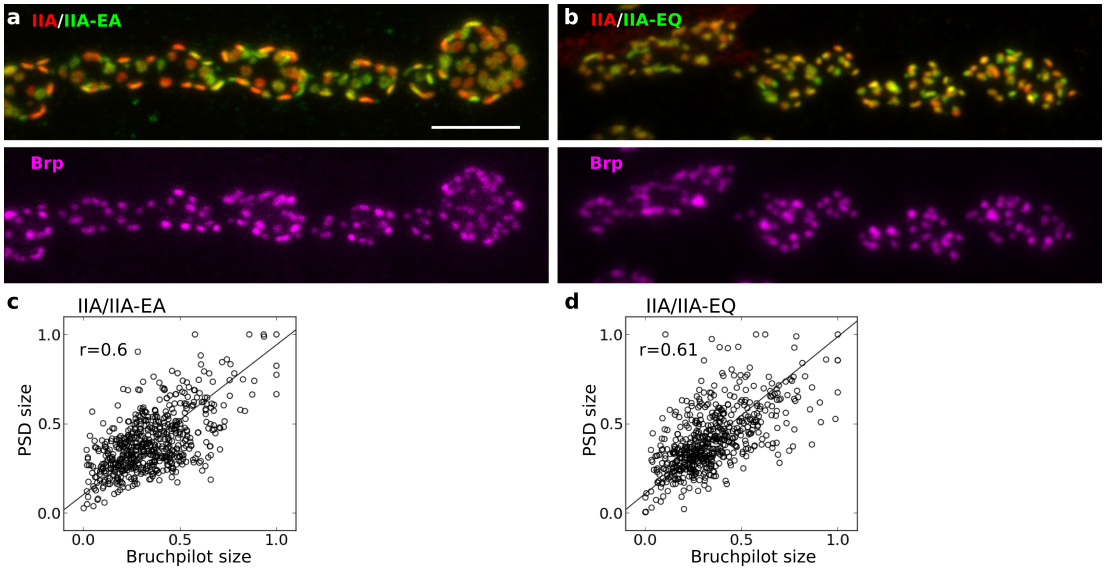

Figure 3.7. Assembly of pre- and postsynaptic sites is coupled. (a,b) NMJs (muscle 4) of the IIA/IIA-EA and IIA/IIA-EQ genotypes were stained with antibody for Bruchpilot. Scale bar for all images, 5 μm. Images by Astrid Petzoldt. **(c,d)** Size of Bruchpilot puncta is correlated with size of receptor field ($P < 0.001$ for both genotypes). IIA/IIA-EA: 583 PSDs from 4 NMJs, IIA/IIA-EQ: 571 PSDs from 4 NMJs.

0.71). Once again, this confirms the very well coordinated assembly process between pre- and postsynaptic sites.

Interestingly, the density of GluRIIA-EA was totally uncorrelated to the Bruchpilot density (Fig. 3.8a,c; r = 0.05). Suggesting that during synaptic assembly GluRIIA-EA loses the ability to match its own level to the assembly state of the presynaptic site. On the contrary, GluRIIA-EQ was still able to adjust its own level to the assembly state of the presynaptic site (Fig. 3.8d,f; r = 0.66).

3.3.3 Receptor segregation depends on evoked glutamate release

Until here the altered localisation of the GluRIIA mutants have been only described. However the mechanisms underlying the segregation have not been addressed. In order to have segregation in a system such as the NMJ, two requirements need to be fulfilled: first the receptors need to be different, and second the synapses need to be different. Obviously, GluRIIA and the GluRIIA mutants are different. On the other side, the synapses differ in their developmental stages. One property that is linked to the developmental stage of a synapse is its transmission property. Larger synapses do have more amounts of Bruchpilot deposited at the active zone. Therefore, larger synapses do have higher probabilities of evoked release, since a recent study linked high levels of Bruchpilot to high probabilities of evoked release (Peled et al., 2014). Thus, evoked glutamate release might be a parameter that is relevant for the segregation of receptors.

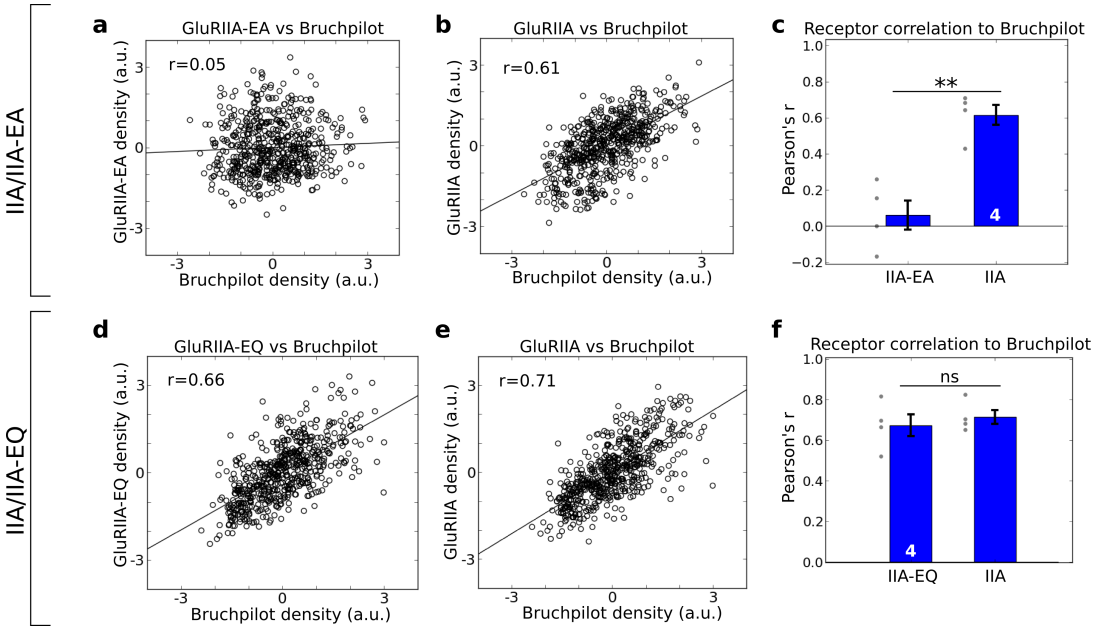

Figure 3.8. Very-fast-gating receptors are uncoupled from Bruchpilot accumulation. Receptor and Bruchpilot density were defined as the total fluorescence intensity in a PSD or Bruchpilot puncta divided by their volume. The correlation between receptor and Bruchpilot was measured using the Pearson's correlation coefficient (r). **(a)** No correlation of GluRIIA-EA (P = ns, 583 PSDs from 4 NMJs), **(b,e)** high correlation of GluRIIA (P < 0.001) and **(d)** high correlation of GluRIIA-EQ to Bruchpilot were observed (P < 0.001, 571 PSDs from 4 NMJs). In **(c,f)** the distribution and mean of the Pearson's correlation coefficient for IIA/IIA-EA and IIA/IIA-EQ is shown (4 NMJs each). Distribution of receptor and Bruchpilot densities were standardised. ns: not significant, ** P < 0.01, two-sided t-test. Dots are single measurements. Error bars represent mean ± SEM.

To test this hypothesis, evoked glutamate release was suppressed by the expression of tetanus toxin light chain (TNT) in a subset of motoneurons in the IIA/IIA-EA genotype. IIA/IIA-EA have been analysed since it exhibited the strongest segregation phenotype. Strikingly, confocal images of NMJs with TNT expression showed that the segregation between GluRIIA and GluRIIA-EA was reduced visually (Khorramshahi, 2012). Moreover, the analysis also revealed that the total synaptic expression level of GluRIIA-EA was decreased, whereas the wild type GluRIIA level was increased (Khorramshahi, 2012). Suggesting the existence of a homeostatic regulation that counteracts the suppression of evoked glutamate release by the preferred incorporation of slow-gating receptors to increase the postsynaptic response.

Here, the decrease in segregation strength was additionally quantitatively explored. Again, receptor composition of single PSDs from TNT and no TNT expressing NMJs were quantified as described in section (2.2). The receptor distribution with regard to PSD size had a much narrower distribution when TNT was expressed (Fig. 3.9a). The quantitative segregation parameter confirmed that the segregation strength in the

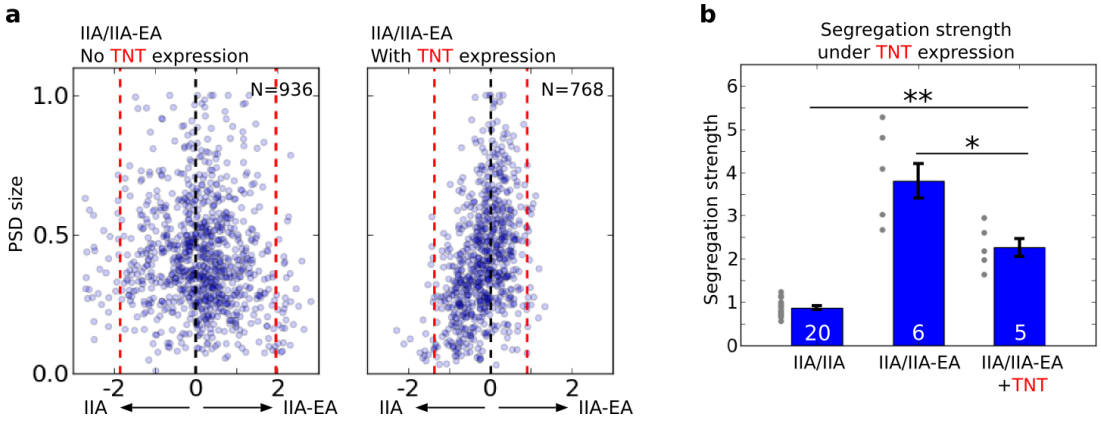

Figure 3.9. TNT expression reduces segregation strength. (a) The red dashed lines denote the average maximum (right line) and minimum (left line) receptor ratio of the analysed NMJs (no TNT: 6 NMJs, with TNT: 5 NMJs). Therefore the width of the area within the lines represents the segregation strength. As indicated by the red dashed lines, TNT expression considerably reduced the segregation between GluRIIA-EA and GluRIIA. The receptor ratio is given as: $\log_2(\text{GluRIIA-EA}^{\text{GFP}}/\text{GluRIIA}^{\text{RFP}})$. The receptor ratio distribution is centred at 0. **(b)** TNT expression reduced significantly the segregation strength. However, the segregation strength was still higher then in the control IIA/IIA genotype. * $P < 0.05$, ** $P < 0.01$, two-sided t-test. Dots are single measurements. Error bars represent mean ± SEM.

TNT expressing NMJs was significantly reduced (Fig. 3.9b). However, the segregation between GluRIIA and GluRIIA-EA was still larger than in the control IIA/IIA genotype. Therefore, segregation was not completely abolished by TNT expression. One possible explanation is that glutamate release from spontaneous vesicle fusions, which are not inhibited by TNT expression (Sweeney et al., 1995), are sufficient to establish receptor segregation.

3.4 Discussion

CTD does not mediate segregation between GluRIIA and GluRIIB

Until recently it has been a common view that the CTD of glutamate receptors plays a major role in receptor trafficking and localisation (Malinow and Malenka, 2002; Bredt and Nicoll, 2003). However, a recent study has cast doubt on the role of the CTD for receptor subunit localisation and trafficking in LTP (Granger et al., 2013).

Here the role of the CTD for receptor subunit localisation was tested at the NMJ, where two different glutamate receptor complexes exist that contain either the subunit GluRIIA or GluRIIB. The two different receptor subunits have distinct localisation and trafficking patterns (Schmid et al., 2008). The results here implicate that the CTD does not determine subunit localisation. The CTD-swap of GluRIIA for the CTD of GluRIIB (IIA/IIA_{IIB} genotype) had neither an effect on the segregation strength (Fig. 3.3d) nor on the receptor distribution with respect to PSD size (Fig. 3.5). In

addition, the CTD-swap of the various GluRIIA mutants had also no effect on the segregation strength (Fig. 3.4). Thus, the CTDs of GluRIIA and GluRIIB alone are not sufficient to mediate subunit localisation at the NMJ.

Gating dynamic as a new parameter in receptor localisation

To find new mechanisms that control receptor localisation, point mutations were introduced into GluRIIA to tune its gating dynamics by increasing or slowing down the desensitisation rate. Importantly, electrophysiological measurements of whole NMJs showed that the point mutations did change the gating dynamics of the receptors as predicted (Petzoldt et al., 2014). Strikingly, the tuned gating dynamics affected the localisation of the GluRIIA mutants. In particular, the localisation of GluRIIA-EA and GluRIIA-EQ were substantially altered on the single synapse level when compared to wild type GluRIIA (Fig. 3.2 and Fig. 3.4).

Moreover, gating dynamics can control receptor localisation during synapse maturation. GluRIIA-EA and GluRIIA-EQ accumulate at young, newly formed synapses earlier than wild type GluRIIA (Fig. 3.6). FRAP experiments also revealed that GluRIIA-EA has an increased surface mobility in comparison to wild type GluRIIA. This fact might explain the premature accumulation of GluRIIA-EA at young synapses, since the increased mobility allows GluRIIA-EA to find new synapses faster (Petzoldt et al., 2014).

Furthermore, GluRIIA-EA exhibited substantial defects regarding synapse assembly. The more Bruchpilot was deposited at the active zone, the more wild type GluRIIA was incorporated into the PSD. However, GluRIIA-EA failed to adjust its own level to the Bruchpilot level (Fig. 3.8). Therefore, gating dynamics is an essential parameter during synapse assembly. Accelerated gating dynamics can cause defects in the usually well-orchestrated assembly process between pre- and postsynaptic sites.

How can gating dynamics control receptor localisation?

Having revealed that gating dynamics influence receptor localisation, the next step is to understand the mechanism behind the gating-dynamic-dependent localisation. For this it is important to know that glutamate receptors at synapses exist not as isolated complexes, but instead are surrounded by many other proteins, which together form supra-complexes (Li et al., 2013). A subgroup of these proteins, called auxiliary subunits, can for example modulate trafficking, localisation and gating properties of receptors (Jackson and Nicoll, 2011). It is possible that the conformational state could determine how receptors interact with those proteins.

Here, the experiments revealed a starting point for future studies. Particularly interesting is the fact that evoked glutamate release is necessary for the strong segregation between GluRIIA-EA and GluRIIA (Fig. 3.9). Thus, it is likely that the conformational changes of a receptor upon glutamate binding might play an essential role in receptor localisation. As mentioned above, the conformation of a protein is important for the interaction to other proteins. Therefore, if the opening time of GluRIIA-EA is dras-

tically reduced, potentially existing protein interactions might be impaired that could be crucial for its localisation.

Recently, the first auxiliary subunit for glutamate receptors in *Drosophila*, called Neto, was revealed by comparative genomics (Kim et al., 2012; Kim and Serpe, 2013). Neto is essential for receptor clustering and synapse functionality and could therefore be a starting point to understand the interactome of glutamate receptors at the NMJ. Furthermore, in mammalians it was observed that presynaptic proteins can trans-synaptically interact with postsynaptic receptors and thereby modify their synaptic transmission (Zhang et al., 2010). Maybe the stability of a receptor subunit within the PSD is not only determined by the PSD itself, but also by signals that arrive from the trans-synaptic site. Therefore, potential presynaptic interaction partners should also be regarded in future studies.

Main conclusions

The CTD does not mediate subunit localisation of GluRIIA and GluRIIB. Gating dynamics tuned by point mutations affect receptor localisation during synaptic maturation and assembly. Very-fast-gating receptors are uncoupled from presynaptic assembly. Gating dynamics therefore should be considered in future models of receptor trafficking.

Chapter 4

Protein Levels between Neighbouring Synapses are Jointly Regulated

4.1 Introduction

In this chapter the hypothesis is tested if receptor localisation depends on the relative position on the axon of the motoneuron. This hypothesis is motivated by two publications from Isacoff's lab. They showed that the synaptic transmission properties at the *Drosophila* larval NMJ is location dependent (Guerrero et al., 2005; Peled and Isacoff, 2011). In the first publication they revealed that the transmission strength along the NMJ is heterogeneous. They were capable to resolve Ca^{2+} influx optically through glutamate receptors in response to single action potentials. Using this method they observed a transmission gradient along axonal branches. The transmission strength decreased linearly from distal boutons to proximal boutons (Fig. 4.1a).

In the second publication they analysed the release probability of multiple synapses at the NMJ simultaneously with single-vesicle resolution (Fig. 4.1b). Under basal conditions, i.e. stimulation at low frequency (0.06 Hz), they observed that half of the synapses have only a very low release probability (< 0.01). Furthermore, they showed that distal boutons have a higher proportion of synapses with high release probability, which is consistent with distal boutons having the highest transmission strength.

In these two publications, however, no molecular counterparts were found that could potentially mediate the transmission gradient. An obvious question is whether or not the distribution of synaptic proteins follow similar spatial patterns. Particularly interesting is the spatial distribution of the receptor subunits GluRIIA and GluRIIB. The receptor composition could determine the transmission strength of a PSD, since GluRIIB desensitises about ten times faster than GluRIIA (DiAntonio et al., 1999). Therefore it is possible that the transmission gradient could be explained by a shift of the PSD receptor composition towards GluRIIA in distal boutons. Also of interest is Bruchpilot (Brp), a presynaptic protein, which is a component of the presynaptic

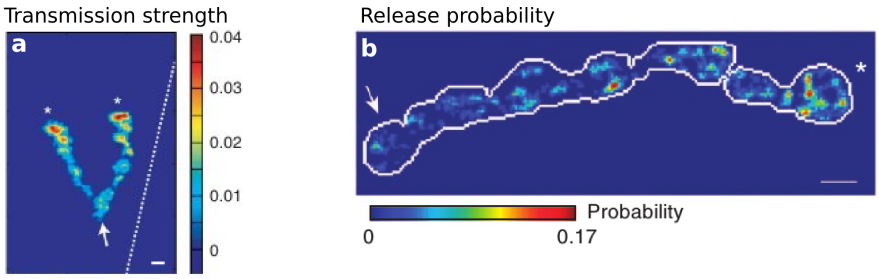

Figure 4.1. Synaptic transmission at the NMJ is location dependent. (a) Distal boutons (marked by asterisks) are stronger in transmission strength than proximal boutons (marked by arrow). The white dashed line represents the muscle border. Scale bar, 8 μm. (Modified from Guerrero et al., 2005). **(b)** Release probability map of an NMJ. In the distal bouton the proportion of high release probability sites is higher than in the proximal bouton. Scale bar, 5 μm. (Modified from Peled and Isacoff, 2011).

release machinery that plays an important role in efficient evoked glutamate release (Kittel et al., 2006; Fouquet et al., 2009; Matkovic et al., 2013). Thus it is possible that the amount of Bruchpilot at distal boutons is increased compared to proximal boutons.

4.2 Synaptic proteins are enriched in distal boutons

To systematically study the spatial distribution of Bruchpilot and receptor composition at the NMJ, the same approach as in chapter (2) was used. GluRIIA and GluRIIB were genetically tagged to RFP and GFP, respectively, and expressed in a gluRIIA^{null};gluRIIB^{null} background (Schmid et al., 2008). Additionally, larval NMJs (muscle 4) were stained for the protein Bruchpilot. The experimental part and the imaging of the larval NMJs were performed by Astrid Petzoldt (Fig. 4.2a-d). Subsequent image processing was conducted as described in section (2.2). Bruchpilot puncta were processed the same way as PSDs. Hereafter Bruchpilot puncta are referred to as presynaptic active zones. A software (NMJ viewer 1.0) in python was specifically written to visualise the Bruchpilot level and the receptor composition in space using a colour code that goes from blue over white to red. For instance in (Fig. 4.2e) red circles represent active zones with high Bruchpilot densities, while blue circles represent active zones with low Bruchpilot densities. In (Fig. 4.2f) red circles indicate PSDs enriched in GluRIIB, whereas blue circles indicate PSDs enriched in GluRIIA.

Besides the visual analysis of synaptic proteins in space, a quantitative approach was needed to test if gradients along the NMJ exist. Therefore a similar approach was used that resembles the one also applied in (Guerrero et al., 2005; Peled and Isacoff, 2011). PSDs were grouped according to their bouton location into three groups: proximal, middle and distal. For each group the average value of interest (e.g. Bruchpilot density) was calculated and then divided by the overall average value. In this way the existence of a gradient along the three groups can be tested.

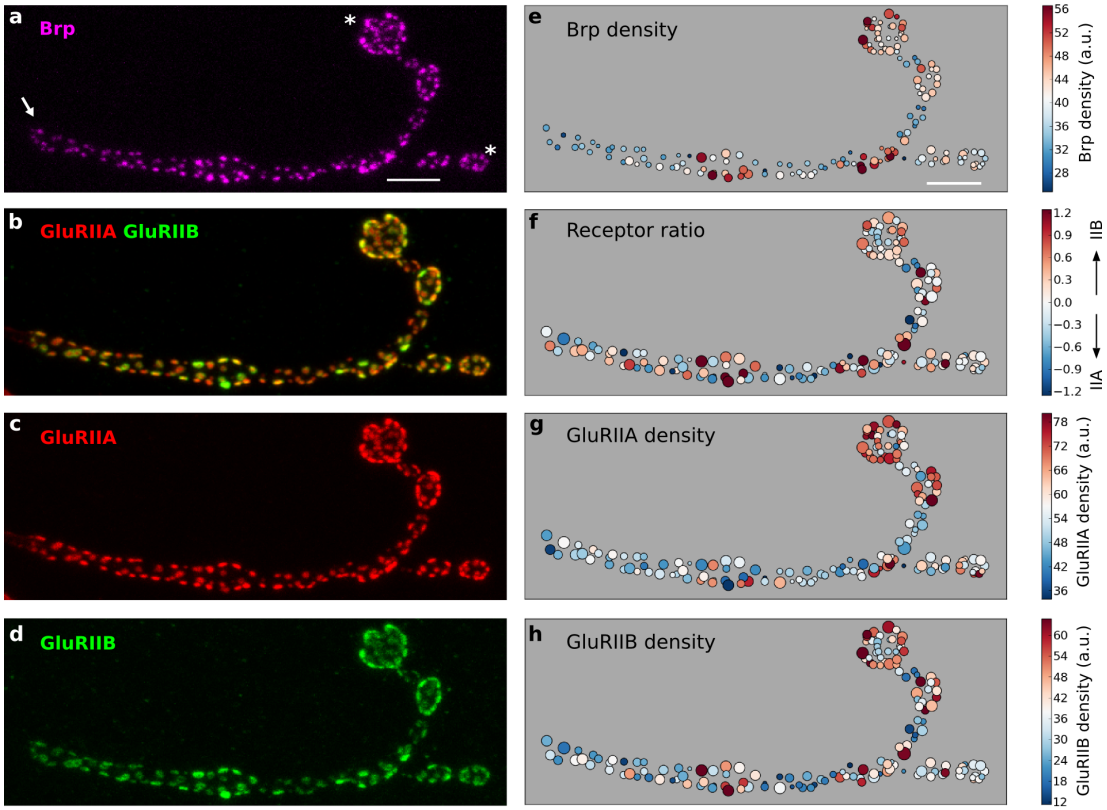

Figure 4.2. Spatial distribution of Bruchpilot, GluRIIA and GluRIIB. (a-d) Confocal images of an NMJ (muscle 4) expressing $\text{GluRIIA}^{\text{RFP}}$ and $\text{GluRIIB}^{\text{GFP}}$. Bruchpilot was labelled with antibody. The distal boutons are marked by asterisks, the proximal bouton is marked by an arrow. **(e-h)** The circle size represents either the size of the Bruchpilot puncta or the size of the receptor field. It seems that Bruchpilot, GluRIIA and GluRIIB are enriched in distal boutons, whereas the receptor ratio does not show any obvious spatial patterns. The receptor ratio is given as: $\log_2(\text{GluRIIB}^{\text{GFP}}/\text{GluRIIA}^{\text{RFP}})$. Scale bar for all images, $5\,\mu m$. Confocal images were taken by Astrid Petzoldt.

Active zones in distal boutons have high Bruchpilot densities

The Bruchpilot density of each active zone was extracted from the confocal image (Fig. 4.2a) and was then visualised in space using the software "NMJ viewer 1.0". The Bruchpilot density was calculated the same way as the receptor density (see section 2.2). Interestingly, the spatial distribution of Bruchpilot at the NMJ is heterogeneous and shows a high degree of order (Fig. 4.2e). It seems that active zones with similar Bruchpilot density cluster together in space. Furthermore, it appears that high-density Bruchpilot active zones (red circles) are more likely to be located in larger boutons, while low-density Bruchpilot active zones (blue circles) are more likely to be located in smaller (intermediate) boutons. In other words, these two groups of active zones seem to segregate in space. The next section specifically addresses how the segregation or the

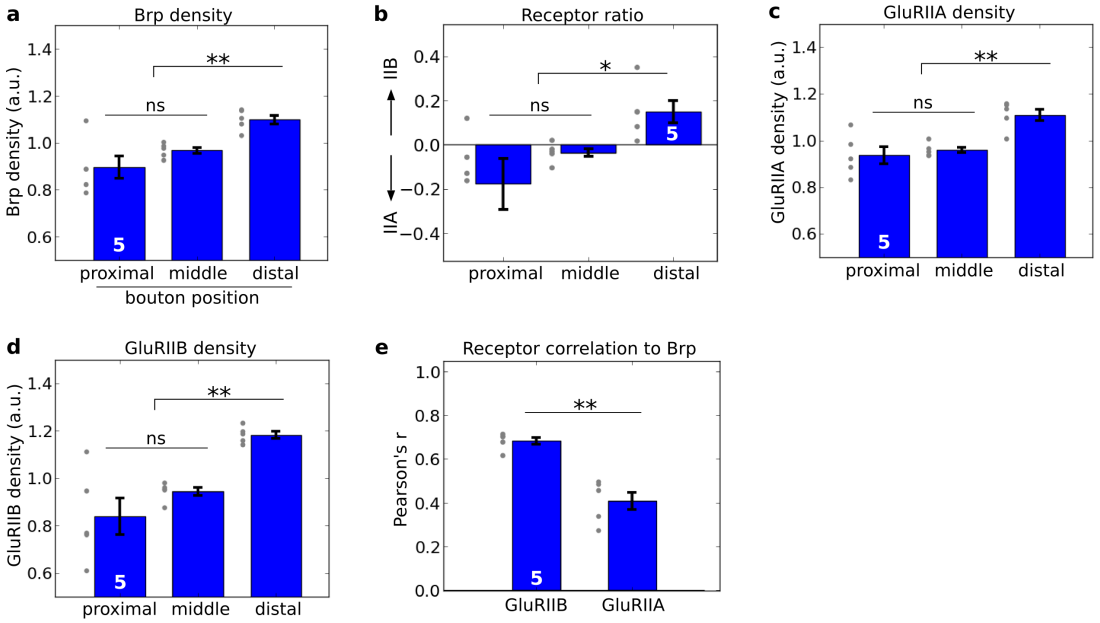

Figure 4.3. Bruchpilot, GluRIIA and GluRIIB are enriched in distal boutons. **(a-d)** The densities of Bruchpilot, GluRIIA and GluRIIB are location dependent. They are significantly higher in distal boutons than in middle or proximal boutons. Furthermore, the receptor composition is shifted towards GluRIIB in distal boutons. **(e)** The densities of GluRIIA and GluRIIB are correlated to the density of Bruchpilot on a single synapse level. N = 5 NMJs. ns: not significant, * $P < 0.05$, ** $P < 0.01$, two-sided t-test. Dots are single measurements. Error bars represent mean ± SEM.

correlation of Bruchpilot density in space can be quantified. In addition, quantification shows that active zones in distal boutons are enriched in Bruchpilot (Fig. 4.3a). Since Bruchpilot is directly involved in efficient evoked glutamate release (Kittel et al., 2006), the results here suggest that high Bruchpilot density at active zones might directly account for the increased release probabilities observed in distal boutons.

PSDs in distal boutons have high receptor densities

Next, the receptor composition of PSDs was analysed in space. It is conceivable that the transmission gradient (Fig. 4.1a) is mediated by a gradient of receptor composition, where GluRIIA is enriched in distal boutons and GluRIIB in proximal boutons. However, the spatial distribution of the receptor ratio shows no apparent gradient nor spatial patterns at all (Fig. 4.2f). Unexpectedly, the quantification revealed that the receptor composition in distal boutons is shifted towards GluRIIB (Fig. 4.3b). This seems to be in contradiction to the fact that GluRIIB desensitises about ten times faster than GluRIIA and thus has a smaller charge flow. However, on the other hand it is possible that the total amount of receptors is increased without changing the receptor composition of a PSD. Therefore, the density of receptors along the NMJ was analysed.

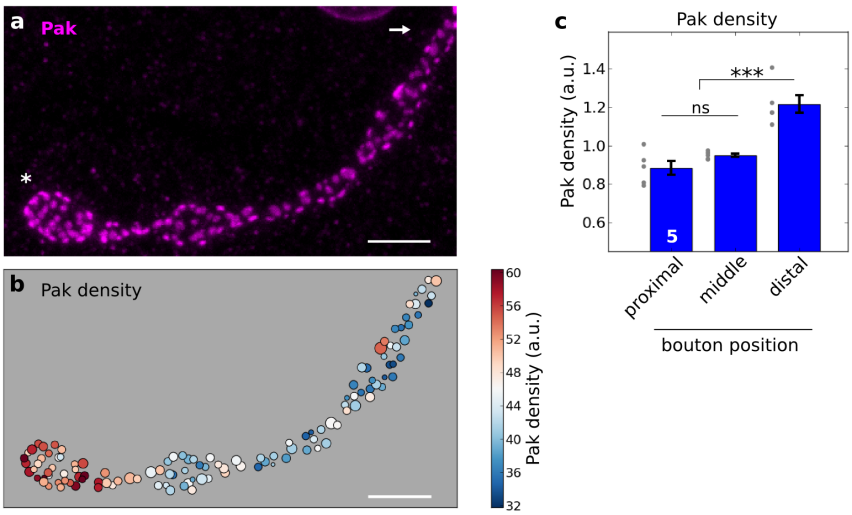

Figure 4.4. The density of Pak is in distal boutons significantly higher. (a) Confocal image of an NMJ (muscle 4) from the genotype IIA/IIA-EA, where Pak was labelled with antibody. The distal bouton is marked by an asterisk, the proximal bouton is marked by an arrow. Confocal image was taken by Astrid Petzoldt. **(b)** The spatial distribution of Pak density is shown. **(c)** Pak is significantly enriched in distal boutons (5 NMJs). ns: not significant, *** $P < 0.001$, two-sided t-test. Dots are single measurements. Error bars represent mean ± SEM. Scale bar for all images, 5 μm.

Strikingly, the densities of GluRIIA and GluRIIB show similar spatial patterns as the Bruchpilot density (Fig. 4.2g,h). They are enriched in the same boutons and even at the same synapses as correlation measurements show (Fig. 4.3e). However, they seem not to exhibit the same degree of order in space, as can be seen for Bruchpilot (see next section for a quantitative comparison).

Quantification along the NMJ confirms that the densities of GluRIIA and GluRIIB are indeed significantly higher in distal boutons. Therefore, it is likely that the increased number of receptors at distal boutons mediate the high transmission strength observed in the publication of Guerrero et al. (2005). However, no gradient could be statistically proven here, possibly due to the small sample size (5 NMJs here, Guerrero et al. (2005) used 34 NMJs). Some example NMJs from other genotypes (IIA/IIA, IIA/IIA-KE see Fig. 3.2 for description of the genotypes) are shown in Tab. (4.1), where gradients of GluRIIA are clearly visible and similar to those observed by Guerrero et al. (2005). Nonetheless, it should also be noted that not all NMJs exhibited clear gradients.

The density of Pak, a cytosolic protein, is increased in distal boutons

The results show that synapses located in distal boutons compared to synapses in proximal boutons have higher densities of Bruchpilot, GluRIIA and GluRIIB. This raises the question whether synaptic proteins are in general enriched in distal boutons. Here, this hypothesis was tested for another synaptic protein called p21-activated kinase

Table 4.1. Transmission strength and receptor density have similar spatial patterns. Four typical spatial patterns of transmission strength observed in Isacoff's lab are similar to spatial patterns found here for GluRIIA density. Distal boutons are marked by asterisks. Proximal boutons are marked by arrows. Scale bar, 8 μm (transmission strength), 5 μm (receptor density). Images for transmission strength are modified from Guerrero et al. (2005). NMJs are from the following genotypes (top to bottom): IIA/IIA, IIA/IIA, IIA/IIA-KE, IIA/IIA-KE.

Transmission strength	Correspondence	Receptor density
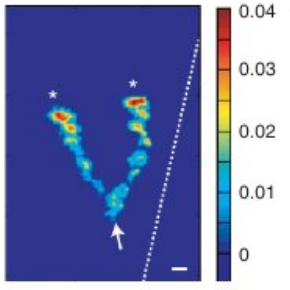	Gradients of transmission strength and receptor density are not only observed for simple but also for complex branching patterns.	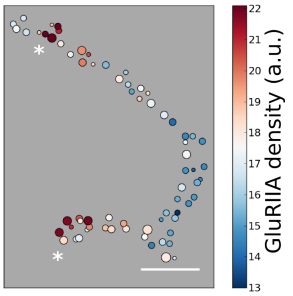
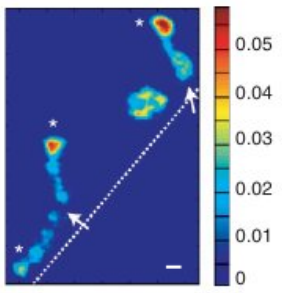	Different branches from the same NMJ can have different absolute transmission strengths and receptor densities.	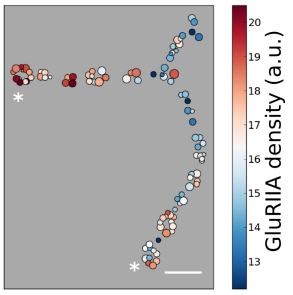
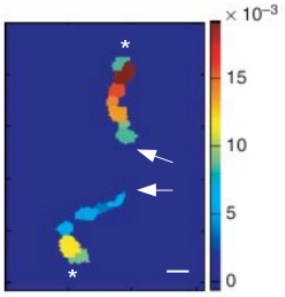	Transmission strength and receptor density of budding boutons at the end of a branch are weaker.	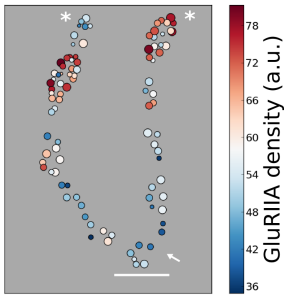
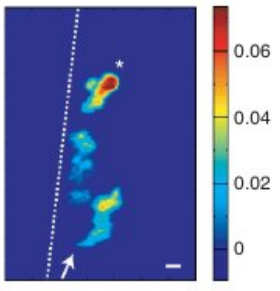	Boutons located on the proximal side of a sharp kink have higher transmission strength and receptor density than boutons following it.	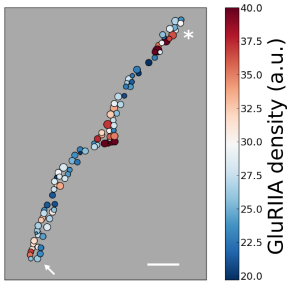

(Pak). Pak is a serine threonine kinase which localises to the PSD and controls GluRIIA abundance (Sone et al., 2000; Albin and Davis, 2004).

Confocal images of Pak puncta at NMJs (Fig. 4.4a) were processed the same way as PSDs (see section 2.2). The analysis shows that the density of Pak is also highly heterogeneous (Fig. 4.4b). Pak seems to exhibit the same degree of order as Bruchpilot. Quantification confirms that the density of Pak is significantly higher in distal boutons than in proximal boutons (Fig. 4.4c). Interestingly, Pak is a cytosolic protein which has a relatively fast turnover rate compared to GluRIIA (Rasse et al., 2005). Thus, the amount of Pak has to be linked to some structural components at the PSD, which control the abundance of Pak. All in all, more synaptic proteins need to be quantified to test if in general proteins are enriched at synapses in distal boutons.

4.3 Synaptic protein levels are regulated in spatial clusters

The motivation of this section is to introduce a spatial parameter to describe the spatial distribution of receptors and other synaptic proteins in a more general way. Using this more general description it will be possible to elucidate the relation of GluRIIA and GluRIIB on the level of single synapses (see next chapter).

The results above suggest that Bruchpilot and glutamate receptors differ in their degree of order in space. It appears that the spatial distribution of Bruchpilot is more regular or less "noisy" (compare Fig. 4.2e with Fig. 4.2g and h). The clusters of synapses with similar Bruchpilot densities are clearer and larger. In other words, Bruchpilot seems to be better correlated in space than GluRIIA or GluRIIB or the receptor ratio. Here, a quantitative parameter for the correlation in space is introduced. This parameter allows the distinction between random spatial distributions without any correlations and spatial distributions with correlation in space. Additionally, it is possible to measure the degree of spatial correlation, so that the spatial distribution of Bruchpilot and the receptors can be quantitatively compared.

4.3.1 Moran's I: A measure for spatial correlation

Correlation in space can be quantified using either the spatial autocorrelation coefficient Moran's I or Geary's C (Sokal and Oden, 1978). Since Moran's I is the more common one, it was used here, although Geary's C yielded similar results. Moran's I was introduced by P. A. P. Moran in 1950 (Moran, 1950) and it is defined for a given spatial distribution X as:

$$I(X) = \frac{N}{\sum_{ij} w_{ij}} \frac{\sum_{ij} w_{ij}(X_i - \bar{X})(X_j - \bar{X})}{\sum_i (X_i - \bar{X})^2} \tag{4.1}$$

where N is the total number of spatial units (e.g. PSDs), X_i and X_j are the attributes of interest (e.g. receptor density), $\bar{X}$ is the mean of the attribute and w_{ij} is the weight

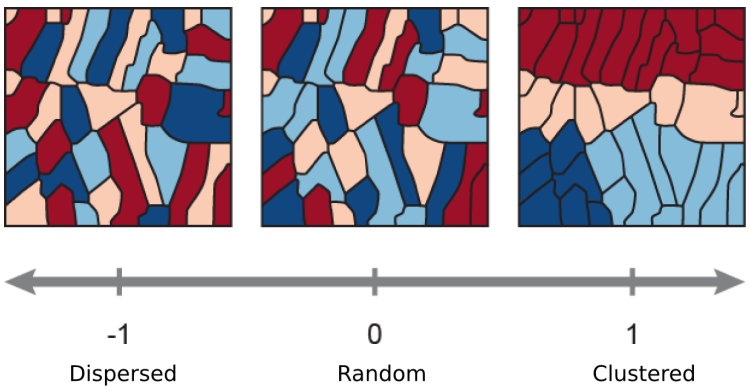

Figure 4.5. Quantifying spatial correlation with Moran's I. Moran's I ranges from 1 to -1, where 1 indicates a clustered and -1 a dispersed distribution in space. The different areas on the map represent the spatial units, whereas the colour represents the values of the attribute.

between the spatial units i and j. In general the weights determine the structure of the spatial data, i.e. they contain a distance measure between the spatial units. The next paragraph will elaborate more on the weights and how they were chosen for the NMJ. Moran's I varies from -1 to 1, whereas -1 indicates a dispersed and 1 a clustered distribution (Fig. 4.5). If no spatial correlation is present, Moran's I approaches 0 for large sample sizes. The significance of Moran's I can either be calculated analytically or empirically. However for the analytical solution the assumption of a normally distributed population has to be made (Sokal and Oden, 1978).

Choosing the weights for the NMJ

The last step before Moran's I can be applied to the NMJ, is the choice of appropriate weights. For each pair of PSDs or active zones a weight has to be defined that is related to their distance in space. Generally the weights should get smaller the further away the PSDs or active zones are from each other. There are several possibilities to define the weights (Sokal and Oden, 1978; Rey and Anselin, 2007). For instance the gravity distance can be used to calculate the weights. The weights are then defined as $1/d^2$, whereas d is the distance between two spatial units. When analysing certain spatial relationships, one can even disconnect two spatial units by setting the weight to 0. Depending on the particular problem some weight definitions are more suitable than others.

At a first glance, the gravity distance seems to be appropriate to define the weights between PSDs or active zones. However, the NMJ exhibits complex branching patterns, where different branches exist next to each other in space. Therefore, it is possible that two PSDs are next to each other although they belong to different branches. In other words, the gravity distance does not always represent the distance along a branch. Thus to avoid these difficulties, the nearest neighbour definition was used to define the weights. Each PSD or active zone was only connected to its nearest neighbour by

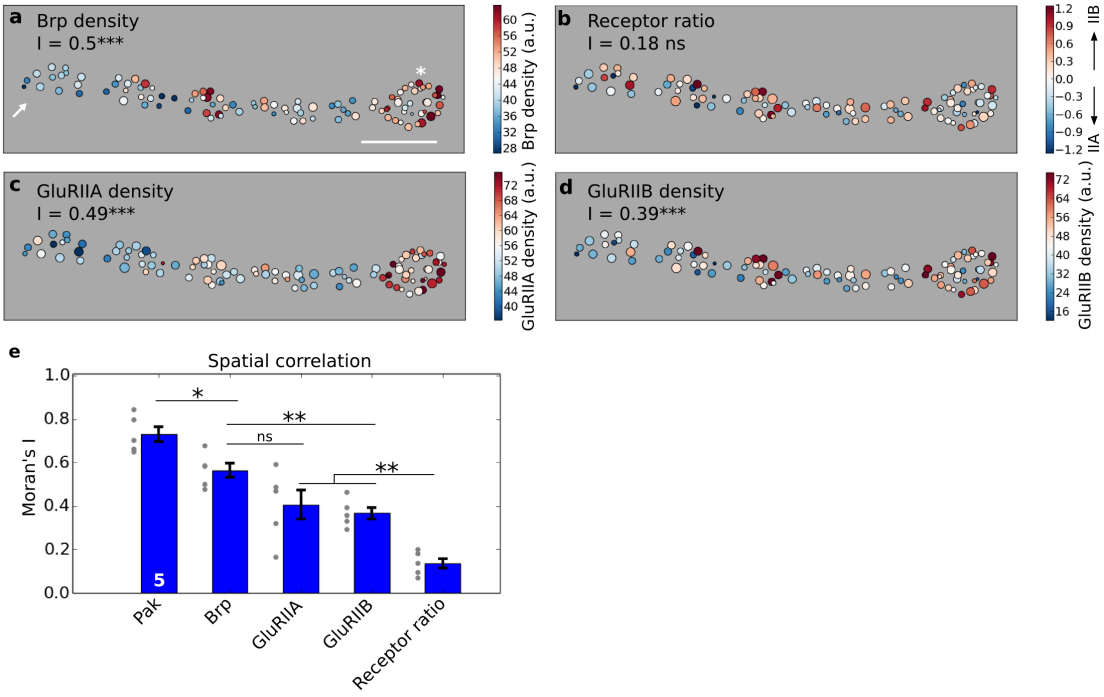

Figure 4.6. The quantity of synaptic proteins is correlated between synapses in space. **(a-d)** Degree of spatial correlation was quantified by Moran's I for the Bruchpilot density, receptor ratio, GluRIIA density and GluRIIB density. **(e)** The spatial correlation of Bruchpilot, receptor ratio, GluRIIA and GluRIIB were calculated from NMJs of IIA/IIB genotype. Pak data are from NMJs of IIA/IIA-EA genotype. Spatial correlation of Bruchpilot is significantly higher than GluRIIB density and receptor ratio. Pak has the highest spatial correlation. ns: not significant, * $P < 0.05$, ** $P < 0.01$, *** $P < 0.001$, two-sided t-test. Dots are single measurements. Error bars represent mean ± SEM. Scale bar for all images, 5 μm.

setting the weight to 1. The remaining weights were set to 0. In this way the diverse structures of NMJs have less influences on the quantification.

4.3.2 Neighbouring synapses have similar protein levels

NMJs from last section are reanalysed here using Moran's I. As discussed above, the nearest neighbour definition was applied to choose the weights between the synapses. The python package "PySAL v1.4.0" (www.pysal.org) was used to calculate Moran's I. The significance of Moran's I for a spatial distribution was calculated empirically. For instance, the Moran's I value of 0.5 for the spatial distribution of Bruchpilot is unlikely to come from a random spatial distribution (Fig. 4.6a). It is highly significant ($P < 0.001$). Whereas the Moran's I value of 0.18 for the receptor ratio is not significant (Fig. 4.6b). Thus the low degree of spatial correlation might just be due to chance. On the contrary, the densities of GluRIIA and GluRIIB show highly significant spatial correlations (Fig. 4.6c,d).

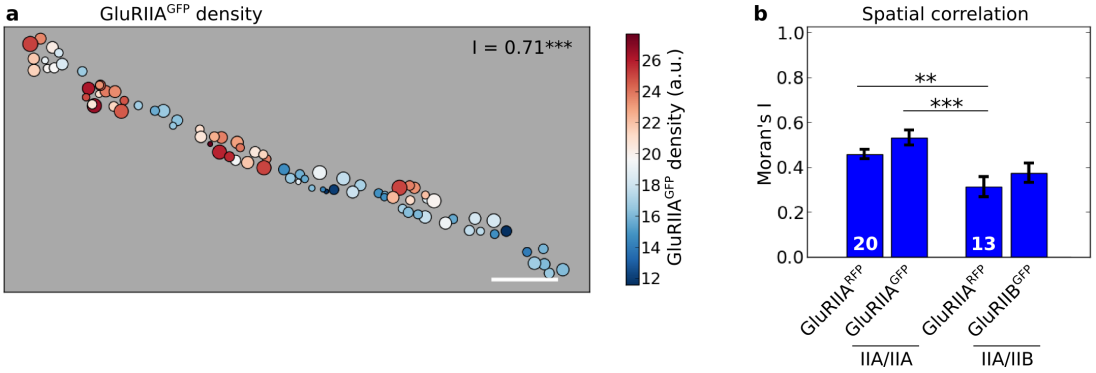

Figure 4.7. GluRIIB decreases the spatial correlation of GluRIIA. (a) In the IIA/IIA genotype, where no GluRIIB is present and where two copies of GluRIIA were expressed (labelled with GFP and RFP, respectively), GluRIIA has a high degree of spatial correlation. Scale bar , 5 μm. **(b)** Quantification revealed that the spatial correlation of GluRIIA is significantly smaller when GluRIIB is coexpressed. Compare GluRIIA in the IIA/IIA genotype with GluRIIA in the IIA/IIB genotype. ** $P < 0.01$, *** $P < 0.001$, two-sided t-test. Dots are single measurements. Error bars represent mean ± SEM.

Quantification on the population level confirms that there are differences in the degree of spatial correlation (Fig. 4.6e). Bruchpilot has as expected a high spatial correlation and the receptor ratio has the lowest spatial correlation. The spatial correlation of GluRIIA and GluRIIB lies in between. Although not visually apparent Pak has a significant higher spatial correlation than Bruchpilot (Fig. 4.6e). Altogether these results confirm the observation that pre- and postsynaptic protein levels between neighbouring synapses are correlated. Thus the amount of proteins is not regulated on a single synapse level, but is regulated jointly between adjacent synapses.

4.3.3 GluRIIB influences the synaptic localisation of GluRIIA

Here a surprising observation was made that motivates the analysis of the next chapter. There seems to be systematical differences between the genotypes with regard to the degree of spatial correlation. The spatial correlation of GluRIIA in the IIA/IIA genotype, where no GluRIIB is expressed, appears to be more prominent than in the IIA/IIB genotype (compare Fig. 4.2g with Fig. 4.7a). Indeed, quantification shows that the spatial correlation of GluRIIA in the IIA/IIA genotype is significantly higher than in the IIA/IIB genotype (Fig. 4.7b). Therefore it is possible that the presence of GluRIIB alters the localisation of GluRIIA on the level of single synapses. The next chapter resolves the discrepancies between the different genotypes and also proposes a model why the spatial correlation of GluRIIA decreases in the presence of GluRIIB.

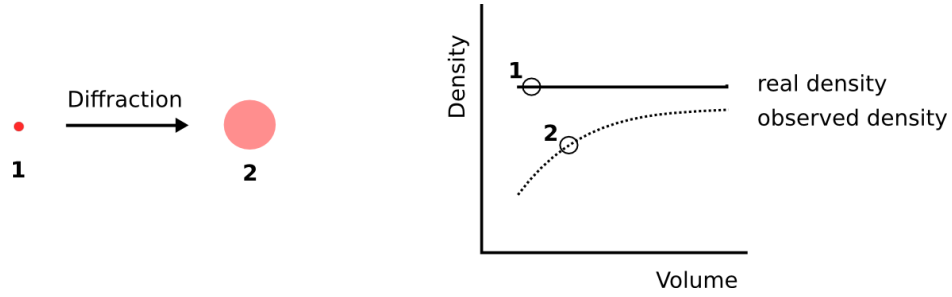

Figure 4.8. Effect of diffraction limited resolution on the measurement of protein densities. Diffraction causes small synapses to appear larger, while the fluorescence intensity does not change. As a consequence the observed density is falsely smaller (compare 1 vs 2).

4.3.4 Different protein densities are not caused by diffraction artefacts

Last, the issue has to be addressed whether different protein densities exist or are caused by artefacts, since the size of a synapse ($\sim 0.3\,\mu m^2$, Atwood et al. 1993) lies in the magnitude of the resolution limit of the microscope ($\sim 0.25\,\mu m$ lateral). Diffraction causes small synapses to appear larger and thus decreasing its density (Fig. 4.8). It is therefore necessary to check if the different protein densities simply reflect the size of a synapse. Based on the previous results this would mean that large synapses are primarily located in distal boutons and small synapses are located in proximal boutons. Or large synapses cluster together and small synapses cluster together in space. Here, the spatial distributions of active zone size (Bruchpilot size) and PSD size were analysed (Fig. 4.9a,b). If the different densities are mainly caused by the diffraction artefact, then the spatial correlation of active zone size and PSD size should be similar to that of Bruchpilot, GluRIIA and GluRIIB. However the quantification revealed that neither active zone size nor PSD size show spatial correlation in space (Fig. 4.9c). Thus it is very likely that different protein densities exist at the NMJ.

4.4 Discussion

Receptor localisation depends on the relative position on the axon

In order to find molecular candidates that mediate increased synaptic transmission and release probability in distal boutons (Fig. 4.1), the spatial distributions of Bruchpilot, GluRIIA and GluRIIB along the NMJ were extracted from confocal images (Fig. 4.2a-d) and analysed. The visualisation of their densities revealed that synaptic proteins are not distributed randomly across the NMJ but show spatial orders (Fig. 4.2e-h). Quantification showed that synaptic proteins are enriched in distal boutons (Fig. 4.3), i.e. synapses located in distal boutons have high densities of Bruchpilot, GluRIIA and GluRIIB. Moreover, some spatial patterns of GluRIIA density had strong similarities to patterns of transmission strength (Tab. 4.1).

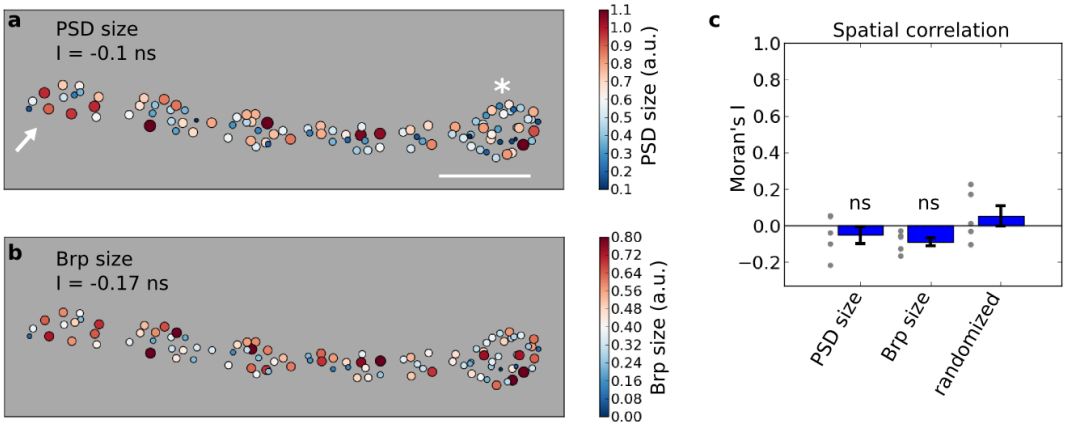

Figure 4.9. Different protein densities are not caused by the diffraction limited resolution. (a-b) Spatial distribution of PSD and active zone size for an NMJ (muscle 4). Both spatial distributions do not exhibit spatial correlations. Scale bar for all images, 5 μm. **(c)** On the population level, the spatial correlation of PSD and active zone size cannot be distinguished from randomised distributions. Thus potential diffraction artefacts cannot explain the spatial correlation of protein densities. ns: not significant, two-sided t-test. Dots are single measurements. Error bars represent mean ± SEM.

However, in the study by Guerrero et al. (2005, see supplementary Fig. 2) no correlation was found between transmission strength and receptor density. Furthermore, in the study by Peled and Isacoff (2011, see supplementary Fig. 6a,b) the Bruchpilot density in wild type larva was not significantly higher in distal boutons. One possible reason to explain these discrepancies is that they used a two dimensional approach to quantify the Bruchpilot and receptor densities. Here, a three dimensional approach was used for quantification (see section 2.2). The three dimensional approach is more precise since the projection onto a two dimensional plain inevitably leads to an information loss.

In summary, two conclusions can be drawn from these results. First, high densities of Bruchpilot might directly account for increased release probabilities and high transmission strength could be mediated by high receptor densities. This is in good agreement with a recent study, where it was shown that the Bruchpilot level was correlated with release probability (Peled et al., 2014). Second, receptor localisation is affected by the relative position on the axon. Thus future studies of receptor trafficking should take into account where a synapse is located, since the location does affect the receptor quantity.

Synapses at the NMJ are regulated in spatial clusters

Interestingly the results suggest that the density of synaptic proteins are jointly regulated in spatial clusters. Neighbouring synapses or synapses in the same bouton tend to have similar protein densities of Bruchpilot, GluRIIA, GluRIIB and Pak (Fig. 4.6). This result is in good agreement with a recent study, which shows that active zones

with similar release probabilities can cluster in space within single boutons (Melom et al., 2013).

How can the regulation of synaptic protein levels be constrained to local clusters of synapses in space? One possible way is the usage of local protein synthesis (Martin et al., 2000). For instance Sigrist et al. (2000) showed that local translational machinery at the NMJ exists, which are located within or adjacent to the subsynaptic reticulum. Along with these results, they also noted that the staining of GluRIIA mRNA was particularly strong in terminal and branch-point boutons (Sigrist et al., 2000). It is therefore conceivable that the local translational machinery could establish the regulation of synaptic protein levels in local spatial clusters.

How can different protein densities be organised on a molecular level?

First at all, it was important to show that different protein densities at the NMJ exist and were not an artefact caused by the diffraction limited resolution of the microscope (Fig. 4.8). By comparing the spatial distribution of active zone size and PSD size to the spatial distribution of the protein densities, it could be ruled out that a diffraction artefact might have caused the different protein densities (Fig. 4.9).

Interestingly, there are already proposals on how different receptor densities might be organised at inhibitory synapses (Heine et al., 2013, see fig. 1b). For instance, it could be possible that gaps are introduced into an existing lattice, which anchors receptors, to decrease the receptor density. Another way to regulate the receptor density at a lattice is to change the mesh size of the lattice (Heine et al., 2013). If Bruchpilot itself is also attached to a lattice, the same model could be used to explain the different Bruchpilot densities.

Main conclusions

Receptor localisation depends on the relative position on the axon. Synapses in distal boutons are enriched in Bruchpilot, GluRIIA, GluRIIB and Pak. This could explain the observed high transmission strength and high release probabilities in distal boutons. The protein level at synapses is not individually regulated on a single synapse level. Instead the protein level is regulated in spatial clusters of synapses.

Chapter 5

GluRIIA and GluRIIB Compete for Incorporation into Synapses

5.1 Introduction

In this chapter the relation between GluRIIA and GluRIIB is analysed on a single synapse level. GluRIIA and GluRIIB are glutamate receptor subunits at the *Drosophila* NMJ that are redundant for the viability of the larva. Their localisation and trafficking characteristics have been studied extensively in the past (e.g. Marrus et al., 2004; Rasse et al., 2005; Guerrero et al., 2005; Schmid et al., 2008). GluRIIA and GluRIIB segregate on the level of single synapses, i.e. they are differently localised at single synapses (see section 1.2). Furthermore, in several studies the observation was made that GluRIIA and GluRIIB had an effect on each other's synaptic expression level (Sigrist et al., 2002; Marrus et al., 2004). For instance, a study by Sigrist et al. (2002) described that the overall synaptic expression level of GluRIIA at the NMJ was negatively affected by the expression of GluRIIB. Marrus et al. (2004) explained this behaviour by a model where GluRIIA and GluRIIB compete for the incorporation into the receptor complex, since both are exchangeable for the proper surface expression of the receptor complex. Thus the expression of GluRIIB would reduce the total number of receptor complexes with GluRIIA.

However, this model cannot explain the results from chapter (4), where the spatial correlation of GluRIIA was dependent on whether GluRIIB was coexpressed or not (Fig. 4.7). If GluRIIB only reduced the total number of receptor complexes with GluRIIA, then the spatial correlation of GluRIIA in the IIA/IIB genotype would not have been decreased. This is because the parameter Moran's I is invariant to scaling with a constant factor. Thus it is very likely that the results from chapter (4) point to a more complex relation between GluRIIA and GluRIIB on the level of single synapses.

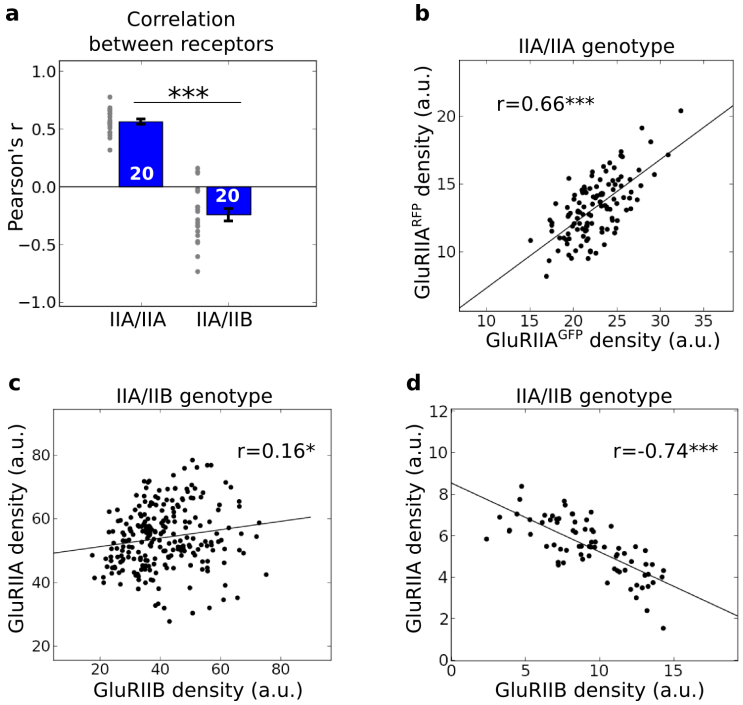

Figure 5.1. The densities of GluRIIA and GluRIIB are negatively correlated. (a) The Pearson's correlation coefficient was used to quantify the correlation between the densities of receptors at NMJs (muscle 4 and muscle 26/27). On average GluRIIA and GluRIIB are negatively correlated. The correlation coefficient lies in the range from 0.16 to −0.74. On the other hand, two copies of GluRIIA show positive correlation at single PSDs. Dots are single measurements. Error bars represent mean ± SEM. *** $P < 0.001$, two-sided t-test. **(b)** An example NMJ is shown, where $GluRIIA^{GFP}$ and $GluRIIA^{RFP}$ are positively correlated (N = 118 PSDs). **(c,d)** Two example NMJs are shown, where GluRIIA and GluRIIB once exhibit a slight positive correlation (N = 237 PSDs) and once a negative correlation (N = 73 PSDs).

5.2 On a small spatial scale GluRIIA and GluRIIB are linearly related

To start analysing the relation between GluRIIA and GluRIIB, their densities at single PSDs were analysed in the receptor density plot. NMJs from either muscle 4 or 26/27 of the IIA/IIB genotype were processed the same way as before (see chapter 2). As a control, the relation between two copies of GluRIIA (IIA/IIA genotype) was also analysed. As expected, a positive correlation was observed between the densities of $GluRIIA^{GFP}$ and $GluRIIA^{RFP}$, since they should localise the same way (r = 0.56 ± 0.02) (Fig. 5.1a,b). Interestingly, the densities of GluRIIA and GluRIIB are negatively correlated at single PSDs (r = -0.24 ± 0.05) (Fig. 5.1a). However, the Pearson's correlation coefficient shows a high variability, which can be as positive as r = 0.16 and as negative as r = −0.74 (Fig. 5.1c,d). In general it appeared that NMJs from muscle 4 have a less negative correlation coefficient than NMJs from muscle 26/27.

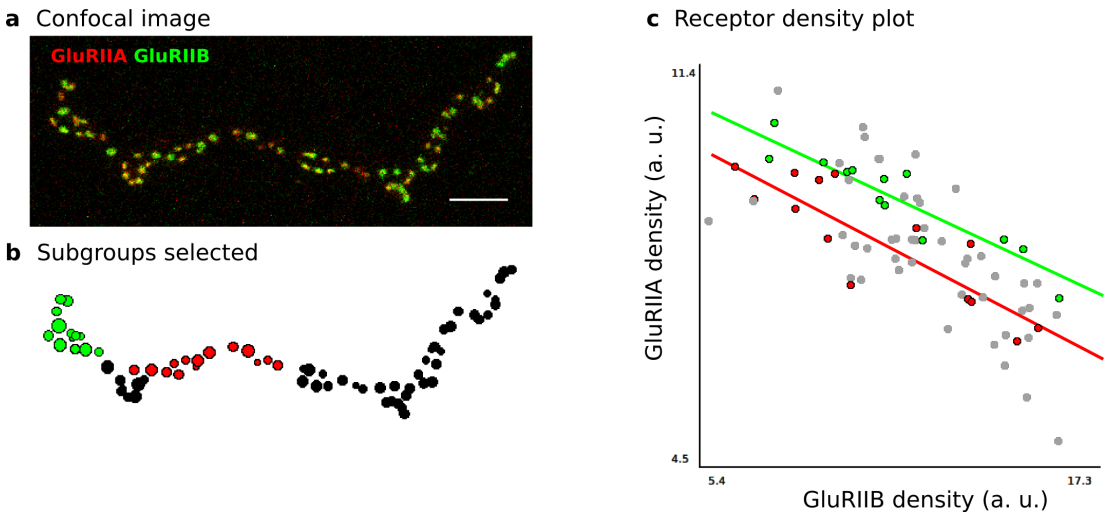

Figure 5.2. The receptor density plot contains subgroups that are clustered in space. **(a)** Confocal image of an NMJ from muscle 26/27 (IIA/IIB genotype). Image was taken by Omid Khorramshahi. Scale bar, 5 μm. **(b)** Two spatial clusters of PSDs (green and red) were selected for further analysis in the receptor density plot. **(c)** In the receptor density plot the two spatial subgroups have a strong negative correlation (green: $r = -0.93$, $N = 13$, $P < 0.001$; red: $r = -0.86$, $N = 14$, $P < 0.001$). Interestingly, the two subgroups seem to lie on lines that are parallel to each other. In total there are 73 PSDs from one NMJ.

Strikingly, when analysing the density plot from (Fig. 5.1d) in more detail, subgroups of PSDs become visible that are clustered in space (Fig. 5.2). The spatial size of these subgroups lie in the magnitude of the size of boutons. In the case of the green subgroup, the subgroup contains all the PSDs from one bouton (Fig. 5.2b). The densities of GluRIIA and GluRIIB are in both subgroups highly anti-correlated (green line: $r = -0.93$; red line: $r = -0.86$) (Fig. 5.2c). Moreover, in the density plot the two subgroups seem to lie on lines that are parallel to each other. Notably, this result shows that the precision of the experimental setup is extremely good, since it is able to resolve such fine structures in the density plot. It should be pointed out that spatial clusters of PSDs with a strong negative correlation are not always that large or do not always contain all PSDs from a bouton. This is especially true for boutons from NMJs of muscle 4.

All in all, the analysis of the density of GluRIIA and GluRIIB revealed that they are highly anti-correlated in local spatial clusters of PSDs (along the red or the green line in Fig. 5.2c). Thus the quantities of GluRIIA and GluRIIB are linearly related.

5.3 A model for the relation of GluRIIA and GluRIIB

GluRIIA and GluRIIB are highly anti-correlated at local spatial clusters of PSDs. This relation can be translated into a negative linear equation:

$$D_{\mathrm{IIA}} \;=\; -m \cdot D_{\mathrm{IIB}} \;+\; b \tag{5.1}$$

where D_{IIA} and D_{IIB} are the densities of GluRIIA and GluRIIB, respectively. Also, two variables m and b occur in this equation that have yet to be defined. Now, the question arises how this negative linear equation can be interpreted in a biologically meaningful way. The most straight forward interpretation of this equation is that it describes a 1:1 coupling between GluRIIA and GluRIIB through the total number of receptors at a PSD. That means if the total amount of GluRIIA increases by five receptors at a PSD, the total amount of GluRIIB has to decrease by five receptors. The variable m would then represent the relative brightness between the GFP and the RFP fluorescence (GFP/RFP), because GluRIIA and GluRIIB were genetically labelled with RFP and GFP, respectively. The fact that the green and red lines are nearly parallel to each other (Fig. 5.2c), implies that they have the same slope m and thus, as expected, the same GFP/RFP. The variable b would then represent the total receptor density at a PSD. As a consequence this would mean that the total receptor density along the green and red lines in the density plot does not change (Fig. 5.2c). Therefore PSDs within each subgroup have the same total receptor density, with PSDs from the green subgroup having a higher density.

A model describing the relation between GluRIIA and GluRIIB

The equation (5.1) does only describe the relation between GluRIIA and GluRIIB at local spatial clusters of PSDs. However, it is possible to rewrite the equation (5.1) to include all PSDs from one NMJ by introducing a new variable D_{total}, which describes the total receptor density of a PSD depending on its location at the NMJ. Before introducing the new model of GluRIIA and GluRIIB, three special cases are shown here to motivate the model. In the following the relative brightness GFP/RFP is assumed to be 1. In the first case, when there is no segregation between GluRIIA and GluRIIB, and when all PSDs have the same total receptor density (see Fig 5.3, left diagram), then the density of GluRIIA and GluRIIB can simply be described by a constant:

$$1. \qquad D_{\mathrm{IIA}} \;=\; D_{\mathrm{IIB}} \;=\; \mathrm{const.}$$

In the second case, when there is no segregation between GluRIIA and GluRIIB, but different receptor densities exist (see Fig 5.3, bottom diagram), then the density of GluRIIA and GluRIIB follow the change of the total receptor density:

$$2. \qquad D_{\mathrm{IIA}} \;=\; D_{\mathrm{IIB}} \;=\; D_{\mathrm{total}}$$

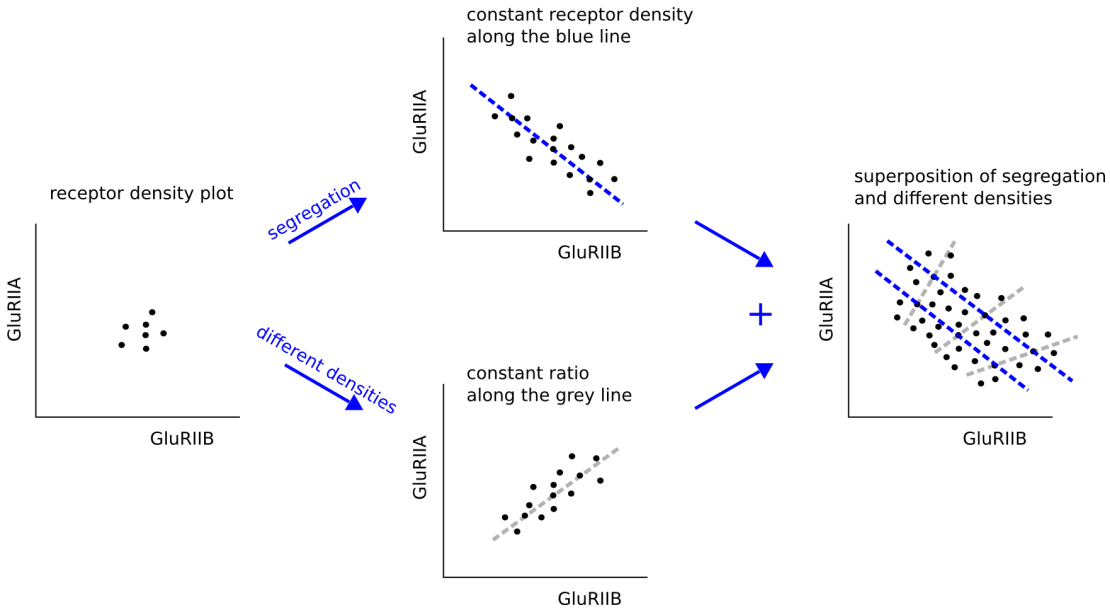

Figure 5.3. Two mechanisms regulate receptor localisation at the NMJ. Illustration of a PSD distribution in the receptor density plot of GluRIIA and GluRIIB, **(left)** when there is no segregation and all PSDs have the same receptor density. Due to noise, all PSDs are randomly distributed around a centre. **(bottom)** PSD distribution when there is no segregation, but different receptor densities exist. **(top)** PSD distribution when there is segregation, but all PSDs have the same receptor density. **(right)** PSD distribution when GluRIIA and GluRIIB segregate and different receptor densities exist.

This case is similar to the IIA/IIA genotype, where $\text{GluRIIA}^{\text{RFP}}$ and $\text{GluRIIA}^{\text{GFP}}$ do no segregate (Fig. 5.1b), but have different densities depending on the location at the NMJ (Fig. 4.7a). In the third case, when there is segregation between GluRIIA and GluRIIB, but all PSDs at the NMJ have the same density (see Fig 5.3, top diagram), then equation (5.1) can be used to describe the densities of GluRIIA and GluRIIB:

$$3. \qquad D_{\text{IIA}} \;=\; -D_{\text{IIB}} \;+\; \text{const.}$$

This equation can be applied to local spatial clusters of PSDs. Finally, the new model describes the relation between GluRIIA and GluRIIB when they do segregate and different receptor densities exist (see Fig 5.3, right diagram):

$$\boxed{D_{\text{IIA}} \;=\; -D_{\text{IIB}} \;+\; D_{\text{total}}} \tag{5.2}$$

The model makes the assumption that the receptor composition and the receptor density are independently regulated from each other. Thus two mechanisms at the NMJ exist. The first mechanism is responsible for the segregation between GluRIIA and GluRIIB. Whereas, the second mechanism is responsible for the different receptor densities. The superposition of the two mechanisms, eventually, define the receptor composition and the receptor density of a PSD at the NMJ.

5.4 The total receptor density is highly correlated in space

Using the model for GluRIIA and GluRIIB (equation 5.2) one can now explain the observed discrepancy in chapter (4), where the spatial correlation of GluRIIA was different between the IIA/IIA and the IIA/IIB genotype (Fig. 4.7). The model can be interpreted in the way that each PSD has a certain number of available anchoring sites for receptors to bind. This number is giving by the variable D_{total} and the size of the PSD (since D_{total} is a density). These anchoring sites can either be populated by GluRIIA or GluRIIB. Now comes the important assumption of the model: the variable D_{total} is highly correlated in space and independent of the expressed receptors. Thus, in the IIA/IIA genotype, where no segregation exists, GluRIIA follows the spatial distribution of D_{total}. As a result, the density of GluRIIA in the IIA/IIA genotype is also highly correlated in space (Fig. 4.7a). In the IIA/IIB genotype, however, neighbouring PSDs can have opposite receptor compositions due to the segregation of GluRIIA and GluRIIB (Schmid et al., 2008). Therefore, the density of GluRIIA has a greater variability in space when coexpressed with GluRIIB. This greater variability in space of GluRIIA, in the end, leads to the observed decrease in spatial correlation (Fig. 4.7b).

To prove that the interpretation and the assumption of the model is correct, one needs to show that the sum of GluRIIA and GluRIIB is highly correlated in space, since it equals D_{total} (rearrangement of equation 5.2):

$$D_{\text{IIA}} \; + \; D_{\text{IIB}} \; = \; D_{\text{total}}$$

Estimating the spatial correlation of the sum of GluRIIA and GluRIIB

In order to quantify the spatial correlation of the sum of GluRIIA and GluRIIB, the quantities of GluRIIA and GluRIIB have to be add up at all PSDs. Unfortunately, GluRIIA and GluRIIB are both labelled with different fluorophores that differ in their brightness (RFP and GFP, respectively). Therefore, one GluRIIA molecule has a different fluorescence intensity than one GluRIIB molecule. Theoretically, one could apply the method from section (2.2) to measure the relative brightness between GFP and RFP. The measured GFP/RFP factor could then be used to normalise the different fluorophores. However, this kind of calibration has not been conducted here for all NMJs. Thus, the following approach was used to estimate the spatial correlation of the sum of GluRIIA and GluRIIB. If the sum is highly correlated in space, then by varying the GFP/RFP factor in equation (5.3) the spatial correlation of the sum will be maximal near the true GFP/RFP factor (Fig. 5.4a).

$$\frac{\text{GFP}}{\text{RFP}} \cdot D_{\text{IIA}} \; + \; D_{\text{IIB}} \; = \; \text{Sum} \tag{5.3}$$

The maximum was then used as an estimator for the spatial correlation of the sum. To exclude any artefacts that could lead to a false maximum when adding together two spatial distributions (e.g. better signal to noise ratio due to the averaging of two measurements), a control is needed. Therefore, the increase in spatial correlation in the

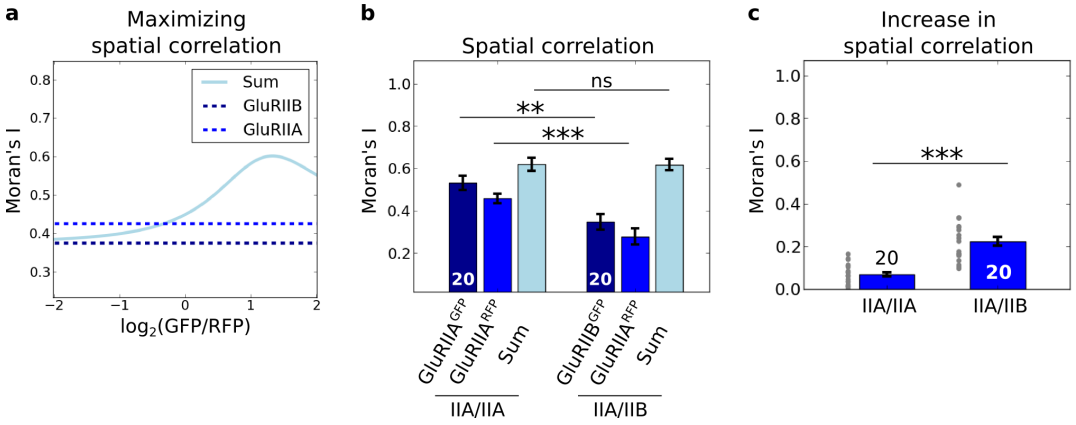

Figure 5.4. The spatial correlation of the sum of GluRIIA and GluRIIB increases significantly. (a) The spatial correlation of the sum of GluRIIA and GluRIIB was estimated by varying the GFP/RFP factor in equation (5.3). The spatial correlation at the maximum was used as an estimator. **(b)** The spatial correlation of GluRIIA and GluRIIB is significantly smaller when compared to the spatial correlation of GluRIIA in the IIA/IIA genotype. However, the spatial correlation of the sum of GluRIIA and GluRIIB is comparable to the spatial correlation of the sum in the IIA/IIA genotype. **(c)** The increase in spatial correlation of the sum is in the IIA/IIB genotype significant larger than in the control IIA/IIA genotype. ns: not significant, ** $P < 0.01$, *** $P < 0.001$, two-sided t-test. Dots are single measurements. Error bars represent mean ± SEM.

IIA/IIB genotype is compared to the control IIA/IIA genotype, where no increase in spatial correlation is expected, since GluRIIA$^{\mathrm{RFP}}$ and GluRIIA$^{\mathrm{GFP}}$ do not segregate.

Neighbouring PSDs have similar total receptor densities

Indeed, the sum of GluRIIA and GluRIIB is highly correlated in space. In particular the degree of spatial correlation is not distinguishable from the spatial correlation of the IIA/IIA genotype (Fig. 5.4b). Artefacts increasing the spatial correlation can be ruled out, since the increase is significantly larger than in the control IIA/IIA genotype (Fig. 5.4c). Notably, the increase in spatial correlation is visible at the NMJ. The single distributions of GluRIIA and GluRIIB (Fig. 5.5a,b) are clearly less correlated than their sum (Fig. 5.5c). As expected, PSDs within each subgroup from (Fig. 5.2b) have similar total receptor densities (Fig. 5.5c, PSDs in green and red boxes). Whereby PSDs from the green group have higher total receptor densities than PSDs from the red group. Interestingly, PSDs next to each other can have inverse receptor compositions, but at the same time can have the same total receptor density (Fig. 5.5, PSD pairs marked with asterisks and arrowheads). This is a very good indication for a model where glutamate receptors bind to defined anchoring sites within PSDs.

To verify the results in a different way, one can also stain for the subunit GluRIID, since GluRIID is an essential subunit of the tetrameric receptor complex. Thus the fluorescence signal of GluRIID represents the total number of receptors within a PSD

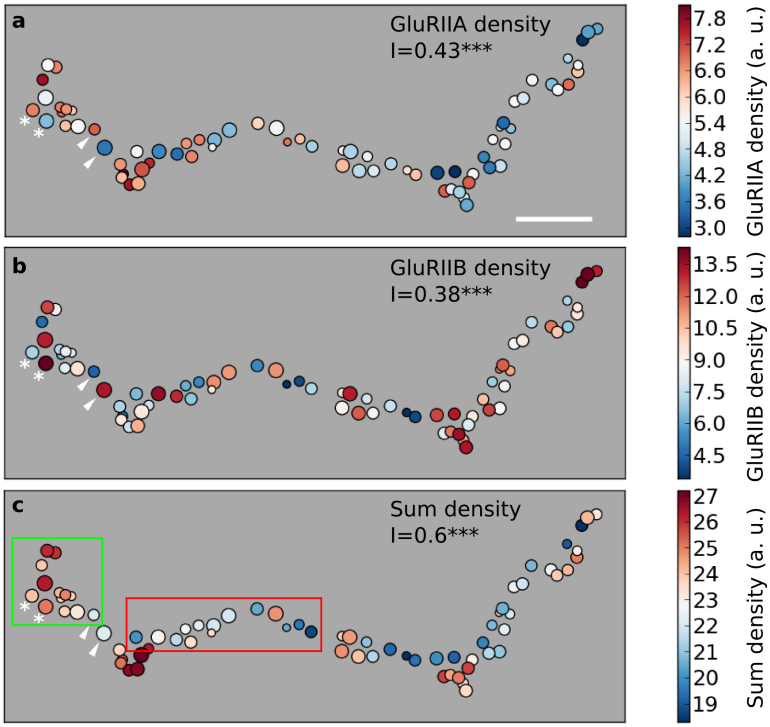

Figure 5.5. The spatial correlation increases when the sum of GluRIIA and GluRIIB is analysed. The increase in spatial correlation of the sum of GluRIIA and GluRIIB is shown for the example NMJ from (Fig. 5.2a). The spatial correlation of GluRIIA **(a)** and GluRIIB **(b)** is smaller then the spatial correlation of the sum **(c)**. Particularly interesting is that the PSDs within the analysed groups from (Fig. 5.2b, green and red) have similar total receptor densities (PSDs in green and red boxes). Neighbouring PSDs can have inverse receptor compositions, but can have the same total receptor density (see PSD pairs marked by asterisks and arrowheads). Scale bar for all images, 5 μm.

and therefore the sum of GluRIIA and GluRIIB. Indeed, the labelling of GluRIID with antibody showed that its density is similarly distributed in space and has a similar degree of spatial correlation as the sum of GluRIIA and GluRIIB (Fig. 5.6). Therefore, future experiments analysing the spatial correlation of the IIA/IIB genotype can be simplified by analysing only the subunit GluRIID.

All in all, the results confirm the proposed assumption that the variable D_{total} in the model (equation 5.2) is highly correlated in space. The results also support the interpretation of the model that GluRIIA and GluRIIB are sharing the total number of available anchoring sites in a PSD (1:1 coupling between GluRIIA and GluRIIB). Furthermore, the segregation between GluRIIA and GluRIIB is the reason why the spatial correlation of GluRIIA in the IIA/IIB genotype is reduced when compared to GluRIIA in the IIA/IIA genotype (Fig. 4.7).

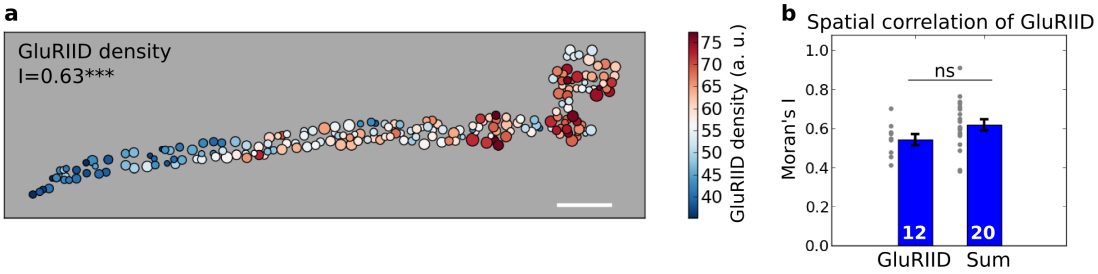

Figure 5.6. The subunit GluRIID shows high correlation in space. (a) At an NMJ from muscle 4, where GluRIIA and GluRIIB are coexpressed, the GluRIID subunit was stained with antibody. The spatial patterns of the GluRIID density are similar to the patterns observed for the sum of GluRIIA and GluRIIB. **(b)** Quantification shows that the density of GluRIID is highly correlated in space (I = 0.54 ± 0.03) and not significantly different from the sum of GluRIIA and GluRIIB.

5.5 Pre- and postsynaptic protein densities are coupled

The sum of GluRIIA and GluRIIB (D_{total}) seems to be an interesting variable, since it is highly correlated in space. In (Fig. 4.3e) the correlation between Bruchpilot and the two receptors, GluRIIA and GluRIIB, was analysed and both receptors showed significant correlation with Bruchpilot (Fig. 5.7a,b). Now, an interesting question arises whether D_{total} is also better correlated with Bruchpilot. To test this hypothesis, the correlation between the sum and Bruchpilot was maximised by varying GFP/RFP in equation (5.3) as it has been done in the last section for the spatial correlation. The results show that D_{total}, indeed, has a significant better correlation to Bruchpilot (Fig. 5.7d,e). This increase in correlation is not trivial, since GluRIIA is not positively correlated with GluRIIB (Fig. 5.7c).

Another way to analyse the relation between D_{total} and the Bruchpilot density is to ask if they localise similarly at synapses (colocalisation or co-occurrence is not the same as correlation, see chapter 6). In other words, do their densities show the same localisation behaviour? The same kind of question has been addressed in chapter (3). There the question was if the GluRIIA mutants show the same localisation as the wild type GluRIIA. Therefore the segregation parameter from equation (3.1) can also be applied here. Analysing the segregation strength between D_{total} and Bruchpilot reveals that they are tightly coupled (Fig. 5.8). They colocalise as well as $\text{GluRIIA}^{\text{GFP}}$ and $\text{GluRIIA}^{\text{RFP}}$ do in the control IIA/IIA genotype.

As a conclusion, D_{total} does not only show high correlation in space, but is also highly correlated to Bruchpilot and shows the same localisation as Bruchpilot. D_{total} seems to represent an important variable at the NMJ and therefore should be regarded in future receptor analyses.

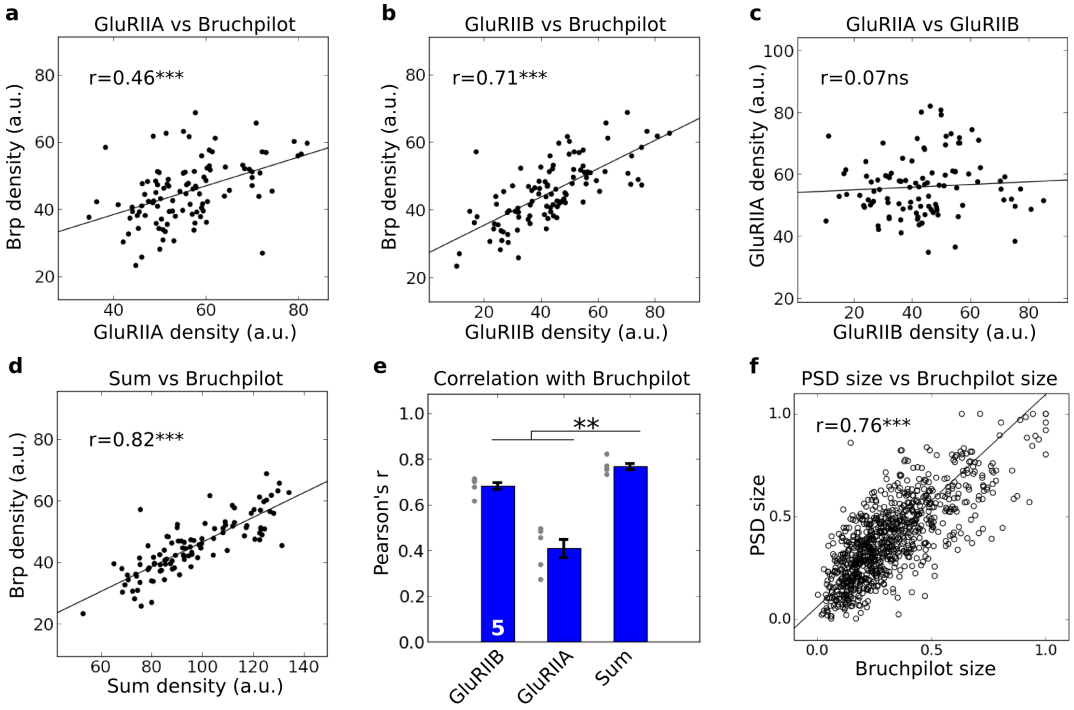

Figure 5.7. The sum of GluRIIA and GluRIIB is highly correlated to Bruchpilot. **(a,b)** Correlation of GluRIIA and GluRIIB with Bruchpilot for one example NMJ from muscle 4 is shown (N = 104 PSDs). **(c)** No correlation between GluRIIA and GluRIIB exists. **(d)** The correlation between the sum of GluRIIA and GluRIIB with Bruchpilot is maximised. The maximised correlation is higher than the single receptor correlations with Bruchpilot. **(e)** The maximised correlation ($r = 0.77 \pm 0.01$) is significantly larger than the single receptor correlations with Bruchpilot ($N = 5$ NMJs). Dots are single measurements. Error bars represent mean ± SEM. ** $P < 0.01$, two-sided t-test. **(f)** High correlation between Bruchpilot size and PSD size is observed for the IIA/IIB genotype (850 PSDs from 5 NMJs).

5.6 Discussion

GluRIIA and GluRIIB compete for synaptic anchoring sites

Here the results strongly suggest that GluRIIA competes with GluRIIB for synaptic anchoring sites at type Ib NMJs. The results revealed that the sum of GluRIIA and GluRIIB has interesting properties. First, the sum is better correlated in space than the single distributions of GluRIIA and GluRIIB (Fig. 5.4). Second, the sum is also better correlated to the presynaptic protein Bruchpilot (Fig. 5.7). Third, neighbouring PSDs can have the same sum densities but inverse receptor compositions (Fig. 5.5). Altogether, the results point to a model (equation 5.2) where GluRIIA and GluRIIB are exchanged for each other at single PSDs in a 1:1 ratio, while the total number of receptors remains constant. In addition the competitive nature between GluRIIA and GluRIIB is strengthened by the observation that in the absence of GluRIIB, GluRIIA

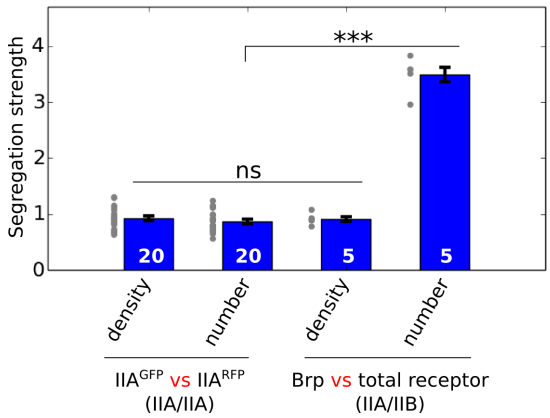

Figure 5.8. The total receptor density is highly coupled to the Bruchpilot density. To study how similar D_{total} and the Bruchpilot density are localised, the segregation parameter from equation (3.1) is used as a measure. The IIA/IIA genotype is again used as a baseline where no segregation is expected. The number of receptors or Bruchpilot proteins is represented by the fluorescence intensity within a PSD or an active zone. The density of receptors or Bruchpilot is calculated by dividing their number by the volume. As expected the receptor density and the receptor number of GluRIIA$^{\text{GFP}}$ and GluRIIA$^{\text{RFP}}$ exhibit the same degree of segregation. Interestingly, D_{total} and the Bruchpilot density also have a similar segregation strength. This indicates that they colocalise or co-occur very well, as if their densities are coupled to each other. This relation is not trivial since the number of total receptors and the number of Bruchpilot proteins have a high segregation strength. Also the density of the single receptors segregate significantly from the Bruchpilot density (not shown in this figure; GluRIIA: S = 1.52 ± 0.07, P < 0.001; GluRIIB: S = 2.05 ± 0.08, P < 0.001). Dots are single measurements. Error bars represent mean ± SEM. ns: not significant, *** P < 0.001, two-sided t-test.

shows the same degree of spatial correlation as their sum (Fig. 4.7). Thus GluRIIB occupies synaptic anchoring sites that could have been otherwise occupied by GluRIIA. In consistence with this interpretation, a recent study showed that the total number of receptors at NMJs is conserved (Morel et al., 2014).

Interestingly, as already mentioned in the previous chapters, a recent study has shown that after LTP synapses can incorporate a broad variety of receptors and are not limited to specific receptor subunits (Granger et al., 2013). This is in good agreement with the results shown here. If no GluRIIB is present than the PSD instead accumulates receptor complexes with GluRIIA to fill the empty synaptic anchoring sites. All in all the segregation between GluRIIA and GluRIIB is of a competitive nature.

The receptor localisation is shaped by two mechanisms that superimpose

Peled and Isacoff (2011) suggested from their results that synaptic transmission properties at the NMJ are regulated on two different spatial scales. An intra-bouton regulation at the level of single synapses and an inter-bouton regulation at the level of single boutons. A similar kind of regulation is observed here for the receptor localisation of GluRIIA and GluRIIB. The receptor composition shows little to no correlation in

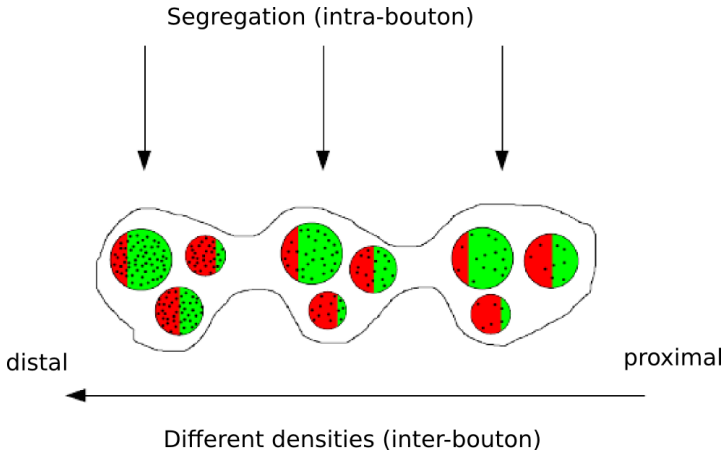

Figure 5.9. At the NMJ receptor localisation is regulated on two spatial scales. Illustration of an NMJ with three boutons. Circles represent PSDs, black dots represent receptors. The receptor composition is regulated on the level of single synapses. Whereas the receptor density is regulated on the level of single boutons. GluRIIA (receptors in red area) and GluRIIB (receptors in green area) are anti-correlated within a bouton, but at the same time they are also correlated from bouton to bouton.

space, i.e. adjacent synapses can have inverse receptor compositions (Fig. 4.6). On the other hand, the sum of GluRIIA and GluRIIB is highly correlated in space, i.e. synapses from the same bouton are likely to have similar total receptor densities. Together with equation (5.2) these findings suggest that there might exist two separate mechanisms at the NMJ that shape receptor localisation (Fig. 5.3). One mechanism regulates the receptor density, i.e. the total amount of receptors at single PSDs. The second mechanism regulates the receptor composition, which is responsible for the segregation between GluRIIA and GluRIIB. The first mechanism at the NMJ is independent of the expressed receptors, while the second one depends on the expressed receptors. The superposition of the two mechanisms define, eventually, the receptor composition and receptor density of a PSD (Fig. 5.9). It is conceivable that the two spatial scales of regulation proposed by Peled and Isacoff (2011) corresponds to the two mechanisms observed here. The difference between their study and this study would then be the analysed attributes - synaptic transmission versus receptor localisation.

Protein densities are tightly coupled between pre- and postsynaptic sites

Pre- and postsynaptic sites are highly coordinated during synapse assembly (Collins and DiAntonio, 2007; Owald et al., 2012). Strikingly the segregation parameter showed that the total receptor density D_{total} is distributed very similar as the Bruchpilot density. The degree of similarity is the same as the degree of similarity between GluRIIA$^{\text{GFP}}$ and GluRIIA$^{\text{RFP}}$. As one can assume that GluRIIA$^{\text{GFP}}$ and GluRIIA$^{\text{RFP}}$ are passively coupled to each other, it is possible that D_{total} and the Bruchpilot density are also passively coupled to each other.

One can now speculate how the coupling of protein densities between pre- and postsynaptic sites are regulated. One possibility would be that either Bruchpilot or the glutamate receptors directly regulate the quantity of the other protein. However, the accumulation of Bruchpilot seems not to be dependent on glutamate receptors and vice versa, since the absence of either one is not affecting the accumulation of the other one (Schmid et al., 2006; Kittel et al., 2006). Thus, it is likely that both lie in the same pathway and receive the same molecular input signals that regulate their densities. The signal could be in the form of scaffold proteins that are located on the pre- and postsynaptic sites and are connected across the synaptic cleft. Good candidate proteins are for example Neurexin and Neuroligin. They interact trans-synaptically and are important for proper synapse assembly (Craig and Kang, 2007). They also accumulate earlier than glutamate receptors and Bruchpilot during synapse assembly (Owald et al., 2012). Bruchpilot and glutamate receptors would then interact with such scaffold proteins to stabilise their localisation and thus matching their densities passively to each other.

Main conclusions

GluRIIA and GluRIIB compete for synaptic anchoring sites within PSDs. Their quantities are negatively coupled in a 1:1 ratio through the total number of receptors:

$$D_{\mathrm{IIA}} = \underbrace{-D_{\mathrm{IIB}}}_{\text{segregation (intra-bouton)}} + \underbrace{D_{\mathrm{total}}}_{\text{different densities (inter-bouton)}}$$

Two mechanisms at the NMJ regulate receptor localisation on two different spatial scales: at the level of single synapses and at the level of single boutons. The Bruchpilot density and the total receptor density (D_{total}) are tightly coupled between pre- and postsynaptic sites.

Chapter 6

Conclusion & Outlook

In this thesis the *Drosophila* neuromuscular synapse was used as a model system to study basic principles of receptor trafficking. New statistical parameters were developed and existing statistical parameters were applied to quantify the distribution of receptors. Moreover the precision of the experimental setup was studied to distinguish experimental noise from biological noise (chapter 2). Based on these findings, future studies can focus on the inherent variability of the biological system and study which components covary to dissect dependencies in pathways.

In particular the main results of this thesis are that receptor trafficking is affected by gating dynamics. Proper coordination between pre- and postsynaptic sites during synapse assembly and maturation is disrupted in very-fast-gating receptors. The results also suggest that receptors compete with each other for synaptic anchoring sites in PSDs. The number of anchoring sites depends on the location at the NMJ (proximal vs distal boutons). Since competition can alter receptor localisation, receptor competition should be considered in future models of receptor trafficking.

The segregation parameter as a new colocalisation parameter?

The imaging of two fluorophores simultaneously with the confocal microscope allows to analyse if two proteins are colocalised or not. In general colocalisation can be divided into co-occurrence and correlation (Fig. 6.1). Co-occurrence analyses if the ratio of two fluorophores are similar from pixel to pixel, whereas correlation analyses the relationship between the two fluorescence intensities.

Different coefficients have been used and developed to quantify colocalisation (Bolte and Cordelières, 2006; Zinchuk et al., 2007). The most common used colocalisation coefficients are the Pearson correlation coefficient (PCC) and the Mander's overlap coefficient (MOC). MOC is based on PCC and was developed to overcome problems with PCC, since negative values of PCC were hard to interpret in colocalisation studies (Manders et al., 1993). However a study by Adler and Parmryd (2010), where the coefficients were quantitatively compared, suggested to abandon the MOC, since it is affected by correlation and co-occurrence in the data and thus also hard to interpret.

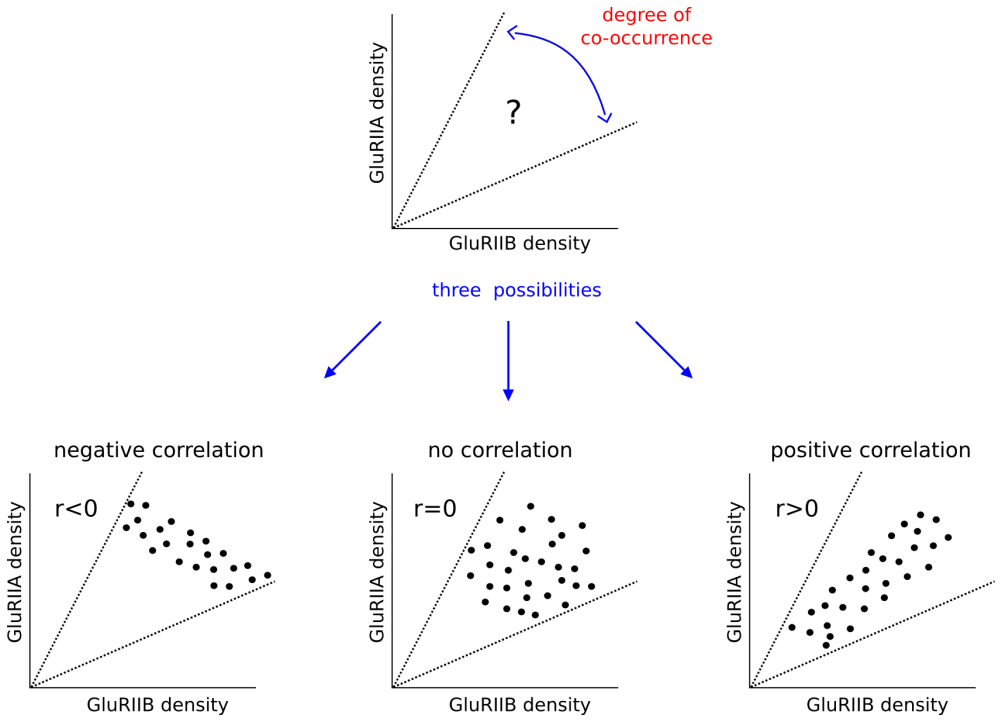

Figure 6.1. Correlation and co-occurrence describe different issues in colocalisation. Correlation and co-occurrence can overlap, but are not the same. Three cases are shown, where the degree of co-occurrence is the same, but the correlation can take any values from -1 to +1.

In this thesis colocalisation was analysed under the aspect of co-occurrence (here called segregation). For this a segregation parameter was developed to quantify the colocalisation of GluRIIA mutants with wild type GluRIIA. The segregation parameter was also applied to study if the densities of total receptors and Bruchpilot colocalise at the same synapse.

Here the suggestion is made that, in general, the segregation parameter could be used to measure the co-occurrence of fluorophores in confocal images. For this purpose the segregation parameter has to be slightly changed and a new variable X_i is introduced:

$$X_i = \log(\frac{\mathrm{GFP}_i}{\mathrm{RFP}_i})$$

where GFP_i and RFP_i are the intensities of one pixel in the green and red channel, respectively. Since one has to consider the stochastic aspects of the pixel intensities, not the full range of ratios is measured, as it has been done for the segregation parameter in chapter (3). Instead the standard deviation of X_i can be used as a measure for the degree of co-occurrence, here also called S:

$$S = \sigma_{X_i} = \sqrt{\mathrm{Var}(X_i)}$$

This new colocalisation parameter could replace the MOC and complement the PCC.

PCC would measure the correlation and S would measure the co-occurrence of two differently labelled proteins. In a future study S should be tested in the same way as Adler and Parmryd (2010) tested the other colocalisation coefficients.

Analysing basic mechanisms of synaptic plasticity at the NMJ

The level of proteins at synapses is tightly regulated during synaptic plasticity processes, since it regulates the synaptic transmission strength. The results from chapter (4) have shown that at the NMJ synapses can have different protein densities. Interestingly the localisation of high density synapses correlates with the localisation of high transmission sites from previous studies. Importantly the difference in protein densities cannot be explained by the size of the synapse. Small synapses can have high densities and large synapses can have low densities.

It is conceivable that the mechanisms underlying the expression of different protein densities could play a role in synaptic plasticity processes. In the last decade a lot of work has been committed to understand receptor trafficking during LTP. It was believed that the CTD of the AMPAR subunit GluA1 was necessary for LTP induction. Hence in LTP research the focus had been on the receptors. However, Granger et al. (2013) have shown that LTP is independent of the GluA1 subunit. Instead it seems that synapses are capable to accumulate a broad variety of glutamate receptors independent of subunit type. Granger et al. (2013) concluded that LTP might be understood as an immediate increase in the "ability" of the PSD to trap receptors. Interestingly, synapses in distal boutons at the NMJ have the "ability" to accumulate more receptors and also more Bruchpilot and Pak proteins. Huganir and Nicoll (2013) proposed a PSD centric model for LTP, where PSD anchoring sites are increased after LTP and thus more AMPARs can be captured.

All in all there seems to be a shift in the field of LTP research. Granger et al. (2013) suggest to focus in future more on structural aspects of the synapse during LTP. The *Drosophila* neuromuscular synapse can be used to study these basic mechanisms, where synapses with different protein densities coexist at the same NMJ. Interestingly, in chapter (5) it has been shown that the density between the pre- and postsynaptic site is highly coupled. The quantitative parameters from chapter (3) and (4) could be used to compare different mutants quantitatively with each other. Especially it would be interesting to understand how it is regulated that not all synapses have the same protein density. Or what proteins are involved to increase the protein density of a synapse. And is the increase in protein density controlled by pre- or postsynaptic mechanisms.

Bibliography

Adler, J. and Parmryd, I. (2010). Quantifying colocalization by correlation: the Pearson correlation coefficient is superior to the Mander's overlap coefficient. Cytometry A *77*, 733–742.

Albin, S. D. and Davis, G. W. (2004). Coordinating structural and functional synapse development: postsynaptic p21-activated kinase independently specifies glutamate receptor abundance and postsynaptic morphology. J Neurosci *24*, 6871–6879.

Anggono, V. and Huganir, R. L. (2012). Regulation of AMPA receptor trafficking and synaptic plasticity. Curr Opin Neurobiol *22*, 461–469.

Atwood, H. L., Govind, C. K. and Wu, C. F. (1993). Differential ultrastructure of synaptic terminals on ventral longitudinal abdominal muscles in Drosophila larvae. J Neurobiol *24*, 1008–1024.

Bailey, C. H., Bartsch, D. and Kandel, E. R. (1996). Toward a molecular definition of long-term memory storage. Proc Natl Acad Sci USA *93*, 13445–13452.

Banovic, D., Khorramshahi, O., Owald, D., Wichmann, C., Riedt, T., Fouquet, W., Tian, R., Sigrist, S. J. and Aberle, H. (2010). Drosophila neuroligin 1 promotes growth and postsynaptic differentiation at glutamatergic neuromuscular junctions. Neuron *66*, 724–738.

Bolte, S. and Cordelières, F. P. (2006). A guided tour into subcellular colocalization analysis in light microscopy. J Microsc *224*, 213–232.

Bredt, D. S. and Nicoll, R. A. (2003). AMPA receptor trafficking at excitatory synapses. Neuron *40*, 361–379.

Budnik, V. and Ruiz-Canada, C., eds (2006). The fly neuromuscular junction: structure and function. Acadamic Press.

Campbell, R. E., Tour, O., Palmer, A. E., Steinbach, P. A., Baird, G. S., Zacharias, D. A. and Tsien, R. Y. (2002). A monomeric red fluorescent protein. Proc Natl Acad Sci USA *99*, 7877–7882.

Chen, K. and Featherstone, D. E. (2005). Discs-large (DLG) is clustered by presynaptic innervation and regulates postsynaptic glutamate receptor subunit composition in Drosophila. BMC Biol *3*, 1.

Chen, K., Merino, C., Sigrist, S. J. and Featherstone, D. E. (2005). The 4.1 protein coracle mediates subunit-selective anchoring of Drosophila glutamate receptors to the postsynaptic actin cytoskeleton. J Neurosci *25*, 6667–6675.

Collins, C. A. and DiAntonio, A. (2007). Synaptic development: insights from Drosophila. Curr Opin Neurobiol *17*, 35–42.

Craig, A. M. and Kang, Y. (2007). Neurexin-neuroligin signaling in synapse development. Curr Opin Neurobiol *17*, 43–52.

DiAntonio, A., Petersen, S. A., Heckmann, M. and Goodman, C. S. (1999). Glutamate receptor expression regulates quantal size and quantal content at the Drosophila neuromuscular junction. J Neurosci *19*, 3023–3032.

Fouquet, W., Owald, D., Wichmann, C., Mertel, S., Depner, H., Dyba, M., Hallermann, S., Kittel, R. J., Eimer, S. and Sigrist, S. J. (2009). Maturation of active zone assembly by Drosophila Bruchpilot. J Cell Biol *186*, 129–145.

Frank, C. A., Wang, X., Collins, C. A., Rodal, A. A., Yuan, Q., Verstreken, P. and Dickman, D. K. (2013). New approaches for studying synaptic development, function, and plasticity using Drosophila as a model system. J Neurosci *33*, 17560–17568.

Füger, P., Behrends, L., Mertel, S., Sigrist, S. and Rasse, T. (2007). Live imaging of synapse development and measuring protein dynamics using two-color fluorescence recovery after photo-bleaching at Drosophila synapses. Nature Protocols *2*, 3285–3298.

Granger, A. J., Shi, Y., Lu, W., Cerpas, M. and Nicoll, R. A. (2013). LTP requires a reserve pool of glutamate receptors independent of subunit type. Nature *493*, 495–500.

Guerrero, G., Reiff, D. F., Agarwal, G., Ball, R. W., Borst, A., Goodman, C. S. and Isacoff, E. Y. (2005). Heterogeneity in synaptic transmission along a Drosophila larval motor axon. Nat Neurosci *8*, 1188–1196.

Guzman, S. J. and Jonas, P. (2010). Beyond TARPs: the growing list of auxiliary AMPAR subunits. Neuron *66*, 8–10.

Hebb, D. O. (1949). The organization of behavior. New York: Wiley & Sons.

Heine, M., Karpova, A. and Gundelfinger, E. D. (2013). Counting gephyrins, one at a time: a nanoscale view on the inhibitory postsynapse. Neuron *79*, 213–216.

Hoang, B. and Chiba, A. (2001). Single-cell analysis of Drosophila larval neuromuscular synapses. Dev Biol *229*, 55–70.

Horning, M. S. and Mayer, M. L. (2004). Regulation of AMPA receptor gating by ligand binding core dimers. Neuron *41*, 379–388.

Huganir, R. L. and Nicoll, R. A. (2013). AMPARs and synaptic plasticity: the last 25 years. Neuron *80*, 704–717.

Jackson, A. C. and Nicoll, R. A. (2011). The expanding social network of ionotropic glutamate receptors: TARPs and other transmembrane auxiliary subunits. Neuron *70*, 178–199.

Kandel, E. R., Schwartz, J. H., Jessell, T. M., Siegelbaum, S. A. and Hudspeth, A. J., eds (2013). Principles of neural science. 5th edition, McGraw-Hill Companies.

Khorramshahi, O. F. (2012). A transsynaptic mechanism regulates glutamate receptor clustering at the Drosophila neuromuscular junction. PhD thesis, Freie Universität Berlin.

Kim, Y.-J., Bao, H., Bonanno, L., Zhang, B. and Serpe, M. (2012). Drosophila Neto is essential for clustering glutamate receptors at the neuromuscular junction. Genes Dev *26*, 974–987.

Kim, Y.-J. and Serpe, M. (2013). Building a synapse: a complex matter. Fly *7*, 146–152.

Kittel, R. J., Wichmann, C., Rasse, T. M., Fouquet, W., Schmidt, M., Schmid, A., Wagh, D. A., Pawlu, C., Kellner, R. R., Willig, K. I., Hell, S. W., Buchner, E., Heckmann, M. and Sigrist, S. J. (2006). Bruchpilot promotes active zone assembly, Ca2+ channel clustering, and vesicle release. Science *312*, 1051–1054.

Lee, H.-G., Zhao, N., Campion, B. K., Nguyen, M. M. and Selleck, S. B. (2013). Akt regulates glutamate receptor trafficking and postsynaptic membrane elaboration at the Drosophila neuromuscular junction. Dev Neurobiol *73*, 723–743.

Li, K. W., Chen, N. and Smit, A. B. (2013). Interaction proteomics of the AMPA receptor: towards identification of receptor sub-complexes. Amino Acids *44*, 1247–1251.

Liebl, F. L. W. and Featherstone, D. E. (2008). Identification and investigation of Drosophila postsynaptic density homologs. Bioinform Biol Insights *2*, 369–381.

Madden, D. R. (2002). The structure and function of glutamate receptor ion channels. Nat Rev Neurosci *3*, 91–101.

Malinow, R., Mainen, Z. F. and Hayashi, Y. (2000). LTP mechanisms: from silence to four-lane traffic. Curr Opin Neurobiol *10*, 352–357.

Malinow, R. and Malenka, R. C. (2002). AMPA receptor trafficking and synaptic plasticity. Annu Rev Neurosci *25*, 103–126.

Manders, E. M. M., Verbeek, F. J. and Aten, J. A. (1993). Measurement of co-localization of objects in dual-colour confocal images. J Microsc *169*, 375–382.

Marrus, S. B., Portman, S. L., Allen, M. J., Moffat, K. G. and DiAntonio, A. (2004). Differential localization of glutamate receptor subunits at the Drosophila neuromuscular junction. J Neurosci *24*, 1406–1415.

Martin, K. C., Barad, M. and Kandel, E. R. (2000). Local protein synthesis and its role in synapse-specific plasticity. Curr Opin Neurobiol *10*, 587–592.

Matkovic, T., Siebert, M., Knoche, E., Depner, H., Mertel, S., Owald, D., Schmidt, M., Thomas, U., Sickmann, A., Kamin, D., Hell, S. W., Bürger, J., Hollmann, C., Mielke, T., Wichmann, C. and Sigrist, S. J. (2013). The Bruchpilot cytomatrix determines the size of the readily releasable pool of synaptic vesicles. J Cell Biol *202*, 667–683.

Melom, J. E., Akbergenova, Y., Gavornik, J. P. and Littleton, J. T. (2013). Spontaneous and evoked release are independently regulated at individual active zones. J Neurosci *33*, 17253–17263.

Moran, P. A. P. (1950). Notes on continuous stochastic phenomena. Biometrika *37*, 17–23.

Morel, V., Lepicard, S., Rey, A. N., Parmentier, M.-L. and Schaeffer, L. (2014). Drosophila Nesprin-1 controls glutamate receptor density at neuromuscular junctions. Cell Mol Life Sci *71*, 3363–3379.

Morimoto, T., Nobechi, M., Komatsu, A., Miyakawa, H. and Nose, A. (2010). Subunit-specific and homeostatic regulation of glutamate receptor localization by CaMKII in Drosophila neuromuscular junctions. Neuroscience *165*, 1284–1292.

Owald, D., Khorramshahi, O., Gupta, V. K., Banovic, D., Depner, H., Fouquet, W., Wichmann, C., Mertel, S., Eimer, S., Reynolds, E., Holt, M., Aberle, H. and Sigrist, S. J. (2012). Cooperation of Syd-1 with Neurexin synchronizes pre- with postsynaptic assembly. Nat Neurosci *15*, 1219–1226.

Peled, E. S. and Isacoff, E. Y. (2011). Optical quantal analysis of synaptic transmission in wild-type and rab3-mutant Drosophila motor axons. Nat Neurosci *14*, 519–526.

Peled, E. S., Newman, Z. L. and Isacoff, E. Y. (2014). Evoked and spontaneous transmission favored by distinct sets of synapses. Curr Biol *24*, 484–493.

Peron, S., Zordan, M. A., Magnabosco, A., Reggiani, C. and Megighian, A. (2009). From action potential to contraction: neural control and excitation-contraction coupling in larval muscles of Drosophila. Comp Biochem Physiol A Mol Integr Physiol *154*, 173–183.

Petersen, S. A., Fetter, R. D., Noordermeer, J. N., Goodman, C. S. and DiAntonio, A. (1997). Genetic analysis of glutamate receptors in Drosophila reveals a retrograde signal regulating presynaptic transmitter release. Neuron *19*, 1237–1248.

Petzoldt, A. G., Lee, Y.-H., Khorramshahi, O., Reynolds, E., Plested, A. J. R., Herzel, H. and Sigrist, S. J. (2014). Gating characteristics control glutamate receptor distribution and trafficking in vivo. Curr Biol, accepted.

Qin, G., Schwarz, T., Kittel, R. J., Schmid, A., Rasse, T. M., Kappei, D., Ponimaskin, E., Heckmann, M. and Sigrist, S. J. (2005). Four different subunits are essential for expressing the synaptic glutamate receptor at neuromuscular junctions of Drosophila. J Neurosci *25*, 3209–3218.

Rasse, T. M., Fouquet, W., Schmid, A., Kittel, R. J., Mertel, S., Sigrist, C. B., Schmidt, M., Guzman, A., Merino, C., Qin, G., Quentin, C., Madeo, F. F., Heckmann, M. and Sigrist, S. J. (2005). Glutamate receptor dynamics organizing synapse formation in vivo. Nat Neurosci *8*, 898–905.

Rey, S. J. and Anselin, L. (2007). PySAL: a Python library of spatial analytical methods. The Review of Regional Studies *37*, 5–27.

Schmid, A., Hallermann, S., Kittel, R., Khorramshahi, O., Frölich, A., Quentin, C., Rasse, T., Mertel, S., Heckmann, M. and Sigrist, S. (2008). Activity-dependent site-specific changes of glutamate receptor composition in vivo. Nat Neurosci *11*, 659–666.

Schmid, A., Qin, G., Wichmann, C., Kittel, R., Mertel, S., Fouquet, W., Schmidt, M., Heckmann, M. and Sigrist, S. (2006). Non-NMDA-type glutamate receptors are essential for maturation but not for initial assembly of synapses at Drosophila neuromuscular junctions. J Neurosci *26*, 11267–11277.

Schuster, C. M., Ultsch, A., Schloss, P., Cox, J. A., Schmitt, B. and Betz, H. (1991). Molecular cloning of an invertebrate glutamate receptor subunit expressed in Drosophila muscle. Science *254*, 112–114.

Shaner, N. C., Patterson, G. H. and Davidson, M. W. (2007). Advances in fluorescent protein technology. J Cell Sci *120*, 4247–4260.

Sheng, M., Sabatini, B. L. and Südhof, T. C., eds (2012). The synapse. Cold Spring Harbor Laboratory Press.

Shepherd, J. D. and Huganir, R. L. (2007). The cell biology of synaptic plasticity: AMPA receptor trafficking. Annu Rev Cell Dev Biol *23*, 613–643.

Sigrist, S. J., Thiel, P. R., Reiff, D. F., Lachance, P. E., Lasko, P. and Schuster, C. M. (2000). Postsynaptic translation affects the efficacy and morphology of neuromuscular junctions. Nature *405*, 1062–1065.

Sigrist, S. J., Thiel, P. R., Reiff, D. F. and Schuster, C. M. (2002). The postsynaptic glutamate receptor subunit DGluR-IIA mediates long-term plasticity in Drosophila. J Neurosci *22*, 7362–7372.

Sokal, R. R. and Oden, N. L. (1978). Spatial autocorrelation in biology. 1 Methodology. Biol J Linn Soc *10*, 199–228.

Sone, M., Suzuki, E., Hoshino, M., Hou, D., Kuromi, H., Fukata, M., Kuroda, S., Kaibuchi, K., Nabeshima, Y. and Hama, C. (2000). Synaptic development is controlled in the periactive zones of Drosophila synapses. Development *127*, 4157–4168.

Sweeney, S. T., Broadie, K., Keane, J., Niemann, H. and O'Kane, C. J. (1995). Targeted expression of tetanus toxin light chain in Drosophila specifically eliminates synaptic transmission and causes behavioral defects. Neuron *14*, 341–351.

Ulbrich, M. H. and Isacoff, E. Y. (2007). Subunit counting in membrane-bound proteins. Nat Methods *4*, 319–321.

Wagh, D. A., Rasse, T. M., Asan, E., Hofbauer, A., Schwenkert, I., Dürrbeck, H., Buchner, S., Dabauvalle, M.-C., Schmidt, M., Qin, G., Wichmann, C., Kittel, R., Sigrist, S. J. and Buchner, E. (2006). Bruchpilot, a protein with homology to ELKS/CAST, is required for structural integrity and function of synaptic active zones in Drosophila. Neuron *49*, 833–844.

Yelshansky, M. V., Sobolevsky, A. I., Jatzke, C. and Wollmuth, L. P. (2004). Block of AMPA receptor desensitization by a point mutation outside the ligand-binding domain. J Neurosci *24*, 4728–4736.

Zhang, C., Atasoy, D., Araç, D., Yang, X., Fucillo, M. V., Robison, A. J., Ko, J., Brunger, A. T. and Südhof, T. C. (2010). Neurexins physically and functionally interact with $GABA_A$ receptors. Neuron *66*, 403–416.

Zinchuk, V., Zinchuk, O. and Okada, T. (2007). Quantitative colocalization analysis of multicolor confocal immunofluorescence microscopy images: pushing pixels to explore biological phenomena. Acta Histochem Cytochem *40*, 101–111.

Zito, K., Parnas, D., Fetter, R. D., Isacoff, E. Y. and Goodman, C. S. (1999). Watching a synapse grow: noninvasive confocal imaging of synaptic growth in Drosophila. Neuron *22*, 719–729.

Acknowledgements

Foremost I want to thank my supervisor Hanspeter Herzel from the ITB for the possibility to do this research in his group. During this time he always encouraged me and was open for my ideas. I am grateful for all the discussions we had and the guidance that he gave me. During this time I learned a lot.

I also want to thank Stephan Sigrist for the possibility to work together with his excellent research group. All the data I have analysed originated from his lab. There I have to thank Omid Khorramshahi, who created the mutant receptors and did the initial imaging before Astrid Petzoldt took over. I am especially grateful to Astrid with whom I worked together most of the time and who was very patient to explain all the experimental "things" to me. She also did a careful reading of the manuscript. Altogether it was a nice and fruitful collaboration, where I learned a lot about the biology of synapses.

At the ITB I want thank all the current and former members of Herzel's group for constructive discussions and the comfortable working conditions. There I have to mention Willi who started with me on this project years ago, but then went on to do some other stuff - metabolic modelling. We also had a lot of fun playing Go. I also want thank all my old roommates from the Invalidenstr. 42, where I spent most of the time before we got separated during the move of the ITB to the new building. Jan-Hendrik, Janina, Bartosz, Agnes and Fabian, thank you all for the pleasant and comfortable atmosphere in this room! And I want to thank the Doktorandenkreis at the ITB for nice discussions about the non-scientific side of a PhD student. Of course, I want to thank all the other ITB members for the enjoyable discussions during the occasional encounters in the mensa.

Finally, I want to thank my parents and my brother for their lifelong support. And I want to thank Chien-Hui for her patience and help during all the time of this thesis.

Deutsche Zusammenfassung

Einleitung

Eines der wichtigsten Themen in der Neurowissenschaft ist die Erforschung der molekularen Grundlagen des Lernens. Was passiert auf der zellulären und molekularen Ebene, wenn wir etwas lernen oder neue Erinnerungen machen? Die heutige Sicht ist, dass die Verbindung zwischen den Neuronen plastisch ist. D.h. die Stärke der synaptischen Übertragung kann sich auf Grund der Aktivität im neuronalen Netzwerk ändern. Dieses Phenomän wird synaptische Plastizität genannt.

Auf der molekularen Ebene sind bereits viele Proteine bekannt, die notwendig sind, um die Stärke der synaptischen Übertragung zu ändern. Hierbei spielen Glutamatrezeptoren eine wichtige Rolle, da sie durch ihre Leitfähigkeit, die Übertragungsstärke einer Synapse direkt beeinflussen. Ihre Anzahl ist maßgebend für die Übertragungsstärke einer Synapse. Deshalb beschäftigt sich ein breites Feld in der Neurowissenschaft mit den Grundlagen, wie der Transport der Glutamatrezeptoren zu den Synapsen auf molekularer Ebene reguliert wird.

Methoden

In dieser Arbeit wird der Transport von Glutamatrezeptoren an der neuromuskulären Synapse von *Drosophila melanogaster* Larven untersucht. Die Glutamatrezeptoren sind hierbei genetisch mit Fluorophoren markiert und können so mit Hilfe eines konfokalen Fluoreszenzmikroskops aufgenommen werden. Dieses System, welches in der Arbeitsgruppe von Prof. Stephan Sigrist von der FU Berlin entwickelt worden ist, lässt außerdem auch die Aufnahme von Larven über mehrere Zeitpunkte zu. So kann die Glutamatrezeptorverteilung *in vivo* über mehrere Stunden analysiert werden, während Synapsen wachsen oder neue Synapsen entstehen.

Speziell soll in dieser Arbeit untersucht werden, ob die Leitfähigkeit eines Rezeptors einen Einfluss auf seinen Transport zur Synapse hat. Hierzu wurden in der Arbeitsgruppe von Sigrist Punktmutationen in der Rezeptoruntereinheit GluRIIA eingeführt, die dessen Leitfähigkeit entweder erhöhen oder senken. Die konfokalen Bilder von den markierten Glutamatrezeptoren an der neuromuskulären Endplatte (NMJ) wurden von Dr. Astrid Petzoldt und Dr. Omid Khorramshahi aufgenommen. Zusätzlich wurden elektrophysiologische Messungen von Eric Reynolds durchgeführt, um die Auswirkungen der Punktmutationen zu überprüfen.

Mit Hilfe der aufgenommenen konfokalen Bilder wird in dieser Arbeit festgestellt, ob die veränderten Leitfähigkeiten einen Einfluss auf den Rezeptortransport haben. Die Lokalisation der GluRIIA-Mutanten wird mit dem des GluRIIA-Wildtyps verglichen. Hierzu wird ein statistischer Parameter entwickelt, der die “Segregation” zwischen den GluRIIA-Mutanten und dem GluRIIA-Wildtyp quantifiziert.

Ein anderer Teil in dieser Arbeit beschäftigt sich mit der Analyse der räumlichen Verteilung der GluRIIA und GluRIIB Untereinheiten an der NMJ. Auf der Ebene von einzelnen Synapsen lokalisieren GluRIIA und GluRIIB unterschiedlich. Mit Hilfe eines statistischen Parameters, der die räumliche Autokorrelation misst, wird außerdem die Beziehung zwischen GluRIIA und GluRIIB untersucht.

Ergebnisse

Die Ergebnisse dieser Arbeit zeigen, dass der Transport von Rezeptoren von deren Leitfähigkeit abhängt. Die Rezeptoren mit geringer Leitfähigkeit zeigen eine deutlich veränderte Lokalisation. Die Stärke der Segregation vom Wildtyp-GluRIIA korreliert mit deren Leitfähigkeit. Zusätzlich sind Rezeptoren, die eine geringe Leitfähigkeit besitzen, während des Synapsen-Wachstums von der präsynaptischen Seite entkoppelt. D.h. deren Menge ist nicht mehr mit der Menge von präsynaptischen Proteinen korreliert. Außerdem akkumulieren diese GluRIIA-Mutanten verstärkt an jungen Synapsen. Diese Ergebnisse sind bereits publiziert (Petzoldt et al., 2014).

Im anderen Teil der Arbeit wird gezeigt, dass die Dichte von GluRIIA und GluRIIB vom Ort an der NMJ abhängt. In distalen Boutons ist die Dichte von GluRIIA und GluRIIB am höchsten. Dies gilt übrigens auch für das präsynaptische Protein Bruchpilot. Insgesamt zeigt die Analyse, dass die Dichte von synaptischen Proteinen nicht auf Einzel-Synapsen-Ebene reguliert ist, sondern in Clustern von mehreren Synapsen.

Als letztes wird gezeigt, dass sehr wahrscheinlich vordefinierte Ankerplätze für Rezeptoren auf der postsynaptischen Seite existieren, um die GluRIIA und GluRIIB konkurrieren. D.h. der Transport von Rezeptoren hängt nicht nur von deren eigenen Eigenschaften ab, sondern auch vom Transport anderer Rezeptoren. Interessant ist auch, dass die Dichte von präsynaptischen Proteinen mit der Dichte von postsynaptischen Proteinen eng miteinander gekoppelt ist. Es ist deshalb wahrscheinlich, dass ein transsynaptischer Mechanismus existiert, der die Protein-Dichten zwischen der präsynaptischen Seite und der postsynaptischen Seite aneinander koppelt.

Publikationsliste

Artikel in Fachzeitschriften

1. Petzoldt, A.G.*, Lee, Y.-H.*, Khorramshahi, O., Reynolds, E., Plested, A.J.R., Herzel, H. and Sigrist, S.J. (2014). Gating characteristics control glutamate receptor distribution and trafficking in vivo. Curr Biol, accepted. (*Co-first author)

2. Lee, Y.-H., Benary, M., Baumgrass, R. and Herzel, H. (2010). Prediction of regulatory transcription factors in T helper cell differentiation and maintenance. Genome Inform *22*, 84-94.

Softwarepakete

1. Benary, M.*, Kroeger, S.*, Lee, Y.-H.* and Lehmann, R.* (2013). cobindR: Finding co-occurring motifs of transcription factor binding sites. Bioconductor R package version 1.2.0. (*Equal contributions)

Berlin, den 9. September 2014

Selbständigkeitserklärung

Hiermit erkläre ich, dass ich die vorliegende Arbeit selbständig und nur unter der Verwendung der angegebenen Literatur und Hilfsmittel angefertigt habe.

Berlin, den 9. September 2014